VERTICAL STRUCTURE OF ESTUARINE FINE SEDIMENT SUSPENSIONS

BY

MARK ALLEN ROSS

A DISSERTATION PRESENTED TO THE GRADUATE SCHOOL
OF THE UNIVERSITY OF FLORIDA IN
PARTIAL FULFILLMENT OF THE REQUIREMENTS
FOR THE DEGREE OF DOCTOR OF PHILOSOPHY

UNIVERSITY OF FLORIDA

1988

UNIVERSITY OF FLORIDA LIBRARIES

ACKNOWLEDGEMENTS

My deepest and most heartfelt appreciation is extended to my chairman, Dr. Ashish J. Mehta, Professor of Coastal Engineering. In his capacity as advisor, educator and friend, he has shown me many lofty values by example. My cochairman, Dr. Robert G. Dean, Graduate Research Professor, an individual of unmatched character and inspiration, receives a lion's share of my gratitude.

Special thanks are extended to my committee members and teachers, Drs. Dave Bloomquist, Wayne Huber, Jim Kirby, and Dan Spangler, who served so patiently and were responsible for many fruitful ideas.

My Ecuadorian research partner and friend, Eduardo Cervantes, proved to be a source of much assistance, insight and camaraderie.

Honorable mention must be made of the tireless crew at the Coastal Engineering Laboratory especially Vernon Sparkman and Chuck Broward for their technical assistance. Helen Twedell of the Coastal Engineering Archives also was very helpful.

Perhaps, most importantly for me is the great sense of honor to which I have been imbued by my family. The result of love, patience, encouragement and support shown by my beautiful wife and parents. Their belief in me never faltered.

Finally, financial support for this work was derived from a research grant extended by the U.S. Army Engineers, Waterways Experiment Station,

Contract No. DACW 39-87-P-1064. Particularly, technical and administrative assistance and input provided by Allen Teeter is gratefully acknowledged.

TABLE OF CONTENTS

LIST OF TABLES

LIST OF FIGURES

LIST OF SYMBOLS

Symbol	
b	Buoyancy jump across density interface
b	Body force per unit mass tensor
C	Sediment suspension concentration (mass/unit volume)
C_a	Concentration at upper fluid mud interface
C_b	Concentration at mobile/stationary fluid mud interface
C_c	Concentration at bed surface
C_d	Drag coefficient for sphere fall velocity
C_{eq}	Equilibrium concentration during deposition
C_h	Interference settling velocity concentration
C_{hT}	Hindered settling (flux) concentration
C_i	Concentration of class i for deposition
C_m	Characteristic maximum concentration
C_{ss}	Steady state concentration after deposition
C_T	Total concentration (sum of components)
C_o	Initial concentration for settling; deposition
C_1	Cohesive (class) sediment concentration
C_2	Non-cohesive (class) sediment concentration
$\overline{C}$	Time mean concentration
C'	Instantaneous concentration component about mean
C'	Non-dimensional concentration C/C_m

d	Equivalent spherical diameter of sediment grain
D	Molecular diffusivity
d_{50}	Sediment grain size diameter of 50% greater than fraction
E_{ij}	Turbulent diffusivity components in i,j direction
E_m	Turbulent momentum diffusion rate (eddy viscosity)
E_*	Entrainment coefficient, u_e/u_*
f	Darcy-Weisbach friction factor
F_b	Vertical sediment bed flux (F_e+F_p)
F_d	Vertical sediment flux from diffusion
F_e	Vertical sediment flux from erosion
F_p	Vertical sediment flux at the bed from deposition
F_{pi}	Class i vertical sediment flux from deposition
F_s	Vertical sediment flux from settling
g	Acceleration of gravity
h	Water depth
H	Wave height
H_b	Breaking wave height
H_o	Deep water wave height
k	Wave number ($2\pi/L$)
K	Turbulent mixing tensor
K_n	Local neutral mixing rate
Ks	Local mixing rate in presence of stratification
Kx,y,z	Turbulent mixing components (cartesian)
Kx,y,z'	Non-dimensional turbulent mixing components (cartesian)
k_1	Flocculation settling velocity constant
k_2	Hindered settling velocity constant

l	Mixing length scale of turbulence
L	Lutocline layer; wave length
L_o	Deep water wave length
m	Mass flux of sediment across bed boundary
n_1	Flocculation settling velocity constant
n_2	Hindered settling velocity constant
P	Pressure variable used in the horizontal momentum equation
P	Relative Probability for deposition rate expression
P_i	Relative Probability for deposition (class i)
P_h	Hydrostatic pressure
P_{pw}	Pore water pressure
P'	Non-dimensional pressure $P/\gamma H$
q	Mass flux vector
R	Reynolds' number of sediment grain ($w_s d/\nu$)
Ri	Gradient Richardson number
Ri_*	Bulk Richardson number (bh/u_*^2)
Ri_u	Richardson number based on average velocity
R_w	Wave Reynolds number
R_t	Shear stress ratio, τ_y/τ_o
Sc	Turbulent Schmidt number
t	Time variable
t_o	Characteristic time scale
t'	Non-dimensional time t/t_o
T	Wave period
T	Stress tensor
u	Velocity component in x-direction

u_o	Characteristic velocity scale
U	Imposed velocity on the sheared turbid layer
u_e	Entrainment rate
u_b	Maximum near-bed orbital velocity
u_e	Entrainment rate (dh/dt)
Δu	velocity jump across stratified layer
u_*	Friction velocity ($\sqrt{\tau_o/\rho}$)
$\bar{u}$	Time mean velocity
u'	Non-dimensional velocity u/u_o
u'	Instantaneous velocity component about mean
v	Velocity component in y-direction
w	Velocity component in z-direction
w_s	Sediment settling velocity
w_s'	Non-dimensional settling velocity
w_{sm}	Characteristic maximum settling velocity
w_{so}	Richardson-Zaki reference settling velocity
w_{so1}	Stokes' settling velocity
w_{so2}	Reference settling velocity for average floc size
x	Longitudinal (horizontal) cartesian coordinate direction
x'	Non-dimensional horizontal direction x/L
y	Lateral cartesian coordinate direction
z	Elevation variable (positive upwards)
z'	Non-dimensional veritical direction
Z_a	Upper fluid mud interface elevation
Z_b	Mobile/stationary fluid mud interface
z_c	Bingham plastic yield elevation

Z_c	Bed elevation
α	Wave diffusivity constant
α_s	$\sqrt{\mu_2/\mu_1}$
α_y	Yield strength calculation constant
α_μ	Viscosity/concentration constant
α'	Munk and Anderson constant
α_1, α_2	Erosion rate constants
α_δ	Viscosity ratio, μ_2/μ_1
β	Settling velocity constant
β_i	Settling velocity constant for sediment class i
β_e	Exponential diffusivity constant (mass diffusivity)
β_H	Holtzman constant
β_{MA}	Munk and Anderson constant
β_{OR}	Odd and Rodger constant
β_{RM}	Rossby and Montgomery constant
β_y	Yield strength calculation constant
β_μ	Viscosity/concentration constant
β'	Munk and Anderson constant mass diffusivity
β_δ	Coefficient used in fluid mud calculations
δ	Intermediate entrainment layer
δ_c	Similarity variable $(z_c(t)/2\sqrt{\nu_1 t})$
δ_c'	$\delta_c/\sqrt{\alpha_s}$
δ_{fm}	Mobile fluid mud thickness
δ_i	Upper entrainment layer thickness
δs	Shear layer thickness; Similarity variable $(z/2\sqrt{\nu t})$
δ_s'	$\delta_s/\sqrt{\alpha_s}$
$\dot{\gamma}$	Fluid shear rate $(\partial u/\partial z)$
κ	von Karman constant (0.4)

ρ	Density of water
ρ_b	Bulk density of suspension
ρ_o	Fluid reference density for stratification
ρ_s	Granular density of dry sediment
ρ_w	Density of suspension fluid (water)
ρ'	Non-dimensional density ρ/ρ_m
μ_w, μ	Dynamic viscosity of suspension fluid (water)
μ_m	Dynamic viscosity of mud suspension
ν_m	Kinematic viscosity of mud suspension (μ_m/ρ)
ν'	Non-dimensional kinematic viscosity
Ψ	Odd and Rodger peak gradient Richardson number
ε	Munk and Anderson constant mass diffusivity
ε_o	Erosion rate constant
σ'	Bed effective stress
σ	Total stress; wave frequency ($2\pi/T$)
τ_b	Applied (time-mean) bed shear stress
τ_{bm}	Critical bed shear stress for partial deposition
τ_{cd}	Critical bed shear stress for total deposition
τ_o	Bed shear stress
τ_s	Bed shear strength for erosion
τ_{xz}	Shear stress component acting in x-direction on z-face
τ_y	Yield strength of bed deposits
χ	Log average of sediment concentration
∇	Vector operator

Abstract of Dissertation Presented to the Graduate School
of the University of Florida in Partial Fulfillment of the
Requirements for the Degree of Doctor of Philosophy

VERTICAL STRUCTURE OF ESTUARINE FINE SEDIMENT SUSPENSIONS

By

Mark Allen Ross

August 1988

Chairman: Ashish J. Mehta
Major Department: Civil Engineering

Fine sediment suspension concentrations in estuaries vary with depth depending on sediment settling and mixing processes, which are in turn dependent on the turbulent flow field and the type of sediment. Two important phenomena, fluid mud and lutoclines, are characteristic of high concentration suspensions. Understanding the physical significance of these phenomena is of paramount importance to quantifying the mixing process and the rate of material transport advected with the prevailing currents. This research investigated the physical characteristics (vertical structure) of estuarine fine sediment suspension profiles within a comprehensive descriptive framework. Suspension related mechanisms of erosion, entrainment, diffusion (in the presence of buoyancy stabilization), advection, settling and deposition were examined in this context. A vertical mass transport model developed from functional relationships between the above processes was used to explain some of the important physical characteristics.

Lutoclines, sharp steps (gradients) in the concentration profile, are regions where the local mixing rate is minimal. The mechanisms for their formation have been shown to be the non-linear relationships between 1) vertical diffusion and concentration gradient and 2) vertical

settling and concentration. The effect of sediment settling is to further stabilize the lutocline layer thereby making it much more persistent in high energy environments than other pychnoclines (e.g., haloclines). Application of the vertical transport model to data from settling column tests, wave flume resuspension tests, and estuarine field investigations provided reasonable predictive agreement for lutocline dynamics.

Fluid mud, a near-bed, high concentration layer with negligible structural integrity, results from high bed erosion or fluidization rates relative to upward entrainment fluxes and from rapid deposition. Sensitive pore pressure and total pressure measurements made in a laboratory flume have been used to demonstrate that waves, for example, provide one mechanism for fluid mud formation by rapid destruction of effective stress in the sediment bed. The upper interface of the fluid mud layer, by definition a lutocline, represents a local maximum in net downward settling flux (i.e., maximum settling minus diffusive flux). The fluid mud layer thus forms (and grows) from rapid deposition whenever the depositional flux at the bed exceeds the rate at which the sediment can develop effective stress (usually very low).

Fluid mud has been shown to be either horizontally mobile or stationary depending on the depth of horizontal momentum diffusion vertically downward into the high concentration layer. Fluid mud tends to occur over a density range between 1.01 - 1.1 g/cm^3 but due to the dependence on hydrodynamic action near the bed a precise definition cannot be made on the basis of density alone.

CHAPTER 1
INTRODUCTION

1.1 Problem Significance

Fine-grained, cohesive sediment is transported in suspension from fluvial and marine sources to depositional environments including navigation channels and harbors. This sediment affects water quality by transport of sorbed nutrients (or pollutants) and light penetration (Hayter, 1983). Shoaling is often one other critical issue. In the continental United States alone, the cost of maintenance dredging of coastal waterways, including estuarine ports and harbors, is approximately one-half billion dollars per year (Krone, 1987). Estimates of contaminant removal or dredging requirements are dependent upon a knowledge of the rates of horizontal transport of the suspended material over periods ranging from days to years. The accuracy of predictions, typically via numerical solutions of the sediment mass transport equation, is therefore strongly contingent upon an understanding of the structure of the vertical profile of sediment concentration and interaction with the turbulent flow field.

Present day modeling of cohesive sediment transport is limited by knowledge of the fundamental transport processes of erosion, entrainment, settling, deposition and consolidation of these sediments. In particular, the dynamics of estuaries with relatively high concentration suspensions typical of macro-tidal (tidal range > 4 m) environments are

poorly understood (Parker, 1987). In this context engineers and other scientists are beginning to deal with the important question of fluid mud, loosely defined as a high concentration slurry transported in the form of a relatively thin suspension layer near the bed by the prevailing currents. At present, there are difficulties associated with measuring the slurry concentration and transport velocity. The result is that large errors often occur in calculating the associated horizontal flux of sediment transport over the water column.

Fluid muds also occur in meso- (2-4 m) and micro-tidal (< 2 m) estuaries and along the open coasts where waves play a more important role than in macro-tidal environments. Wells and Kemp (1986) observed that waves traveling over nearshore mud shoals principally acted as an agent for softening and fluidizing the muddy bed. Maa and Mehta (1987) made similar observations in laboratory flume tests. In nearshore areas waves can thus significantly assist currents in transporting fluidized material to sites prone to sedimentation. Consequently, in micro-tidal waters the generation and transport of fluid mud is far more episodic than under macro-tidal conditions.

Understanding the dynamics of fluid mud is central to the issue of understanding the response of the vertical concentration profile to hydrodynamic forcing by currents and waves. Unlike the boundary of beds composed of cohesionless material (e.g., sandy beds), the cohesive bed boundary is often poorly defined as it is not evident, e.g., from echo sounder data, at what depth the near-bed suspension ends and the bed begins. Parker (1986) noted ambiguities when lead lines, echo sounders or nuclear transmission or backscatter gauges are used to identify the

bed. In fact, Ross et al. (1987) noted that due to the dynamic nature of the cohesive bed boundary which responds significantly to hydrodynamic forcing, the density of the suspension by itself cannot be used either to identify the cohesive bed boundary or the fluid mud layer which occurs immediately above this boundary. An understanding of the interaction between the concentration (or density) profile with the flow field is critically important.

Kirby (1986) recently published a summary of extensive field observations made in the Severn estuary, a macro-tidal estuary (maximum tidal range 14.8 m) on the west coast of England. Large mass transport rates via fluid mud generation regularly occur in this estuary. The dynamic interaction between the concentration field and flow field are further complicated by the extremely high concentrations. Surface concentrations reach 1000 mg/l easily, which may be compared with ≈ 20 mg/l in Florida's coastal waters (Mehta et al., 1984). A significant observation in the Severn was the generation of rather sharp gradients in concentration termed lutoclines, which rise and fall through the water column depending upon the flow condition. According to Kirby (1986), lutoclines, which are analogous to other types of pycnoclines, e.g., haloclines, seem to occur where the suspension concentration exceeds ≈ 500 mg/l. However, they differ from other pycnoclines by the added process of sediment settling. Sediment settling further supports stabilization and resulting high density gradients. For this reason lutoclines are much more persistent than for example haloclines in high energy environments. An example of a lutocline is the upper level of fluid mud within which concentrations can typically exceed ≈ 10,000 mg/l.

Above this level, lutoclines often show up as multiple "steps," which represent local complex imbalances between diffusive and settling fluxes. Kirby (1986) observed that lutoclines often are not simulated properly by numerical models with resulting errors in the estimates for the rates of mass transport.

The aforementioned issues illustrate the strong need to examine the entire question of the vertical structure of concentration and its interaction with the flow field within a comprehensive framework. An attempt is made in this thesis to approach the problem via analysis of laboratory and field measurements within a descriptive framework for the vertical concentration structure. New definitions are proposed and the dynamics of the concentration profile are adduced through relatively simple mathematical models which are verified by laboratory and field data. The objectives and scope are accordingly as follows.

1.2 Objective and Scope

The objectives of this study were to

1. Define the physical characteristics of fine sediment suspension profiles in estuaries including lutoclines, fluid mud, and the cohesive bed within a comprehensive descriptive framework.

2. Determine the important physical mechanisms and processes which influence these characteristics.

3. Develop simple but useful qualitative and quantitative descriptions for these processes which could be used in a predictive capacity to model suspensions in the prototype environment.

To meet these objectives the scope of this research was as follows:

1. Laboratory tests were conducted, using natural estuarine

sediment, to measure the parameters important to cohesive bed and suspension profile definitions.

2. For the simple vertical structure model development, only vertical transport fluxes were considered. Analysis of turbulent diffusion was based on classical mixing length approximations and gradient Richardson number bouyancy stabilization relationships. Sediment settling velocity expressions were concentration dependent.

3 Horizontal transport in the fluid mud layer was calculated from consideration of momentum diffusion resulting from applied interfacial shear stress.

4. Verification of model applicability was limited to comparisons with selected field and laboratory data (e.g., time series concentration profiles).

1.3 Outline of Presentation

The study is presented in the following order. Chapter 2 can be regarded as a description and definition chapter. Specific justification is presented for delineating processes influencing vertical suspended sediment structure. Physically based, qualitative definitions are given for lutoclines, stationary and mobile fluid mud layers, and bed elevation. This chapter also describes many of the complexities associated with defining the cohesive bed from theoretical and applied perspectives.

Chapter 3 presents the theoretical development of the vertical transport and momentum diffusion models. For the transport model, the advection-diffusion equation is given and the individual terms are discussed. Entrainment, diffusion, settling and bed fluxes are addressed. For the fluid mud momentum diffusion model, theoretical formulations are presented with assumptions concerning rheological and temporal responses.

Chapter 4 presents the objectives, procedures and results of laboratory experiments with three specific themes: cohesive bed dynamics associated with wave-induced bed fluidization and delineation of the cohesive bed boundary; wave resuspension with emphasis on the evolution of the suspension profile with time; and settling velocity determination. The natural estuarine sediment used in the tests is characterized in Section 4.2.2. Historical approaches toward settling velocity determinations are discussed in the context of strengths and weaknesses. Section 4.3.2 presents an improved procedure for determining cohesive sediment settling velocity concentration relationships using settling columns.

The application of the vertical transport model is presented in Chapter 5. An early attempt was made to progressively verify the individual routines in the model, before concurrent simulation. Thus, for example, the settling routine was first tested by reproducing quiescent (column) settling results (a nearly pure settling condition, see, for example, Yong and Elmonayeri, 1984, for diffusion in quiescent settling). Next, the diffusion, erosion and deposition routines were added and tested. Predictions of lutocline formations in field conditions together with fluid mud layer development in a wave-tank illustrating the model's ability to handle sediment fronts (i.e., sharp concentration gradients) are also shown in Chapter 5.

The fluid mud horizontal transport model results also are included in Chapter 5. Steady and unsteady simulations of wave-tank data (presented in Chapter 4) and field data (published by Kendrick and Derbyshire, 1985) are shown.

Conclusions, recommendations for future research and miscellaneous closing comments are given in Chapter 6.

Appendix A presents a dimensional analysis to determine the important terms in the transport equation. Appendix B contains the tabulated laboratory data taken during wave resuspension tests. Appendix C is a printout of the 1-D vertical transport model developed for this study.

CHAPTER 2
VERTICAL STRUCTURE OF SUSPENSIONS

2.1 Introduction

Suspended sediment concentration in estuaries varies greatly with depth, the highest concentrations being usually found nearest the bed. Simply stated, this variance is because gravitational flux (associated with settling) counteracts mixing and prevents the sediment from becoming uniformly mixed as is the case with neutrally buoyant or dissolved constituents. In an equilibrium profile (profile not changing with time) the vertical flux associated with settling is everywhere equal to the vertical flux associated with upward diffusion (typically turbulent mixing). For sediment with a constant settling velocity and mixing based on a Prandtl/von Karman mixing length approximation, analytical solutions for the concentration profile follow the classical works of O'Brien (1933) and Rouse (1937). In a fully developed turbulent flow in the absence of significant density gradients the mixing rate, which is directly proportional to the eddy scale of turbulence, is smallest near the bed and increases upward reaching a maximum approximately at mid-depth (Schlichting, 1979). However, sediment in suspension can greatly increase the bulk density of the water. If high concentration (density) gradients develop, turbulent mixing will be greatly damped locally (Fischer et al., 1979). This has been well documented for stratified flows associated with dissolved salt- and temperature-induced density

gradients (Turner, 1973), but has been generally overlooked by classical solutions of vertical sediment transport (Rouse, 1937; Raudkivi, 1967).

This chapter presents the physically based definitions for the vertical structure (or vertical characteristics) of fine-grained suspended sediment profiles. Much of the terminology and descriptions used have been liberally applied in broad contexts in previous related and unrelated studies. Most were disparate in their objective. The following pages will help clarify the usage.

2.2 Typical Concentration Profile

Figure 2.1 shows a typical instantaneous concentration profile as might be observed in a high sediment load environment such as the Thames River (UK), San Francisco Bay or the Severn Estuary. While the values are assumed, they are representative of those commonly reported in the literature (Parker and Kirby, 1979).

It is noted that there is a 4-5 order of magnitude range in concentration from water surface to bed surface. While most sediment transport models focus primarily on calibrations of the upper water column concentrations, the significance of neglecting the near bed layers should be obvious, but will be shown in detail.

The largest layer is the mobile suspension layer which extends down to reference level, Z_a. This is the layer that is most often turbulent. It is also generally, dominated by pressure gradient driven flow associated with water surface elevation gradients resulting from tides and freshwater discharge. Concentrations in the upper mobile suspension

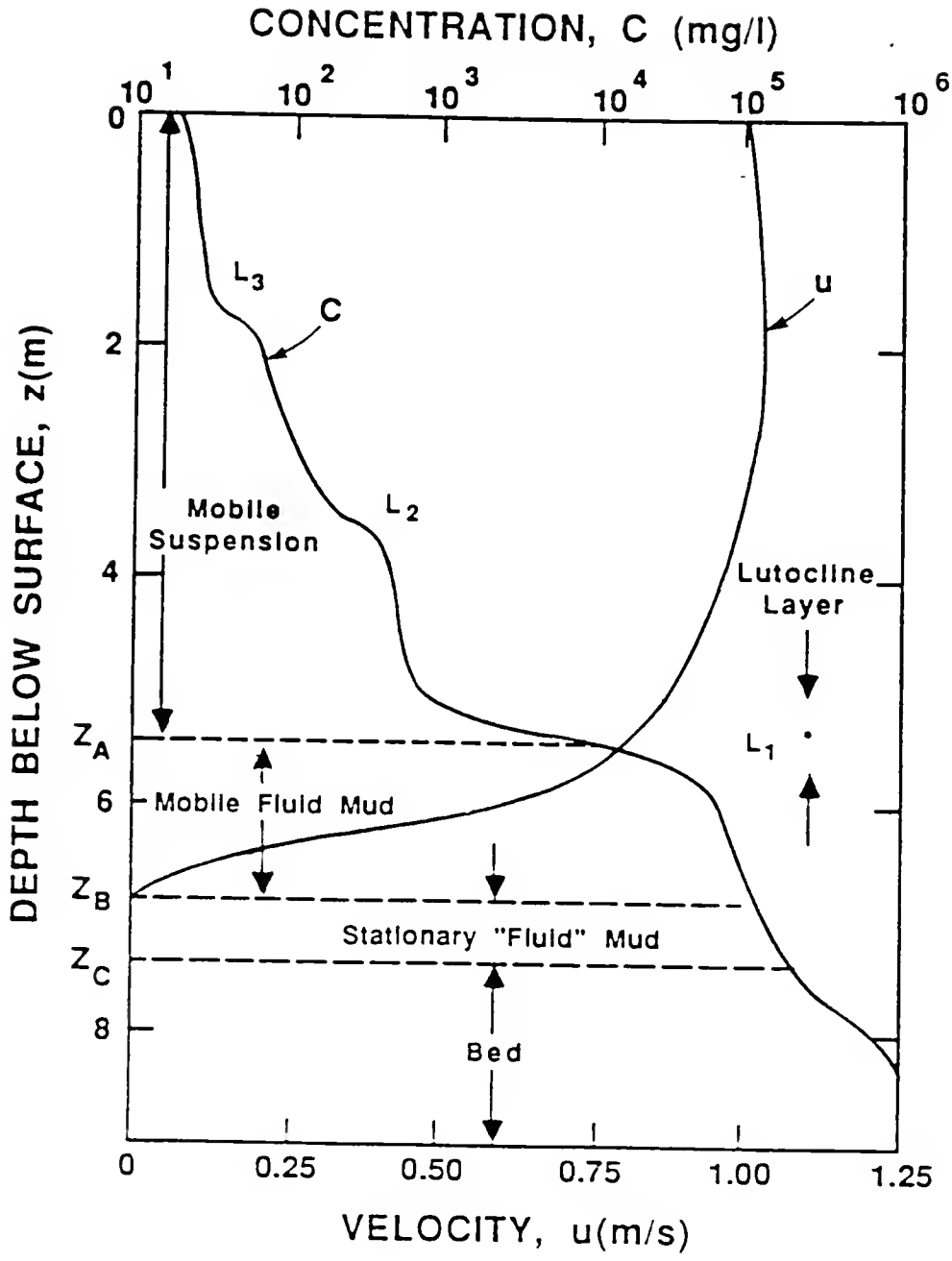

Figure 2-1. Typical Instantaneous Concentration and Velocity Profiles in High Concentration Estuarine Environments

layer are usually 1-1000 mg/l but in rare cases exceed 10,000 mg/l (in the lowest portions) during extreme tides or storm conditions (Parker and Kirby, 1979).

At various levels in the mobile suspension layer there can exist sharp increases in concentration which result from and further support local minima in mixing and upward vertical diffusion. These are termed lutocline layers which are one form of pycnoclines (regions of sharp density gradients). There can be multiple lutocline layers but more than 2-3 is rare. Such multiple layering in salinity or thermal structure is called finestructure (Posmentier, 1977).

Below Z_a there is a sharp increase in concentration above 10,000 mg/l to 100-300 g/l. This is the so-called "fluid mud" layer defined in Section 2.4. Thus, Z_a represents a lutocline between upper column mobile suspensions and near-bed fluid mud. This is often mistaken as the bed on echo sounder records (Kirby, 1986). Depending on the rheological properties of the mud, the magnitude and duration of the applied interfacial (lutocline) shear stress, and/or the internal pressure gradients, a portion of this fluid mud layer is mobilized to flow in a direction with the applied force(s). The interface between the mobile and stationary mud suspensions is labeled reference level Z_b. The symbol, Z_b, will not necessarily be identifiable from concentration profiles but instead must be identified from accurate measurements of the velocity profile. Below the fluid mud layer at reference level Z_c there exists a definable sediment interface below which the sediment exibits bed properties based on classical soil mechanical definitions. This is the cohesive bed elevation, above which only suspension occurs (discussed

in Section 2.3). Strictly speaking, the stationary fluid mud layer (Z_b-Z_c) may not necessarily behave as a fluid (i.e., not supporting shear stresses), but since it fits the general definition for fluid mud (i.e., near-bed, high-concentration layer) the terminology is nevertheless retained.

A typical velocity profile is also shown in Figure 2-1 for reference. It is shown to be of almost logarithmic form in the mobile suspension layer--indicative of turbulent flow. Near the fluid mud layer turbulence is dampened out and there is a transition layer which, proceeding down with depth, gives way to a shear flow viscous layer. This is analogous to stratified flows of salts (Yih, 1980; Narimousa and Fernando, 1987) and is described further in Chapter 3.

2.3 Problems Related to Defining the Bed

When trying to determine the bed elevation, Z_c, to do so on the basis of concentration only is imprecise. As pointed out by Sills and Elder (1986) and in this report, bed properties (i.e., development of effective stess as defined in Section 2.3.2) can exist in concentrations as low as 70-80 g/l, depending primarily on the fluid suspension and bed dynamics (stress, strain and strain rate) at any particular time. Thus, under field conditions, a precise identification of the cohesive bed interface would not be possible without dynamical data (e.g., measurements to determine effective stress). Bed definition is also dependent on previous formation conditions, wave and current actions and consolidation properties of the particular sediment. These phenomena provide justification for a brief discussion of bed formation and

consolidation concepts followed by a subsection (2.3.2) on the concept of bed definition related to effective stresses.

2.3.1 Bed Formation Concepts

To characterize the process of bed formation in a laboratory or field setting it is important to distinguish the mode of deposition. According to Parchure and Mehta (1985), in the laboratory, bed formation can be in the form of a "placed" or "deposited" bed. Placed beds are those developing from high concentration slurries. Deposited beds result from lower concentration, particle by particle deposition. Placed beds, therefore, are more uniform vertically, whereas deposited beds are non-uniform and dewater relatively rapidly. The specific character of each bed type is most pronounced earliest after formation, decaying with time until the properties are nearly indistinguishable. Because of the time scales involved, placed beds are probably more typical of laboratory conditions; however, rapid fluid mud deposition in an estuary would have similar characteristics.

In the field, an alternative to considering the bed based on depositional mode is to examine in detail the physics of mud deposition and bed formation. A schematic representation of the bed formation process is shown below (Figure 2-2).

There are basically two mechanisms responsible for bed formation: sedimentation (deposition) and consolidation. Sedimentation can be defined as the process by which particles or masses of particles leave suspension and settle onto the bed under gravity. Consolidation in a fully saturated environment results from particle framework (mineral

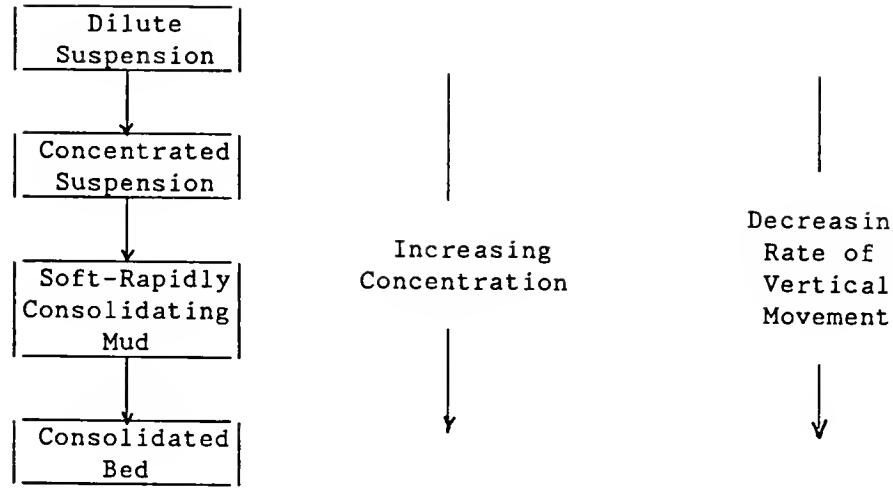

Figure 2-2. Schematic Representation of Bed Formation Process

skeleton) deformation under applied stress. The applied mechanical forces can be either due to net negative buoyancy (self-weight) or imposed overburden (surcharge) loading.

Imai (1981) gave a description and graphical model of the bed formation processes. Figure 2-3 shows this description.

The flocculation stage in Figure 2-3 actually includes the complex process of particle destabilization by doublelayer suppression in the presence of available cations and subsequent aggregation by interparticle collision and cohesion. The floc formation process takes place under settling conditions as pointed out by Krone (1962). The settling zone shown in Figure 2-3 would be more appropriately labeled hindered (or zone) settling. No further discussion of settling will be given here as the settling process is discussed further in Chapter 3. Between times t_1

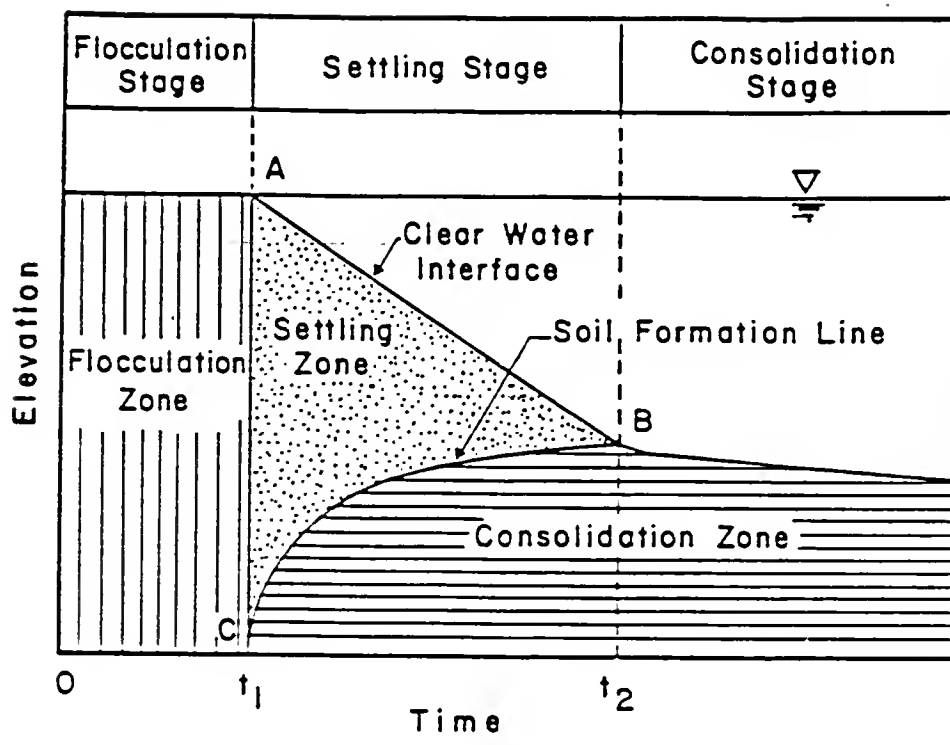

Figure 2-3. Bed Formation Process According to Imai (1981)

and t2, sediment flocs settle to form a soft bed. The bed is continually built up by continuous deposition of these flocs but simultaneously undergoes dewatering and consolidation. During this time, bed properties begin to change with depth due to particle rearrangement and larger floc breakdown (Krone, 1962). After the settling stage, consolidation continues and the bed slowly begins to "harden" as depth-variation in bed properties (i.e., density, effective stresses, etc.) become more pronounced. This self-weight consolidation approaches a steady state condition exponentially.

Since it is not within the scope of this study to discuss the details of consolidation, it will suffice to conclude this section by stating that a vast amount of geotechnical literature on

sedimentation/consolidation theories is available. The pioneering work by Terzaghi (1923) using one-dimensional finite strain theory now has evolved into complex multi-dimensional, non-linear finite strain theories. The reader is directed to the paper by Schiffman et al. (1986), which presents a noteworthy historical, theoretical, and applied account of one-dimensional sedimentation and consolidation.

2.3.2 Effective Stress

Given that the porous medium (the cohesive bed) is a two-phase system consisting of a deformable mineral skeleton filled with an incompressible liquid (water), the effective stress, σ', is defined as the difference between the total stress, σ, and the pore water pressure, P_{pw}, at any point:

$$\sigma' = \sigma - P_{pw} \qquad (2.1)$$

Empirically, it is found to be the controlling parameter in determining soil strain, deformation and strength (Schiffman et al., 1986). Classically, one type of soil failure is defined as a "quick" condition in which the effective stress tends toward zero (Sowers, 1976).

Another important parameter is excess pore pressure, Δu. This is the difference between actual pore water pressure, P_{pw} (e.g., as measured by a manometer), and hydrostatic pressure, P_h. Under dynamic conditions, if the sum of excess pore pressure, Δu, and hydrostatic pressure, P_h, approaches the total stress, σ, liquefaction occurs (Perloff and Baron, 1976),

$$\Delta u + P_h \rightarrow \sigma \qquad \text{(Liquefaction)} \qquad (2.2).$$

Figure 2-4 is a definition sketch for these terms.

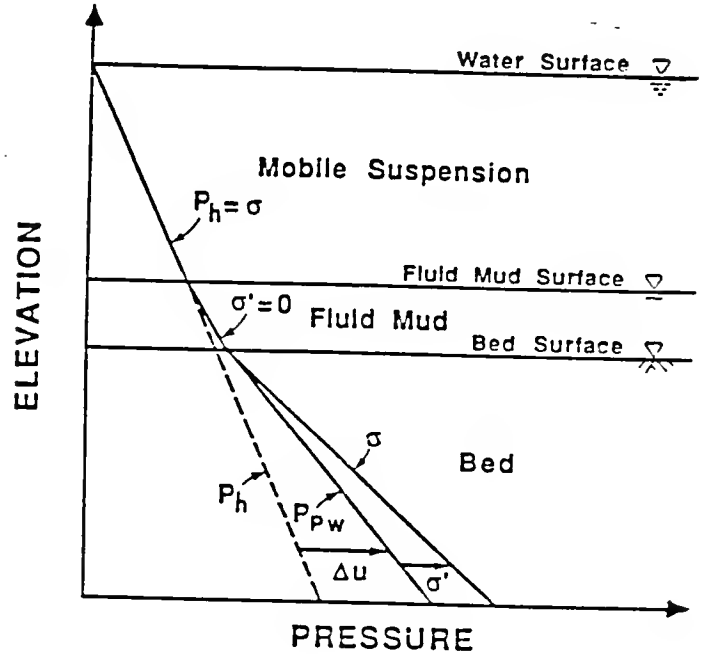

Figure 2-4. Definition Sketch of Bed Stress Terminology

In a non-fluidized sandy (or any large porosity) sediment bed the effective stress everywhere is non-zero. The total pressure is the integral of the density profile over depth (acted on by gravity) and the pore pressure is everywhere hydrostatic. For finer sediments which are much less permeable, pore pressures easily increase to above hydrostatic.

In the upper bed where the pore water pressure is equal to the total pressure, the sediment is in suspension and the water bears the weight of the sediment (increased bouyancy through higher bulk densities). When

the pore pressure drops below the total vertical stress, there is particle interaction. Thus, a weak structure forms that is able to support some of the weight of the sediment. Therefore, the development of effective stress provides a fundamental distinction between suspension and structural bed, i.e.,

$$\sigma' = 0 \; ; \quad P_{pw} = \sigma \quad : \quad \text{Suspension}$$
$$\sigma' > 0 \; ; \quad P_{pw} < \sigma \quad : \quad \text{Bed} \qquad (2.3).$$

The elevation of the (structured) bed, Z_c in Figure 2-1, therefore, should be based on the development of effective stress below this elevation. Within the bed, the interaction between sediment flocs provides a resistance to erosion due to frictional and electrochemical bonding. A reduction in effective stress, therefore, leads also to the reduction in the yield strength and the critical shear stress for erosion. No effective stress means no inter-aggregate contact or friction. This important distinction was pointed out by Sills and Elder (1986).

Been (1980) and Been and Sills (1981) made extensive laboratory measurements of the development of effective stress in quiescent settling/consolidation of fine sediments. A representative plot of measured effective stress profile is shown in Figure 2-5.

In their experiments on Combwich mud using different initial concentrations, no unique concentration was found at which effective stress developed. The concentration range over which structural development occurred was between 80 and 220 g/l depending on the initial

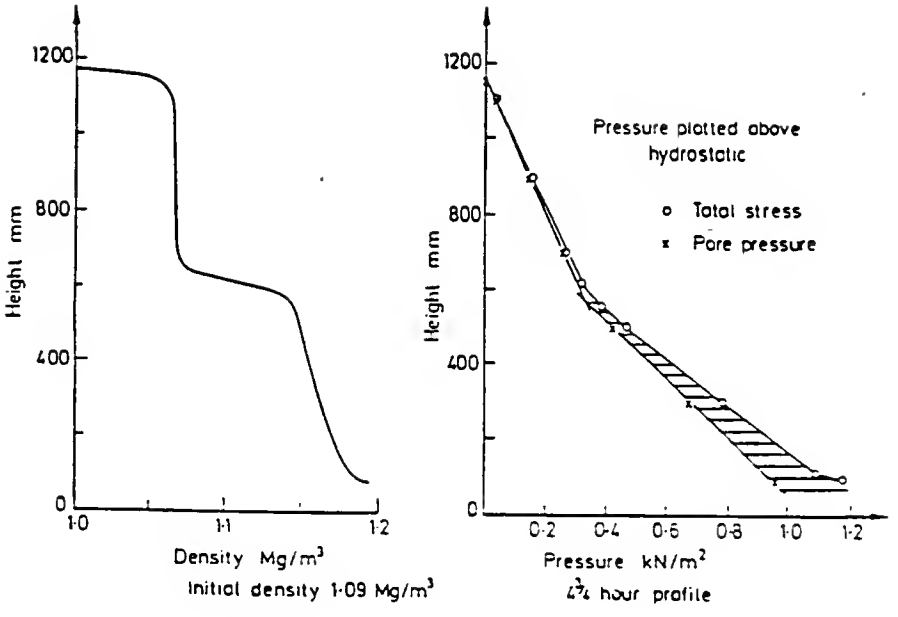

Figure 2-5. Effective Stress Profiles in a Settling/Consolidation Test (reprinted with permission from Been and Sills, 1986)

concentration of the slurry. One significant observation was that effective stress existed always in concentrations greater than 220 g/l. This observation seems to imply that structural phase development is dependent on sedimentation rate especially in low concentration quiescent conditions. It is noted in the following sections that structural phase development is also dependent on hydrodynamic agitation. This dependence is demonstrated in laboratory tests of wave erosion as described in Chapters 4 and 5.

2.4 Fluid Mud

As stated in Chapter 1, fluid mud is defined as a near-bed, high density, cohesive sediment suspension layer (Ross et al., 1987). In

areas with large bed slopes, fluid mud loosened by currents or waves can flow down the slope by gravitational forces similar to mudslides and debris flow on hillsides (Odd and Rodger, 1986). For this reason, navigation channels and basins are especially vulnerable to this type of sedimentation.

Many investigators have identified fluid mud in terms of a range of bulk density (or concentration) of the sediment-fluid mixture, as noted in Table 2-1. It should be pointed out that these investigations were, in general, disparate in terms of their aims, dealing with field observations or laboratory tests. Nevertheless, there seems to be some agreement amongst the proposed densities initially suggesting perhaps an approximate range of 1.03 to 1.20 g/cm^3 (concentration range of 10 to 320 g/l).

To provide a quantitative definition for fluid mud based on a discrete concentration range is not possible because, as pointed out in the previous section, the effect is not simply dependent on concentration but on the flow conditions and sediment settling properties. Therefore, the values given in Table 2-1, without qualifying the particular flow conditions and sediment settling behavior under which the ranges apply, are not amenable to developing a general definition applicable in all cases. All that can be deduced from the tabulated data is that fluid mud seems to occur within a rather wide concentration range of between 3 and 500 g/l (two orders of magnitude).

Fluid mud can form during rapid erosion or deposition. During erosion, if initially the erosion rate greatly exceeds the turbulent entrainment rate, i.e., the rate at which sediment is mixed by turbulence

into the upper column mobile suspension layer, the near-bed high concentration further dampens turbulent mixing and the near-bed

Table 2-1. Fluid Mud Definition by Density/Concentration

Investigator(s)	Density/Conc. Range	
	Bulk Density (g/cm^3)	Concentration x 10^{-3} (mg/l)
Inglis and Allen (1957)	1.03 - 1.30	10 - 480
Krone (1962)	1.01 - 1.11[a]	10 - 170
Wells (1983)	1.03 - 1.30	50 - 480[a]
Nichols (1985)	1.003 - 1.20	3 - 320
Kendrick and Derbyshire (1985)	1.12 - 1.25[a]	200 - 400

[a]Conversion between density and concentration based on assumed sediment density of 2.65 g/cm^3.

suspension can be stabilized as a stratified flow. This effect is often the case in wave erosion (Maa and Mehta, 1987). This is discussed in Chapter 3 and later shown in laboratory wave resuspension tests documented in Chapter 4. During deposition, if the sediment deposition flux exceeds the rate of pore fluid transport upward (dewatering rate of the suspension), dense near-bed suspensions are formed that grow upward and only slowly consolidate (see Section 2.3.1).

As shown in Figure 2.1, fluid mud can occur as a mobile or stationary suspension. This distinction was first made by Parker and Kirby (1977). Both conditions are discussed in the following sections.

2.4.1 Stationary Fluid Mud

Within the fluid mud layer there are typically two distinct regions separated by a level below which no horizontal motion takes place. In the definition sketch (Figure 2-1) this was elevation Z_b. For instance, this elevation might be considered to be the applicable elevation of the bottom boundary condition for a horizontal transport model. However, this level is quite sensitive to the rheological response of the mud from imposed stress (e.g., the lower extent of the vertical momentum diffusion resulting from an applied horizontal shear stress at the upper fluid mud interface). For the purpose of describing why this layer exists and how it is differentiated from the mobile layer above, several simple arguments are presented here and are more formally posed in Chapter 3 (Section 3.7).

It is possible to estimate the stationary layer elevation, Z_b, by making several simplifying assumptions. As a first approach, analogy can be made between flow in the fluid mud layer and unsteady couette flow development beneath an infinite plate moving with a constant velocity after being started from rest. A shear stress results on the upper fluid mud interface, elevation Z_a in the definition sketch (Figure 2-1), because of an imposed velocity in the upper column (mobile suspension). Momentum diffusion then occurs over a finite thickness, δ_{fm}, in the fluid mud layer. For a constant kinematic viscosity, ν_m of the mud, the temporal response (for relative time t after imposing the shear stress) of the mobile fluid mud layer thickness, δ_{fm}, is

$$\delta_{fm} = \beta_\delta \sqrt{\nu_m t} \qquad (2.4)$$

where β_δ is a constant (Eskinazi, 1968). However, this leads to calculations of layer thicknesses of many meters after periods of minutes--unreasonably large values. Also, the viscosity of these high concentration layers is not constant but concentration (and thus depth) dependent (Krone,1962).

Another approach is to consider the slurry to have a concentration dependent dynamic viscosity, $\mu_m(C)$. The density of the bulk suspension, ρ_b, is given by a simple linear relation to the (mass/unit volume) concentration, C, as

$$\rho_b = \rho_w + C\ (1 - \frac{\rho_w}{\rho_s}) \qquad (2.5)$$

where ρ_w is the density of the suspending fluid (water) and ρ_s is the granular density of sediment (typically 2.65 g/cm^3).

A summary of empirical relationships for dynamic viscosity variation with concentration is shown in Figure 2-6. The trend, in the fluid mud range ($10 \leq C \leq 200$ g/l), seems to be of an exponential or polynomial form: i.e.,

$$\mu_m = \mu_w\ e^{\alpha'_\mu C} \qquad (2.6a)$$

or

$$\mu_m = \mu_w(1 + \beta_\mu\ C^{\alpha_\mu}) \qquad (2.6b)$$

where μ_m is the dynamic viscosity of mud suspension, μ_w is the dynamic

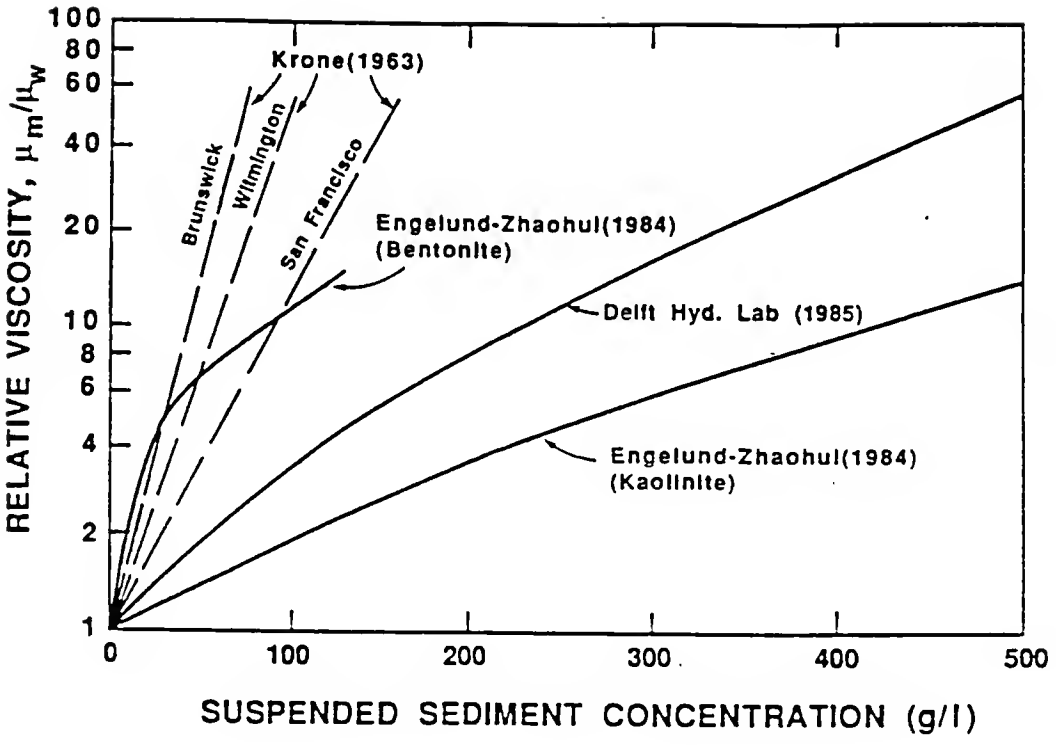

Figure 2-6. Mud Dynamic Viscosity Variation with Concentration

viscosity of clear (free from suspension) water, C is the concentration of suspended sediment, α'_μ, α_μ and β_μ are empirical coefficients. Engelund and Zhaohui (1984) proposed a relationship of the form of Eqn. (2.6b) for kaolinite suspensions. They found $\beta_\mu/\alpha_\mu = 0.206$ and $\alpha_\mu = 1.68$ for kaolinite concentration (in percent) and fresh water ($\mu_w = .001$ N-s/m^2). Equation 2.6b represents a truncated approximation of a power series expansion of $\mu_m(C)$. For a more general form for $\mu_m(C)$, the reader is directed to the discussion by Krone (1963).

However, it must be pointed out that data published by Krone (1963) showed that multiple values for β_μ, α'_μ and α_μ are possible for a particular sediment, depending on the shear rate and degree of

aggregation. Therefore, caution must be advised concerning the validity of Eqn. 2.6 for more detailed application.

By considering the mobile fluid mud as depth varying viscous Rayleigh flow (Stokes' first problem with variable viscosity; see Schlichting, 1979), a numerical solution of the flow and boundary layer thickness can be obtained. This is a non-steady state approach to determining the horizontal transport layer detailed in Section 3.7.

An alternative approach to determining the mobile/stationary interface is considering the non-Newtonian rheological properties of high concentration suspensions. Past research has indicated that concentrations in the fluid mud range behave as Bingham plastics or pseudoplastics (Krone, 1963; Kirby and Parker, 1977; Faas, 1981; 1987; Nichols, 1985). Over short (tidal) time periods the designation of effective yield strengths may be appropriate. In this case, the data seem to suggest a concentration power law relationship. Figure 2-7 shows a very approximate linear (on log-log paper) relationship between yield strength, τ_y, and concentration through the data sets shown. The expression to relate this functional dependence is of the form,

$$\tau_y = \beta_y C^{\alpha_y} \qquad (2.7)$$

where β_y and α_y are empirical constants. The data in Figure 2-7 suggest that $\beta_y = 8.7 \times 10^{-7}$ Pa (1 Pa = 1 N/m^2) and $\alpha_y = 2.55$. With this assumption it is possible to estimate the lower penetration distance (lower extent of horizontal motion), the mobile/stationary fluid mud layer interface, Z_b, based solely on equating the applied bed shear to

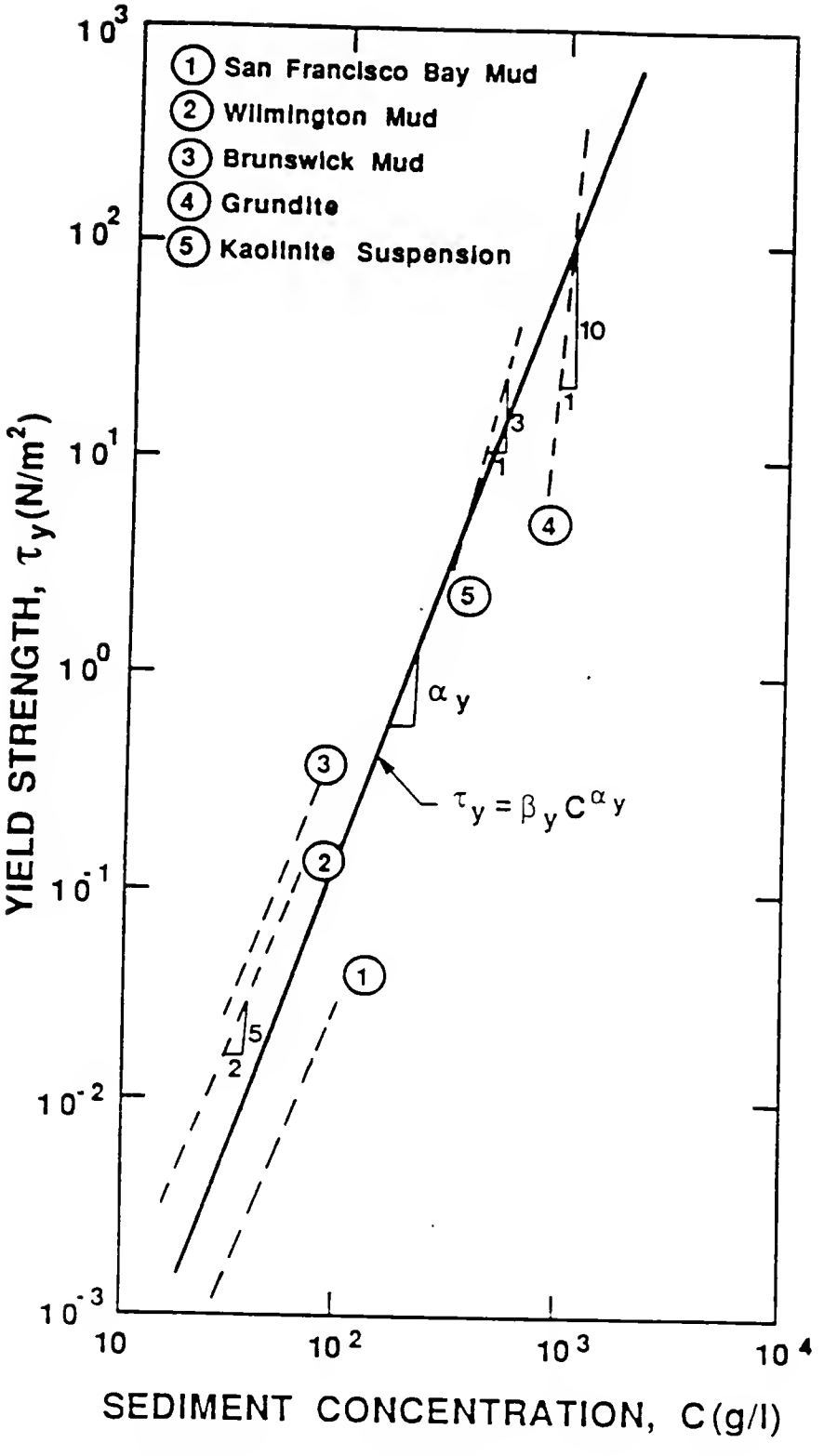

Figure 2-7. Bingham Yield Strength Variation with Concentration

the level of equal yield strength. However, field observations of fluid mud flows (Kendrick and Derbyshire, 1985) do not seem to support this approach (see Section 5.5). This is because flow occurs when the applied shear stress is less than the reported shear strength (Figure 2-7). This suggests that the behavior is more pseudoplastic than Bingham. Further discussion of possible means of determining the elevation, Z_b, is described in Section 3.7.

2.4.2 Mobile Fluid Mud

The mobile fluid mud layer as described in Section 2.2 is that part of the fluid mud layer which is advected along with the mobile suspension layer current. It may also be gravitational slump flow along a sloping bed (Kendrick and Derbyshire, 1985). The elevation, Z_a, (Figure 2-1) which defines the upper bound of the layer represents a local maximum in net downward vertical flux.

The settling velocity of cohesive sediments varies with concentration in suspension, $w_s(C)$. Initially constant, the velocity rises with increasing concentration (due to flocculation) to a level where it becomes constant again then rapidly drops. An example of the settling characteristic of a natural estuarine sediment is shown in Figure 2-8. The point beyond which no further increase in settling velocity occurs has been termed "hindered settling" (Owen, 1970; Imai, 1980; Teeter, 1986a). For purposes that will become clear with the following arguments, it is important to distinguish hindered settling velocity from hindered settling flux. The details of free, flocculation and hindered settling velocity are discussed in Chapter 3 (Section 3.4).

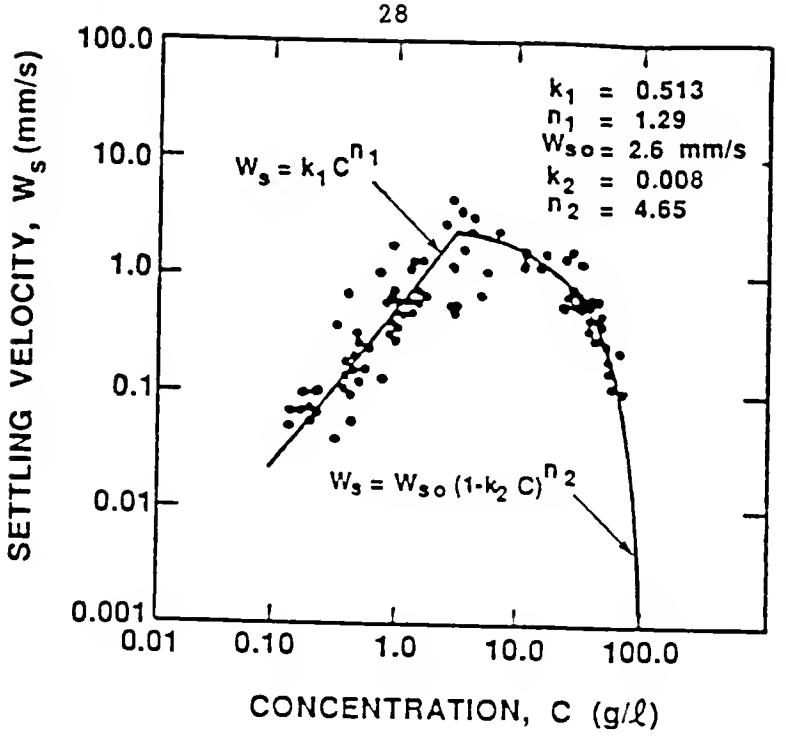

Figure 2-8. Settling Velocity Variation with Concentration Severn Estuary Mud (adapted from Mehta, 1986)

The vertical flux of sediment (mass per unit area per unit time) from settling, F_s, is the product of the local settling velocity and concentration as

$$F_s(C) = w_s(C) \cdot C \qquad (2.8)$$

For the data of Figure 2-8 (source: Thorn, 1981) the vertical flux, F_s, is plotted against concentration, C, in Figure 2-9 below.

From Figures 2-8 and 2-9 it is observed that the peak flux occurs at a much higher concentration (i.e., ≈ 20 g/l) than that at which the peak settling velocity occurs (i.e., ≈ 3 g/l). This is due to settling velocity being either constant or only slightly decreasing from the

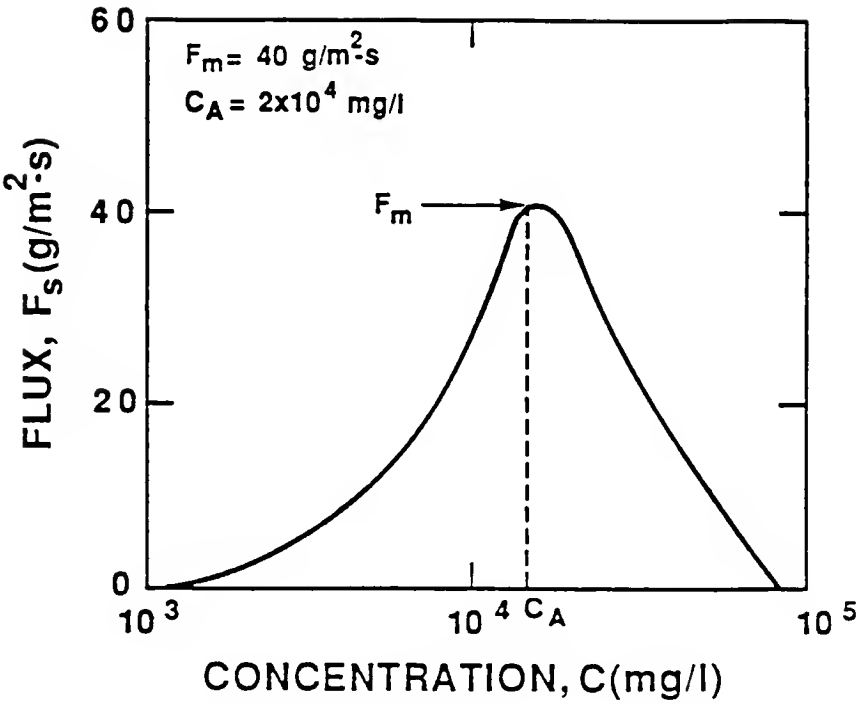

Figure 2-9. Vertical Settling Flux Variation with Concentration (reprinted with permission from Ross et al., 1987)

maximum (≈ 2-3 g/l) over a wide concentration band (2-10 g/l). The peak settling flux (i.e., 20 g/l) represents a more reasonable definition for hindered settling than that based on the peak settling velocity. Beyond this point, the actual vertical mass flux from settling diminishes rapidly with increasing concentration.

The upper elevation, Z_a, of the fluid mud layer under settling conditions therefore occurs at the "hindered" (defined on the basis of flux) concentration. A discrete interface forms because the sediment accumulates at this level because the flux is increasing above and decreasing below this interface.

After all the sediment in the upper suspension layer has settled onto the fluid mud layer, the interface settles according to the

interfacial settling region (shown in Figure 2-3). When the flow in the upper suspension layer is turbulent, diffusion and entrainment at the interface reduce the overall downward vertical flux and the interfacial concentration, C_a, drops from that given by pure settling conditions. Thus, C_a has a maximum value given by the hindered (flux) concentration. In the presence of mixing, the mobile fluid mud layer, $\delta_{fm} = Z_b - Z_a$, does not necessarily become thicker (by becoming more diffuse). Due to the sharp density gradients resulting from the high suspension concentrations, turbulent mass and momentum diffusion across the fluid mud layer is greatly damped. This results in a stable stratification, often termed buoyancy or gravitational stabilization (Fischer et al., 1979). In this case, upward entrainment, which is dependent on the degree of stratification and relative turbulent intensity (Yih, 1980) becomes the dominant mixing mechanism. Stratification development is discussed in greater detail in the next section. Mixing in the presence of gravitational stabilization is discussed in Section 3.3.2.

2.5 Lutoclines

Lutoclines are defined as pronounced "steps" in the vertical concentration profile resulting from complex mixing-settling processes. The upper fluid mud interface, by this definition, is also a lutocline (shown as L_1 in Figure 2-1). However, lutoclines can as well occur in the mobile suspension layer (shown as L_2 and L_3). Lutoclines have a vertical scale (distance between steps) dependent on the local vertical scale of turbulence (Posmentier, 1977). Therefore, only a limited number can exist and over limited periods. The origin of this term stems from

the Latin word lutum which means mud (Kirby, 1986). Lutoclines are analogous to other types of density stratification (pycnoclines) from sharp salinity gradients (haloclines) and temperature gradients (thermoclines) with the exception that suspended sediment exhibits settling independent of the fluid. They are easily recorded by high frequency echo sounders and are characteristically observed in high sediment (> 500 mg/l) environments.

Figure 2-10 shows a typical suspended sediment profile showing the relative temporal stability of two lutoclines.

The velocity data also shown in the figure together with the concentration profiles suggest turbulent, well mixed flow between lutoclines.

The physics of lutocline genesis, growth, and decay is governed by the dynamic interaction between the counteracting processes of turbulent mixing and gravitational settling. Simply stated, lutoclines occur because sediment is heavier than water and it tries to settle out under quiescent conditions. Due to flocculation and hindered settling, fine sediment suspended at large concentration settles as a sharp interface, as opposed to concentration "thinning" (Bosworth, 1956). Turbulent eddies impinging on the interface exchange "parcels" of sediment-laden fluid. However, due to the potential energy difference of each "parcel" with its surroundings, they are returned to near origin levels with only modest mixing. This is in sharp contrast to the rapid mixing which takes place in the low density gradient regions (qualitatively defined below). Thus, the moderate mixing at the interface is counter-balanced by the sediment settling, and the interface remains stable.

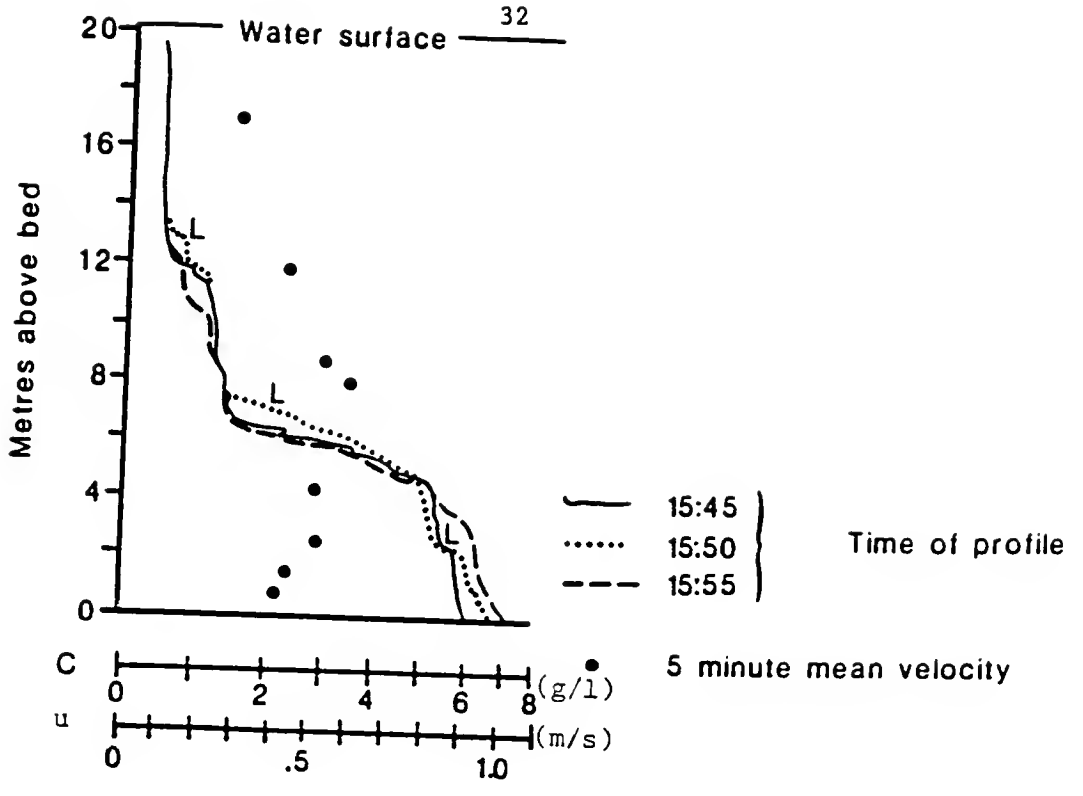

Figure 2-10. Typical Suspended Concentration Profile Showing Multiple Lutocline Stability Over 10 min. Period (Kirby, 1986)

One means of relating the relative magnitudes of gradients in kinetic energy, $\partial(\rho u^2/2)/\partial z$, to potential energy, $\partial(\rho g z)/\partial z$, is through the local gradient Richardson number defined as

$$Ri = - \frac{g}{\rho} \frac{\partial \rho}{\partial z} \left(\frac{\partial u}{\partial z}\right)^{-2} \qquad (2.9)$$

where g is the acceleration of gravity, ρ is the fluid density, u is the horizontal velocity and z is the vertical coordinate direction (positive upwards).

Thus, the implications of equation 2.9 are

Ri $\gtrsim$ 0	:	High rate of kinetic energy dissipation relative to low potential energy gradient → Rapid Mixing
Ri $>>$ 1	:	Low rates of kinetic energy dissipation relative to high potential energy gradient → Minimal Mixing
Ri $<$ 0	:	Density gradient, $\partial\rho/\partial z$, $>$ 0 , the system is unstably stratified → Overturning

As an example, letting the local mixing rate in a neutrally stratified condition (no density stratification) be defined as $K_n(z)$ implying that it is variable with depth, the simplest relationship for mixing in the presence of stratification, based on Richardson number, is

$$K_s(z) = K_n(z)\ (1 + Ri)^{-1} \qquad (2.10)$$

where K_s is the local mixing rate dampened by stratification. The limits on mixing meet the above requirements as it can be seen that $K_s(z) \to K_n(z)$ for Ri → 0 and $K_s(z) \to 0$ if Ri → ∞. This is then one means of quantifying the stratification dampened mixing.

A more general form for the above equation, a review of literature, and a discussion of applicability of buoyancy stabilization are given in Section 3.3.2.

CHAPTER 3
TRANSPORT CONSIDERATIONS

3.1 Introduction

The physics related to the vertical structure of fine sediment suspension can be addressed by considering the important components of the advection-diffusion equation. This equation, simply an Eulerian conservation of sediment mass expression, relates the temporal changes in sediment concentration to the spatial gradients in fluxes. Simple arguments show that for the present purpose the important coordinate in the equation is the vertical, z (positive upwards from the bed), direction. Furthermore, gravitational forces which influence the diffusion and settling flux terms are responsible for the complex structure of lutoclines and fluid mud as defined in Chapter 2.

Theoretical and rationally based relationships for settling velocity, neutral turbulent diffusivity, and buoyancy stabilization are presented in this chapter for explanation and predictive purposes. A simple one-dimensional numerical model, developed from these relationships and the advection-diffusion equation, is used to explain laboratory and field data presented later in this report. Finally, to distinguish the lower layer of mobile fluid mud, a simple numerical model based on momentum diffusion is developed to evaluate the dynamic and steady state characteristics of this layer and to estimate horizontal sediment transport rates.

3.2 Mass Conservation Equation

In Cartesian coordinates (x, longitudinal; y, lateral; and z, directed vertical upwards positive from the water surface), the instantaneous Eulerian conservation of mass equation for (scalar) sediment suspension concentrations C(x,y,z,t) (mass of sediment/volume of suspension) can be written as

$$\frac{dC}{dt} = -\nabla \cdot q \qquad (3.1)$$

where q is the resultant mass flux vector (from diffusion and settling) and ∇ is the vector operator.

For Fickian molecular diffusion, the mean mass flux vector is

$$q_m = - D\nabla C \qquad (3.2)$$

where it is assumed that the molecular diffusivity, D, is isotropic (Fischer et al., 1979).

Since it is implausible to track particles in suspension on an instantaneous, infinitesimal scale, and because natural flows are typically turbulent, it is usual to express equation (3.1) in terms of time averaged values (e.g., time average velocity, $\bar{u}$, and concentration, $\bar{C}$) where the averaging time is sufficiently long to negate turbulent fluctuations but short enough to track longer period temporal behavior (Vanoni, 1975; McDowell and O'Connor, 1977). However, time averaging greatly increases the diffusive mass flux vector. Fortunately, as an

approximation, turbulent diffusion can be expressed analogous to Fickian diffusion in the form

$$q_t = - K \cdot \nabla \overline{C} \qquad (3.2a)$$

where K is the turbulent mixing vector with Cartesian (x,y,z) coordinate components (K_x,K_y,K_z). Since turbulent mixing is much greater (2-8 orders of magnitude) than molecular diffusion, the latter is often neglected (McCutcheon, 1983). Simple perturbation analyses, i.e., letting the velocity (vector) and concentration (scalar) components be represented by mean (e.g., $\overline{u}$,$\overline{C}$) and fluctuating values (e.g., u',C'), have been used to support this result mathematically. The reader is directed to Hayter (1983) or French (1985) for this derivation.

The mass flux vector from settling is, simply,

$$q_s = F_s = -w_s C j \qquad (3.3)$$

where w_s is the mean sediment settling velocity and j is the unit vector directed along the z axis.

The resultant mass flux vector for suspended sediment is then approximated by

$$q = q_t + q_s \qquad 0 < z < Z_b \qquad (3.4)$$

away from the boundaries (water surface z=0 and bed surface, $z=Z_b$).

For the purposes of considering vertical structure, only the vertical transport terms need to be evaluated. Horizontal gradients in concentration are (typically 3-4) orders-of-magnitude smaller than vertical gradients.

$$\left|\frac{\partial C}{\partial x}\right| << \left|\frac{\partial C}{\partial z}\right| \quad , \quad \left|\frac{\partial C}{\partial y}\right| << \left|\frac{\partial C}{\partial z}\right|$$

Non-dimensional scaling arguments have been used to determine the relative importance of the individual terms in Eqn. 3.1 This analysis is included for reference in Appendix A. For typical estuarine conditions (see Appendix A) horizontal and vertical advective fluxes and horizontal diffusive fluxes can be neglected for first order analysis. The governing equation for considering the vertical structure of fine suspended sediments is now reduced to

$$\frac{\partial C}{\partial t} = \frac{\partial q_z}{\partial z} = \frac{\partial}{\partial z}\{w_s C + K_z \frac{\partial C}{\partial z}\} \qquad 0 < z < Z_b \qquad (3.5)$$

where q_z is the resultant vertical flux from settling and vertical diffusion away from the boundaries (z=0 and $z=Z_b$) shown by the bracketed. terms in Eqn. 3.5.

The boundary conditions which must be imposed on Eqn. 3.5 are

Bed Flux Boundary Condition. Application of Eqn. 3.5 at $z = Z_b$ requires that a bed flux term, F_b (mass of sediment per unit bed area per unit time), containing both erosion, F_e, and deposition, F_p, fluxes as

$$F_b = F_e - F_p \tag{3.6}$$

be defined. In addition, the diffusion and settling flux terms at the bed are zero. Thus $q_z(Z_b,t) = F_b$ and $w_s = K_z = 0$ at $z = Z_b$ is the appropriate bed boundary condition. F_b is dependent on sediment and hydrodynamic conditions. Section 3.5 presents a detailed discussion of bed fluxes (erosion and deposition) used in the vertical transport model.

Surface Boundary Condition. The boundary condition at the water surface, z=0, is a no net flux boundary. This means that there is no net transport across the free surface and diffusion flux is always counterbalancing settling flux i.e.:

$$q_z(0,t) = (w_s C) + \{K_z \frac{\partial C}{\partial z}\} = 0 \tag{3.7}$$

The diffusion flux term $F_d = \{K_z \frac{\partial C}{\partial z}\}$ must include entrainment and gravitationally stabilized mixing. In the absence of well defined hydrodynamics (i.e., perhaps the results from a full turbulence model simulation), functional forms for the vertical turbulent diffusivity, K_z, based on first-order closure modeling using mixing length approximations can be used (McCutcheon, 1983). This assumes that the mass diffusivity can be related to the momentum diffusivity. Furthermore, due to differences in time scales, spatial variability, and kinetic energy dissipation, the functional forms for highly oscillatory currents (e.g., waves) are quite different from those for unidirectional flows.

Stratification, in general, dampens turbulent mixing by the mechanisms described in Chapter 2. Through local gradient Richardson

number relationships of the Munk and Anderson (1948) form, buoyancy (gravitational) stabilization can be modeled. Stabilized diffusivity is treated separately in Section 3.3.2.

On the subject of mixing and stratification it must be pointed out that surface waves can create interfacial waves which can build to breaking, thereby greatly enhancing interfacial mixing (Yih, 1970; Dean and Dalrymple, 1984). Due to the limited scope of this research and because this phenomenon was not observed in laboratory or field data for this study, no further discussion is provided. The reader can find additional information on this topic in Lamb (1945), Yih (1976), and Yih (1980).

The settling flux ($w_s C$) as written in Eqn. (3.5) allows for spatial variability in both unknowns, settling velocity and concentration. In general, for both cohesive and non-cohesive sediments, settling velocity is a function of concentration, $w_s(C)$. The settling behavior of cohesive and non-cohesive sediment is covered in Section 3.4.

3.3 Diffusive Transport

3.3.1 Turbulent Diffusion

In turbulent flows mixing occurs mainly because the time-averaged products of the velocity and concentration fluctuations i.e., $\overline{u_i' C'}$, are non-zero. Through adequately measuring the simultaneous fluctuations in velocities and concentrations, turbulent mixing can be precisely quantified. Then, for predictive purposes, correlations to flow parameters such as bottom friction, mean velocity and pressure gradient are required. Reasonable success is beginning to be achieved in the area

of turbulence modeling (Zeman and Lumley, 1977; Sheng, 1983). However, in light of the difficulties in precise measurement of these fluctuations, verification poses difficulties.

For fine sediment suspensions the turbulent diffusion of sediment mass, K_s, is approximately equal to that of the diffusion of momentum, E_m. The turbulent Schmidt number, S_c (Daily and Harleman, 1966), which is the ratio of mass to momentum diffusivity is equal to one (Teeter, 1986b) as

$$S_c = \frac{K_s}{E_m} = 1 \tag{3.8}$$

In turbulent flows momentum diffusion is by Reynolds stress, $\tau_{ij} = -\rho \overline{u_i' u_j'}$, gradients where the time mean product of the velocity fluctuations is nonzero. For mass diffusion, the time mean product of the concentration and velocity fluctuation is nonzero analogously.

This observation (Reynolds' analogy) allows the use of a wide body of literature on first-order closure modeling based on the coefficient of eddy viscosity, relating the Reynolds stress to mean velocity gradient as

$$\tau_{ij} = -\rho E_{ij} \frac{\partial u_i}{\partial x_j} \tag{3.9}$$

where E_{ij} is the i,j component of the momentum diffusivity (eddy viscosity) tensor. It can be seen from Eqn. (2.9) that the eddy viscosity, in general, must be a function of mean shear rate and shear stress. It is also common to assume that turbulent diffusion is

isotropic (i.e., $E_{ij} = E_{ji} = E$, Fischer et al., 1979) in the absence of stratification.

The most commonly applied expression of vertical variation in eddy diffusivity is the formulation given by Rouse (Vanoni, 1975). By following von Karman's assumptions of a linear shear stress distribution with depth leading to a logarithmic velocity profile, the following expression is found:

$$E(z) = \kappa u_* z \left(1 - \frac{z}{h}\right) \tag{3.10}$$

where κ is von Karman's constant, u_* is the friction velocity ($\sqrt{\tau_o/\rho}$) and h is the flow depth. While this expression may be sufficient for describing turbulent-logarithmic uni-directional flows, it does not describe highly oscillatory flows such as under waves. Maa (1986), Kennedy and Locher (1972), and Hwang and Wang (1982) have reviewed currently popular expressions for diffusion coefficients under waves. There seems to be little consistency in the forms. One of the most promising expressions based on energy dissipation is that developed by Hwang and Wang (1982). Their model, applicable outside the wave boundary layer, is of the form

$$E(z) = \alpha H^2 \sigma \frac{\sinh^2 kz}{2\sinh^2 kh} \tag{3.11}$$

where α is a constant, H is the wave height (twice the amplitude), σ is

the wave frequency ($2\pi/T$, T = wave period), and k is the wave number ($2\pi/L$, L = wave length).

Thimakorn (1984) found success using a coefficient similar to that given by Hwang and Wang (1982) to predict vertical profiles of natural clay concentration during resuspension in a wave flume. It should be pointed out that the concentrations reported were small (<1000 mg/l) and any buoyancy stability effects therefore were likely to be negligible.

Next to the bed boundary layer effects greatly increase vertical mixing under waves due to the relatively large velocity gradients and shear (Neilson, 1979). Orbital particle trajectories are significantly altered from those predicted for example by linear wave theory (inviscid potential flow) because viscous (or turbulent) effects dominate. However, this layer is small ($\sigma/(2\nu) < 1$ cm) and is often neglected (Maa, 1986). Further upward, the velocity amplitude gradients increase with distance above the bottom to a maximum at the surface. This is the basis for the Hwang and Wang (1982) form shown above. Maa (1986) conducted dye diffusion tests under waves which showed larger lateral spreading rates near the surface and immediately near the bottom. This is indicative of higher energy dissipation in those regions which would support the proposition of higher vertical mixing rates.

In the presence of density stratification the form of the neutral diffusivity is not as important as the form of the stability coefficient (French, 1985), which provides the basis for a discussion of mixing in the presence of density stratification.

3.3.2 Gravitational Stabilization

In the previous section, theoretical and empirical based expressions for the vertical turbulent diffusivity under current and waves were mentioned. In a continuously, stably stratified flow the vertical diffusion of both momentum and mass is inhibited by stratification, and significant modification of the turbulent diffusivity occurs. Furthermore, the diffusivity of momentum and mass are not affected in the same manner. In the presence of density stratification, the eddy viscosity (i.e., the turbulent momentum diffusity) is larger than the eddy diffusivity of heat and mass (French, 1985). Progress has been made towards estimating values and obtaining expressions for mass and momentum diffusion in a continuously stratified flow. However, it must be emphasized that at the present time an expression does not exist for either eddy viscosity or diffusivity which is considered universally valid. French (1985) provides a summary of several popular forms developed for uni-directional flow only. A brief review of those plus others is given here for the purpose of explaining vertical structure.

Rossby and Montgomery (1935) first proposed an equation relating vertical eddy viscosity for stratified flow, E_s, to the corresponding value for homogeneous or neutral conditions, E_n, of the form

$$\frac{E_s}{E_n} = (1 + \beta_{RM} Ri)^{-1} \tag{3.12}$$

where β_{RM} is an empirical coefficient and Ri is the local gradient Richardson number, Eqn. (2.9). They assumed that the change in kinetic energy per unit mass in going from a neutral or unstratified condition to

a stably stratified condition is equal to the potential energy change due to displacement over the mixing length from the equilibrium position with a different density.

Holzman (1943) suggested a somewhat different relationship

$$\frac{E_s}{E_n} = (1 - \beta_H Ri) \tag{3.13}$$

where β_H is a coefficient. Note the change in sign of the coefficients.

Munk and Anderson (1948) proposed a generalized form of the Rossby and Montgomery (1935) and Holzman (1943) equations as

$$\frac{E_s}{E_n} = (1 + \beta_{MA} Ri)^{\alpha_{MA}} \tag{3.14}$$

where β_{MA} and α_{MA} are free coefficients.

Kent and Pritchard (1957) also used a conservation of energy argument to develop an equation of the Munk and Anderson (1948) form; however, they argued that α=-2 on a theoretical basis.

Delft Hydraulics Laboratory, (DHL) (1974), reported that the ratio of E_S to E_n should decrease exponentially with increasing values of Ri or

$$\frac{E_s}{E_m} = e^{-\beta_e Ri} \tag{3.15}$$

where β_e is an empirical coefficient.

Finally, Odd and Rodger (1978) used the original hypothesis of Rossby and Montgomery (1935) to define equations applicable for two specific cases:

Case 1. Stratified flow with a significant peak in the vertical profile of Ri at a distance $z = z_0$ from the bottom boundary where Ψ is the peak gradient Richardson number, then

$$\frac{E_s}{E_n} = (1 + \beta_{OR}\Psi)^{-1} \qquad \text{for } \Psi \leq 1 \qquad (3.16)$$

and

$$\frac{E_s}{E_n} = (1 + \beta_{OR})^{-1} \qquad \text{for } \Psi > 1 \qquad (3.17)$$

where B_{OR} = a coefficient.

Case 2. No significant peak exists in the vertical profile of Ri: then

$$\frac{E_s}{E_n} = (1 + \beta_{OR}Ri)^{-1} \qquad \text{for } Ri \leq 1 \qquad (3.18)$$

and

$$\frac{E_s}{E_n} = (1 + \beta_{OR})^{-1} \qquad \text{for } Ri > 1 \qquad (3.19)$$

Equations (3.16) through (3.19) are applied throughout the vertical dimension, but near the boundaries, if $E_s > E_n$ then E_n is used. Note that E_s/E_n = constant (not a function of depth) for all cases except conditions when Eqn. (3.18) applies. This is significantly different from the previously proposed forms (Eqns. 3.12 - 3.15) which are everywhere depth variable.

The problem with all the above methodologies is that, in general, they cannot be shown to be universally valid. Suggested values for some of the coefficients used in the above equations are summarized in Table 3-1 below.

Table 3-1. Summary of Coefficient Values for Turbulent Vertical Diffusion of Momentum in Continuously Stratified Flow

Equation	β	α	Source
3.12	2.5	--	Nelson (1972)
"	5.0	--	DHL (1974)
"	30.3	--	French and McCutcheon (1983)
3.14	10	-0.5	Munk and Anderson (1948)
"	30	-0.5	DHL (1974)
3.16-3.19	0.31	0.747	French (1979)
"	0.062	0.379	French and McCutcheon (1983)
"	140-180		Odd and Rodger (1978)

With regard to the data summarized in Table 3-1, the following should be noted:

1. Nelson (1972) used published oceanographic, atmospheric, and pipe flow data for his analysis, and the same was true of the analysis by the Delft Hydraulics Laboratory (1974). Thus, these investigators had no control over the quality of their data.

2. The data used by French (1979) were taken under laboratory conditions, but the flume used for these experiments had a small width-to-depth ratio, and the results may have been unduly affected by this fact.

3. Odd and Rodger (1978) used field data from a reach of tidal channel. Their data set is perhaps the best data presently

available regarding the turbulent vertical diffusion of momentum under stratified conditions.

4. French and McCutcheon (1983) used the Odd and Rodger (1978) data set for their analysis. The coefficients for Eqns. (3.16 - 3.19) used in their work differ from that of Odd and Rodger (1978) due to differences in the definition of reasonable fit.

5. In the past, Eqn. (3.12) has been the most commonly used method of estimating E_s (Nelson, 1972). It is more theoretically justifiable than the methods of Odd and Rodger (1978), French and McCutcheon (1983) or French (1979).

6. Delft Hydraulics Laboratory (1974) concluded that when Ri < 0.7, the scatter of the data available is so great that no best-fit equation can be selected.

A number of models for the eddy (mass) diffusivity in stratified flow have also been proposed. Most have been based on the results from momentum diffusion; however, under stratified conditions, questions arise as to the applicability of this assumption (e.g., see Oduyemi, 1986). One of the most frequently used expression is of the form

$$\frac{K_s}{K_n} = \varepsilon(1 + \beta' Ri)^{-\alpha'} \qquad (3.20)$$

where K_n and K_s are the vertical mass diffusivities for homogeneous and stratified flows, respectively, and ε, β', and α' are coefficients. Munk and Anderson (1948) estimated that $\varepsilon = 1$, $\alpha' = 1.5$, and $\beta' = 3.33$.

It is interesting to note that stratification apparently also acts to reduce the value of the turbulent transverse diffusion coefficient by

turbulence damping; however, the results presently available in this area (see, for example, Sumer, 1976) are inconsistent and are not relevant for vertical structure considerations.

When gravitational stability is considered (e.g., by Eqn. 3.20), nonlinearity between diffusive flux, F_d, and vertical concentration gradient, $C_{,z}$ (note $_{,z}$ denotes differentiation with respect to z), develops. Without regard to stabilization ($K_z = K_n$), by Fickian diffusion, the diffusive flux is linearly proportional to concentration gradient, $F_d = K_z.C_{,z}$. However, from theoretical results presented for gravitational stabilization, the turbulent mass diffusion coefficient ($K_z = K_s$) was shown to be inversely proportional to the gradient Richardson number, Ri (given by Eqn. 2.9), to a power, $\alpha' > 1$. The gradient Richardson number, of course, is directly proportional to the density gradient, $\rho_{,z}$, which is a function of the concentration gradient because bulk density is a function of sediment concentration (Eqn. 2.5). The resulting dependence of diffusion flux to concentration gradient is therefore highly nonlinear.

Figure 3-1 shows an example of the nonlinearity resulting between F_d and $C_{,z}$ using Eqn. 3.20 with Munk and Anderson values for stability coefficients (i.e., $\varepsilon = 1$, $\alpha' = 1.5$, and $\beta' = 3.33$). For this case the flux initially increases with $C_{,z}$ reaches a maximum and then slowly decreases. For a given flux below the maximum two values of $C_{,z}$ (corresponding to the two roots) satisfy the equation. In the absence of settling, discontinuities in concentration profile (two distinct $C_{,z}$'s) are theoretically possible (because $F_{d,z} = 0$) and relatively stable as long as F_d is constant with time (e.g., near the bed during steady

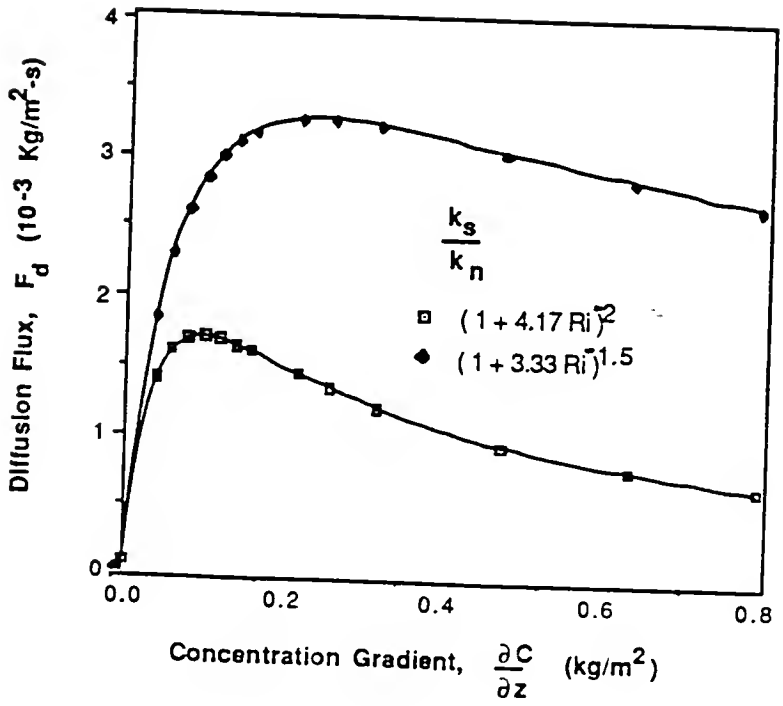

Figure 3-1. Diffusion Flux vs. Concentration Gradient

erosion). For salinity concentrations in estuarine environments, this has been pointed out to be a likely cause of salinity finestructure (Postmentier, 1977). For suspended fine sediment, the nonlinearity in diffusion flux, F_d, (with $C_{,z}$) has the effect of promoting lutocline growth and stability--in addition to the nonlinearity between settling flux, F_s, and concentration, C (pointed out in Section 2.4.2). The settling properties of estuarine fine sediment is presented in the following section (3.4).

3.4 Settling

The predominant distinction between fine sediment suspensions and other density altering constituents (e.g., salt, temperature, etc.) is

that suspended sediment is negatively buoyant and settles independent of the suspending fluid which surrounds it. This counteracts mixing to the extent that under quiescent conditions partial or total clarification is possible only to be later well mixed again under high flow conditions.

While the settling characteristics of non-cohesive sediments (e.g., sand) are reasonably well behaved, i.e., not so strongly dependent on concentration, salinity, etc., cohesive sediments are very sensitive to these variables.

It is convenient to start by discussing the settling characteristics of individual particles and work into high concentration (>20,000 mg/l) settling suspensions.

3.4.1 Free Settling

Free settling was defined in Chapter 2 as the concentration range over which individual settling sediment particles (both dispersed primary particles and aggregates) do not physically interfere with one another. For cohesive sediments, the upper concentration limit is in the range of 300-500 mg/l (Krone, 1962) but for non-cohesive sediments it is one to two orders-of-magnitude higher (McNown and Lin, 1952).

Individual sediment particles settle at a terminal fall velocity which results in a force balance between form and skin friction (viscous) drag and net negative buoyancy. For a spherical particle of diameter, d, settling in a viscous fluid with kinematic viscosity, ν, the settling velocity, w_s, is

$$w_s = \left\{ \frac{4}{3} \frac{gd}{C_D} \frac{(\rho_s - \rho_w)}{\rho_w} \right\}^{\frac{1}{2}} \qquad (3.21)$$

where g is the acceleration of gravity, C_D is the drag coefficient and ρ_s and ρ_w are the sediment and fluid densities, respectively. The coefficient of drag, C_D, is a function of the Reynolds' number of the sphere ($R = w_s d/\nu$), but cannot be determined analytically for $R > 1$ (see, for example, Vanoni, 1975).

In the viscous or Stokes' settling range ($R < 0.1$) the drag coefficient is given by $C_D = 24/R$ and the settling velocity is

$$w_s = \frac{gd^2}{18\nu} \frac{(\rho_s - \rho_w)}{\rho_w} \tag{3.22}$$

Fine estuarial sediment in dispersed or quiescent conditions typically falls well within this range. Therefore, no further discussion of the deviations from Stokes settling will be presented here with one minor exception: fine estuarine sediment is not generally spherical. In dispersed form, cohesive size sediment is plate-like with a large surface area to volume ratio (Van Olphen, 1963). This results in a higher drag coefficient and slower settling velocity than spherical sediment of the same volume. Very fine ($d < 1$ μm) dispersed sediment may not settle at all due to the increased relative importance of Brownian motion. Aggregates, although irregularly shaped, are generally more spherical (and substantially larger than dispersed primary particles). For both particles, it is typical to define an "effective" particle diameter based on measured settling velocity and specific density (ρ_s). A more thorough discussion of the effects of particle shape on settling velocity as well as other deviations from Stokes settling can be found in Vanoni (1975).

3.4.2 Flocculation Settling

In the presence of small amounts of dissolved salts (< 1 ppt NaCl) cohesive sediment in suspension can flocculate greatly, thus changing the settling properties. Flocculation of cohesive sediment particles is the consequence of inter-particle collision and cohesion. Cohesion and collision are discussed in detail by Einstein and Krone (1962), Krone (1962), Partheniades (1964), O'Malia (1972), and Hunt (1980) and reviewed by Hayter (1983).

Cohesion depends primarily on the mineral composition and the availability and charge of cations in the suspended fluid. Colloidal particles have both attractive and repulsive forces (Van Olphen, 1963). The attractive forces predominate when the coulombic repulsive forces are suppressed by sorbed cations near the particle surfaces. A measure of the relative cohesiveness of a particular colloidal sediment is the cation exchange capacity, CEC. A high CEC indicates a highly cohesive sediment. Montmorillinitic sediments have a higher CEC and thus are more cohesive than illitic or kaolinitic sediments with lower CECs.

Collision intensity and frequency are dependent on three mechanisms: Brownian motion, fluid shearing, and differential settling. Brownian motion is the natural thermal agitation of the sediment particles in the suspending medium. Particle movement from Brownian motion is erratic, the collisions are weak and the resulting flocs are "fluffy" (of relatively low density and weakly bound). This motion becomes much less apparent as the floc size grows. Brownian motion in estuaries is the least significant collision mechanism of the three (Krone, 1962). Particle collision from fluid shearing, however, becomes much more

significant as the size of the flocs grows. The result is a greater intensity of collision and stronger flocs. Differential settling becomes increasingly more important as the distribution of the size widens. Under quiescent conditions e.g., at the time of slack water, with a natural non-uniform sediment this becomes the primary collision mechanism. The frequency of all three means of collision increases with increasing concentration.

Two characteristics of flocculated sediment which differ from the dispersed form and which affect the settling velocity are particle density and shape. First, because of interstitial trapped water, the relative particle densities are reduced. This effect alone would lead to reduced settling velocity in the flocculated state. However, because of the larger size and more spherical shape, a decrease in viscous drag results. Since the reduction in drag is much more significant than the reduction in density, the settling velocity of the flocs are up to 4 orders of magnitude larger than dispersed particles (Bellessort, 1973). This can result in rapid sedimentation and shoaling in upper estuaries where flocculation (by introduction of dissolved salts) is first stimulated.

Krone (1962) reasoned that the average (median, by weight) settling velocity of flocculating Mare Island Strait (San Francisco Bay) sediment for equal flocculation time was proportional to the sediment concentration raised to the 4/3 power,

$$w_s \propto C^{4/3} \tag{3.23}$$

His reasoning was based on consideration of collision probability and average floc size. He further supported this argument with data taken in settling column and flume studies.

Burt (1986) used a general relationship for flocculation enhanced variation with concentration as

$$w_s = k_1 C^{n_1} \tag{3.24}$$

where k_1 depends on sediment composition and n_1 can vary from about 1 to 2.

3.4.3 Hindered Settling

As the concentration of sediment in suspension increases beyond the flocculation settling range, the mean sediment settling velocity begins to drop. Aggregates are so closely spaced as to form a continuous network, and the interstitial fluid is forced to escape through smaller and smaller pore spaces. This is commonly termed "hindered settling" in the literature (Mehta, 1986, Lavelle and Thacker, 1978). However, the inadequacies of this definition were pointed out in Section 2.4.2. The pioneering work of Richardson and Zaki (1954) on the settling of uniform glass spheres resulted in a widely accepted relationship for the settling velocity as a function of concentration of the form,

$$w_s = w_{so} (1 - k_2 C)^{n_2} \tag{3.25}$$

where w_{so} is the initial or reference settling velocity, k_2 is a coefficient which depends on the sediment composition and $n_2 \approx 5$. The coefficient k_2 can be considered to be the reciprocal of the hypothetical concentration where hindered settling gives way to primary, first-stage consolidation. This is typically in the neighborhood of 120-160 g/l (Mehta 1986, Einstein and Krone, 1962). For fine sand-coarse silt the reference velocity, w_{so}, is given by Stokes' Law. For cohesive flocculated sediment the reference velocity, w_{so}, is the maximum velocity of the flocculation range. Teeter (1986b) found that most natural fine bay sediments fit this relationship well.

Lavelle and Thacker (1978) used an expression of this type in steady-state analysis of the high concentration data of Einstein and Chien (1955) for coarse-grained sediment. Including a term of $(1-C)^{\alpha}$ in the Rouse (1938) equation allowing for finite and reasonable concentrations at the bed (z=0), they found success in predicting the near-bed high concentration data of Einstein and Chein (1955).

3.5 Vertical Bed Fluxes

The bed flux boundary condition for solution of Eqn. (3.5) plays a critical role in the evolution of the vertical suspension profile as the overall source and sink component of sediment mass in suspension. Bed fluxes can be either erosional or depositional. Both are discussed in the following paragraphs. It is important to point out that defining the elevation at which the erosion or deposition process takes place is, in itself, a formidable task. From a practical viewpoint, simultaneous continuous profiling of concentration, velocity and bed stresses

(pressures and shear) are required in the upper-bed to near bottom layers to define the interface elevation with time and hydrodynamic action. As was pointed out in Chapter 2, it is very important to distinguish the stationary bed material from the fluid mud layer. Additionally, erosion relationships developed for bed/mobile suspension interfaces may not be adequate for erosion and fluidization of the bed beneath a fluid mud layer. This is a possible limitation of the proposed erosion/deposition functions used in the vertical structure model and presented in the following subsections.

3.5.1. Bed Erosion

Bed erosion occurs when the resultant hydrodynamic lift and drag forces on the sediment at or below the bed interface (Z_c in Figure 2-1) exceed the resultant frictional, gravitational and physico-chemical bonding forces of the sediment grain or particle. Continuous inter-particle contact ceases and individual or groups of aggregates become resuspended.

There are two modes of erosion (Mehta, 1986), surface or particle by particle erosion and mass or bulk erosion. In surface erosion, individual particles break free of the bed surface as the hydrodynamic erosive force (i.e., instantaneous turbulent shear stress acting on the particle surface) applied to them exceeds the resultant gravitational, frictional and cohesive bed bonding force. Under mass erosion, failure occurs well below the bed surface resulting in large chunks of sediment being broken from the bed structure and, subsequently, resuspended. Bed fluidization is mass erosion where large structural breakdown occurs with

an initially minimum change in density. Surface erosion is more typical of low concentration, low energy environments while mass erosion occurs under higher flow and higher concentration conditions (Mehta, 1986).

Surface waves and other highly oscillatory currents have a particularly pronounced influence on erosion in comparison with unidirectional currents. Because of the increased inertial forces (e.g., "added mass" drag) associated with a local change in linear momentum, the net entrainment force is much greater than with turbulent unidirectional flows. Much more significant is the effect bed "shaking" and "pumping" can have under highly oscillatory flows. "Shaking" or bed vibrations occur because of the oscillatory bed shear stress which is transmitted elastically (while at the same time damped) down through the bed. "Pumping" occurs from oscillatory fluid hydrostatic pressure at the bed which, given the low permeability of cohesive sediments, can lead to internal pore pressure build up and liquefaction, similar to earthquake failure of saturated terrigenous soils (Seed, 1976). This effect can cause destruction of effective stress in larger layers depending on the bed characteristics leading to mass erosion and fluid mud formation (Alishahi and Krone, 1964; Wells et al., 1978; and Maa and Mehta, 1987). The destruction of effective stress under waves is documented, perhaps for the first time, in laboratory measurements presented in Chapter 4.

Erosion (particles leaving the bed surface) precedes scour (resulting decrease in bed elevation) which will continue under constant loading until the bed shear stress and the bed shear strength are equal. The bed shear strength is a function of the deposition and consolidation

history plus the physico-chemical characteristics of the sediment. The shear strength, in general, increases with depth into the bed.

The rate of erosion (= flux of sediment from the bed), F_e, from surface erosion is linearly related to the "excess shear" stress, $\tau_b - \tau_s$, for spatially and temporally uniform bed properties (Kandiah, 1974) as

$$F_e = \alpha_1 \left(\frac{\tau_b - \tau_s}{\tau_s}\right) \tag{3.26}$$

where α_1, is an empirical rate constant, τ_b is the applied (time-mean) bed shear stress and τ_s is the bed shear strength for erosion. For a given α_1, which is related to the type of flow and sediment characteristics, the erosion rate, F_e, is constant. For non-uniform beds (e.g., soft, partially consolidated) the rate of erosion can be found by (Parchure 1984, Parchure and Mehta, 1983).

$$F_e = \varepsilon_o \exp\{\alpha_2 [\tau_b - \tau_s(z)]^{1/2}\} \tag{3.27}$$

where ε_o and α_2 are constants (determined empirically). Since τ_s increases with depth below bed, the erosion rate, F_e, decreases as scour proceeds.

No currently unique expression exists for mass erosion since it must involve dynamic bed data (i.e., bed stresses and pressures) as well as imposed shear.

For mass erosion under waves the practice is to increase the coefficients to account for the larger magnitude erosion. Maa (1986) showed success with this procedure and demonstrated that the coefficients

were as much as an order-of-magnitude larger for wave erosion than for what has been found for the uni-directional case. Under pure wave flow condition it is difficult to distinguish bed erosion from fluid mud entrainment. Even though wave erosion has a greater ability to break the bonding forces, without high momentum diffusion or turbulent entrainment rates the fluid mud may not become mobile.

3.5.2 Deposition

Sediment particles or aggregates in suspension will redeposit on the bed if the bed shear stress drops below some critical threshold value, τ_{cd}. τ_{cd} is the shear stress below which all initially suspended sediment deposits eventually. In general, it takes lower turbulent bed shear stress to keep cohesive sediment in suspension than it does to erode it (i.e., $\tau_{bm} < \tau_s$). τ_{bm} is the shear stress above which no deposition occurs and it is generally larger than the limit for total deposition, $\tau_{bm} > \tau_{cd}$, (Mehta, 1986). This is because after deposition interparticle bonding and orientation are time-dependent, as well as dependent on consolidation mechanics (e.g., overburden, etc. as discussed briefly in Chapter 2) and the critical shear stress for erosion increases with time. For a uniform sediment $\tau_{cd} = \tau_{bm}$.

For uniform sediment, in a depositional environment (i.e., $\tau_b < \tau_{cd}$), the rate of sediment deposited (= flux of deposited sediment), F_p, on the bed is related to the average aggregate settling velocity, w_s, the near-bed concentration in suspension, C, and the relative probability, P, that the sediment will stay on the bed as

$$F_p = - w_s \, C \, P \quad , \quad \tau_b < \tau_{cd} \tag{3.28}$$

The probability, P, that the sediment will stick to the bed is related to the relative shear stress (Krone, 1962) as

$$P = (1 - \frac{\tau_b}{\tau_{cd}}) \qquad (3.29)$$

As observed, this relationship indicates no deposition when $\tau_b \geq \tau_{cd}$ and rapid settling when the bed shear goes to zero ($\tau_b = 0$). Krone (1962) and Mehta (1973) conducted deposition experiments under steady flows using natural estuarine sediments and commercial kaolinite. τ_{cd} was found to depend on sediment composition, varying from 0.04 to 0.15 N/m^2.

Mehta (1986) made the distinction for critical shear stress for deposition of non-uniform sediment. He pointed out that while deposition proceeds when $\tau_b < \tau_{bm}$, not all of the sediment in suspension deposits when $\tau_b > \tau_{cd}$. This is illustrated by the data in Figure 3-2. Mehta (1986), in reanalyzing earlier data (Mehta, 1973), pointed out that even after long periods the ratio C_{eq}/C_o of ultimate equilibrium concentration, C_{eg}, to initial concentration, C_o, was only a function of τ_b (i.e., $C_{eq}/C_o = f(\tau_b)$), not of C_o.

This, then represents a fundamental distinction between cohesive and cohesionless sediment since for cohesionless sediment the equilibrium concentration, C_{eq}, is dependent on τ_b and independent of initial concentration, C_o, (i.e., $C_{eq} = f(\tau_b)$). For cohesionless sediment, the equilibrium concentration represents a balance between the rates of erosion and deposition, whereas for cohesive sediment simultaneous erosion and deposition did not occur under test conditions relative to

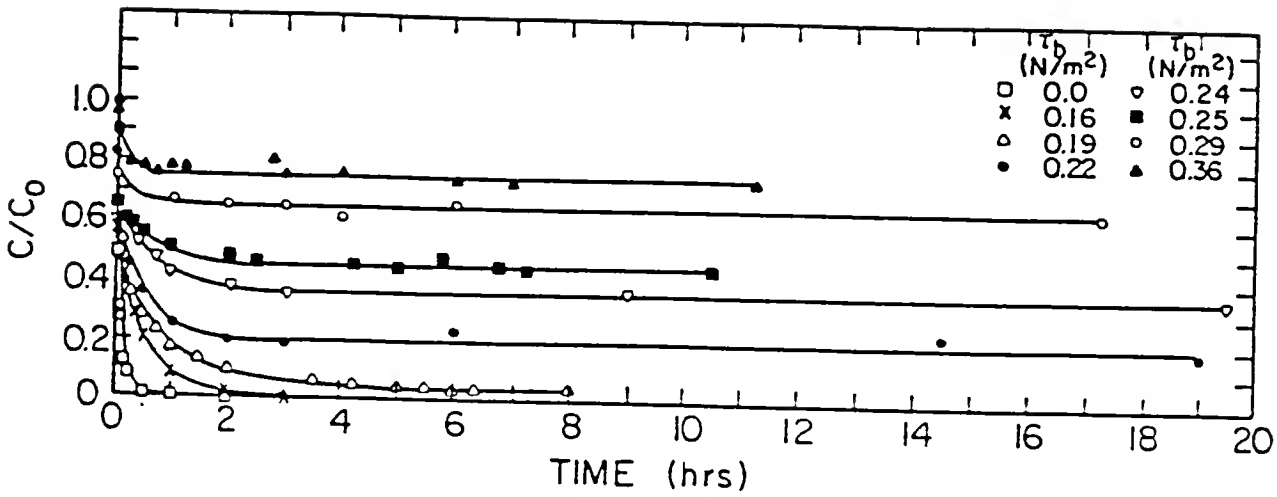

Figure 3-2. Ratio C/C_o of Instantaneous to Initial Suspended Sediment Concentration Versus Time for Kaolinite in Distilled Water (after Mehta, 1973).

Figure 3-2. Thus C_{eq}, for cohesive soils was the steady state concentration, C_{ss}. For cohesive soils, winnowing (coarser material settling out first) is a likely cause of the variable steady state ratios, C_{ss}/C_o (Mehta and Lott, 1987). Thus, the steady state concentration, C_{ss}, results in a suspension with a mean particle grain size finer than the original suspension. For modeling purposes, discretizing non-uniform suspended sediment into a finite number of classes, C_i, and treating erosion and deposition for each class separately would be one means of handling the winnowing (and resulting bed layering) phenomena. The vertical structure model considers independent settling and deposition of multiple classes of suspended

particles after it was found to be significant in settling column tests of natural bay sediment (see Section 4.3). For discretizing the non-uniformity of the deposition Eqn. 3.28 (originally developed for uniform sediment) is assumed to be valid as

$$F_{p_i} = - w_{s_i} C_i P_i \qquad , \tau_b < \tau_{cd_i} \qquad (3.30)$$

where the i subscripted variables must be defined for each class.

3.6 Fluid Mud Entrainment

Once a fluid mud layer is formed, either from high erosion or deposition rates, entrainment of this high concentration sediment suspension can occur at the upper, mobile fluid mud interface (see Figure 2-1). Entrainment is markedly distinguised from bed erosion in that the sediment is already in suspension. Fluid mud entrainment results from interfacial instabilities and dissipation of kinetic energy with, as yet, limited theoretical analysis. However, because it is believed to behave analogously to two-layer density stratified flows associated with salt or temperature gradients, a relatively larger literary and theoretical base exists for these cases (Yih, 1980).

Velocity shear at the interface accounts for the primary mixing mechanism. Unlike mixing in homogeneous or weakly stratified shear layers, strong stratification characterized by a high Richardson Number is composed of events such as interfacial wave generation and breaking, interchange of energy between waves and the mean flow, and local shear-instabilities (Narimousa and Fernando, 1987).

Kato and Phillips (1969) in laboratory experiments of entrainment of linearly stratified fluids found that the entrainment coefficient, $E_* = u_e/u_*$, where u_e is the entrainment rate (dh/dt) and u_* is the friction velocity, decreased with increasing stratification. They found an inverse relation between entrainment rates and bulk Richardson Number, $Ri_* = \Delta bh/u_*^2$ in which $\Delta b = g(\rho-\rho_o)/\rho_o$ is the buoyancy jump, ρ is the fluid density, ρ_o is a fluid reference density, g is the gravitational acceleration, and h is the average depth of mixed layer. They suggested $E_* \propto Ri_*^{-1/2}$. Other research indicates that it should be related to mean velocity, $\bar{u}$, in the mixed (i.e., upper) layer (Price, 1979; Thompson, 1979) as

$$E_v = \frac{u_e}{\bar{u}} = f(Ri_u)^{-4} \qquad (3.31)$$

where $Ri_u = \Delta bh/\bar{u}^2$.

Still other researchers (Phillips, 1977; Price, 1978; Narimousa and Fernando, 1987) showed supporting evidence for using the velocity jump, Δu, across the interface defined as the difference between the mean flow velocities in each layer. Later researchers reasoned that the major portion of the energy for turbulent mixing at the density interface results from shear production at the entrainment zone itself and, therefore, Δu is the significant velocity scale to obtain a measure of the energy dissipation rate.

Narimousa and Fernando (1987) presented a graphical depiction of the entrainment process which is qualitatively descriptive enough to warrant reproduction here.

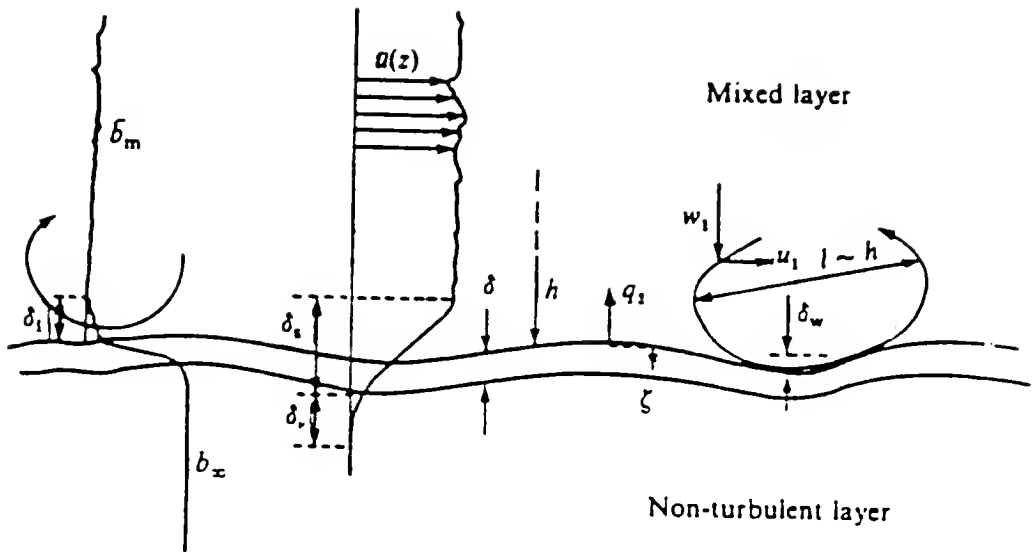

Figure 3-3. Simplified Description of Density Stratified Entrainment (after Narimousa and Fernando, 1987)

Figure 3.3 shows the entrainment process based on experimental observations (Narimousa and Fernando, 1987). The upper turbulent layer of thickness, h, is well mixed and the lower layer is initially stationary. An intermediate entrainment layer, δ, separates the two layers and is the region characterized by high energy dissipation and buoyancy gradients. In the upper entrainment layer, the mean shearing rate, $d\bar{u}(z)/dz$, increases downward reaching a maximum at δ_i, and then decreases as viscous dominant momentum diffusion penetrates deeper and deeper into the stationary layer. The shear layer thickness is shown as δ_s. The highest density gradients occur in the entrainment layer of thickness δ, which is inside the shear layer, δ_s, where turbulence dampening is sufficient to eliminate turbulent penetration into the

lowest layer. The momentum diffusion (viscous) layer, of thickness δ_v, can be dynamic (growing with time) or relatively constant with respect to the interface. Also shown are the flattening of large eddies (with turbulent velocity components u_1 and w_1) at the density interface and local scouring and internal waves of height δ_w in the intermediate entrainment layer by the mixed layer eddies of mixing length scale, l (proportional to the mixed layer depth, h).

As can be deduced from the number of characteristics in the above description, entrainment of density stratified flows of single phase fluids is, in itself, an interesting and challenging field. Add to this, particle settling associated with the two-phase sediment/fluid mixture and one can see that fluid mud entrainment deserves fundamental research. No effort has been made to distinguish fluid mud entrainment from general lutocline mixing in this research. Nevertheless, despite this limitation, reasonable success has been achieved in explaining the observed physical behavior of prototype and field vertical profiles, as shown in Chapter 5. Further research in fluid mud interfacial entrainment is required before a more refined understanding and usable results are obtained.

3.7 Horizontal Fluid Mud Transport

Several approaches to solving for the horizontal transport of mobile fluid mud and the relative thickness of the mobile layer are available. These approaches are based on different simplifying assumptions concerning the rheological and temporal behavior of the fluid/sediment system. The solution approximations (for velocity profile in the fluid

mud layer) together with limitations are presented in order of increasing complexity, beginning with the analytical solution of viscous boundary layer development under an imposed shear stress. The following titles are given for solution approaches:

A. Constant Viscosity Rayleigh Flow

B. Constant Viscosity Unsteady Bingham Flow

C. Variable Viscosity Steady Bingham Flow

D. Variable Viscosity Rayleigh Flow

E. Variable Viscosity Unsteady Bingham Flow

Applicable solution techniques were applied to field and laboratory data, the results of which are presented in Chapter 5.

The constitutive equations which govern fluid mud transport are the conservation of momentum (Cauchy's Equation) and mass (continuity) equations. The Cauchy Equation of motion written in tensor notation is (Malvern, 1969)

$$\rho \frac{du}{dt} = \rho b + \nabla \cdot T \tag{3.31}$$

where ρ is the local fluid density u is the velocity vector, b is the body force per unit mass vector, T is the stress tensor, and ∇ is the vector operator. The first term in Eqn. (3.31) is the time rate of change of momentum per unit volume. The other terms are the body force per unit volume and stress tensor gradient, respectively.

For an incompressible viscous fluid, the conservation of horizontal momentum equation in Cartesian coordinates is

$$\rho \frac{du}{dt} = - \frac{\partial P}{\partial x} + \frac{\partial}{\partial z}\{\mu \frac{\partial u}{\partial z}\} + \frac{\partial}{\partial y}\{\mu \frac{\partial u}{\partial y}\} \qquad (3.32a)$$

where P is the pressure. The dynamic viscosity, μ, is assumed here to be isotropic but, in general, a function of concentration, $\mu=\mu(C)$. Together with the continuity equation,

$$\frac{\partial u}{\partial x} + \frac{\partial v}{\partial y} + \frac{\partial w}{\partial z} = 0 \qquad (3.32b)$$

sufficient boundary and initial conditions (outlined below), the problem is said to be closed and formally defined.

For a tractable solution to the horizontal flow problem, somewhat far reaching assumptions must be made. First, one-dimensional horizontal flow in the x direction is assumed (no v and w components in the velocity vector). Next, the assumption of lateral uniformity is made. Then, by continuity, the horizontal velocity component must only vary in the z direction, $u = u(z,t)$. The third assumption is by far the most stringent. It is assumed, analogous to the laminar sub-layer next to a boundary (Schlichting, 1979) and the shear layer in a stratified fluid (Narimousa and Fernando, 1987), that the horizontal pressure gradient is much smaller than the vertical shear stress gradient,

$$\frac{\partial P}{\partial x} << \frac{\partial \tau_{xz}}{\partial z} \qquad (3.33a)$$

To more formally show the conditions under which this assumption is valid, scaling arguments are used to evaluate the relative magnitude of

the terms of Eqn. 3.32a for dynamic momentum diffusion into the fluid mud layer. First, defining non-dimensional (primed) variables as

$$t' = \frac{t}{t_o} \quad , \quad u' = \frac{u}{u_o} \quad , \quad x' = \frac{x}{L} \quad , \quad z' = \frac{z}{\delta} \, ,$$

$$P' = \frac{P}{\gamma H} \quad , \quad \rho' = \frac{\rho}{\rho_o} \quad , \quad \mu' = \frac{\mu}{\nu_o} \tag{3.33b}$$

where t_o and u_o are the characteristic maximum time and velocity, L is the length scale of the estuary, δ is the length scale of the fluid mud layer depth, H is the differential height of the water surface over L, γ is the specific weight of mud, ρ_o and μ_o are the characteristic mud density and dynamic viscosity. Substituting the above variables in Eqn. 3.32a and considering only vertical shear gives

$$[\frac{u_o}{t_o}] \frac{du'}{dt'} = -[\frac{\gamma H}{\rho_o L}] \frac{1}{\rho'} \frac{\partial P'}{\partial x'} + [\frac{\mu_o u_o}{\rho_o \delta^2}] \frac{1}{\rho'} \frac{\partial}{\partial z'} \{\mu' \frac{\partial u'}{\partial z'}\} \tag{3.32c}$$

where all terms not in brackets, [ ], are order 1. Multiplying Eqn. 3.33c through by $[\frac{t_o}{u_o}]$ gives,

$$[1] \frac{du'}{dt'} = -[\frac{gHt_o}{L\, u_o}] \frac{1}{\rho'} \frac{\partial P'}{\partial x'} + [\frac{t_o \mu_o}{\rho_o \delta^2}] \frac{1}{\rho'} \frac{\partial}{\partial z'} \{\mu' \frac{\partial u'}{\partial z'}\} \tag{3.32d}$$

Substituting typical numerical values for fluid mud layers in estuaries of $g = 10^1$ m/s^2, $H = 10^0$ m, $t_o = 10^3$ s, $L = 10^5$ m, $u_o = 10^0$ m/s, $\nu_o = \mu_o/\rho_o = 10^{-4}$ m^2/s, and $\delta = 10^{-1}$ m, the order of magnitude of the pressure gradient term is

$$\left[\frac{(10^{1}\ \mathrm{m/s^{2}})(10^{0}\ \mathrm{m})(10^{3}\ \mathrm{s})}{(10^{5}\ \mathrm{m})(10^{0}\ \mathrm{m/s})} \right] = [10^{-1}] \qquad (3.33d)$$

The viscous shear term is

$$\left[\frac{(10^{-4}\ \mathrm{m^{2}/s})(10^{3}\ \mathrm{s})}{(10^{-1}\ \mathrm{m})^{2}} \right] = [10^{1}] \qquad (3.33e)$$

which, for the particular set of conditions, is two orders of magnitude greater than the pressure gradient magnitude. Hence, neglecting horizontal pressure gradients in Eqn 3.32a for qualitative understanding of the dynamic momentum diffusion depth is justified, albeit weakly. It must be emphasized that under fully developed steady flow, the order of magnitude of the viscous shear stress and horizontal pressure gradient terms are the same (since they are the only two non-zero terms in the equation).

Under the above constraints the momentum equation becomes

$$\frac{\partial u}{\partial t} = -\frac{1}{\rho}\frac{\partial}{\partial z}\left(\mu\frac{\partial u}{\partial z}\right) \qquad (3.34)$$

The equation is now in a form in which analytical and simple numerical solutions are possible with careful specification of initial and boundary conditions and rheological behavior.

A. Constant Viscosity Rayleigh Flow. For the case of constant mud viscosity, μ_m, and unsteady shear flow, an analytical solution proposed by Stokes (see Schlichting, 1979) is appropriate. With the boundary conditions, 1) imposed velocity, U, at the upper interface $u(z)=U$ @ $z=Z_a$ (in Figure 2-1), and 2) $U(z)=0$ @ $z\to\infty$. The solution for the horizontal flow velocity is (Eskinazi, 1968)

$$u = U\,(1 - \mathrm{erfc}\delta_s) \tag{3.35}$$

where δ_s is the similarity variable $z/2\sqrt{\nu t}$ and erfc is the complementary error function defined as

$$\mathrm{erfc}\delta_s = 1 - \frac{2}{\sqrt{\pi}}\int_0^{\delta_s} e^{-\eta^2}d\eta \tag{3.36}$$

The penetration depth of the mobile fluid mud layer (Z_b defined in Figure 2-1) can be found by considering the boundary layer thickness, defined by $u/U = 0.01$ which is

$$\delta = 3.64\sqrt{\nu t} \tag{3.37}$$

The inadequacy of this solution is that even for viscosities ten times higher than water (i.e., 10^{-5} m^2/s), the predicted boundary layer thickness over several hours is too large; e.g.,

$$\delta = O\{3.64(10^{-5}.10^4)^{1/2}\} = O(3.64\ m) \tag{3.38}$$

Additionally, the approach does not adequately represent the rapid depth variation in concentration (i.e., increasing concentration with depth) of the fluid mud.

B. Constant Viscosity Unsteady Bingham Flow. For the steady state flow of a Bingham plastic with constant viscosity (and constant yield strength), an analytic similarity solution has been presented by Phan-Thien (1983). He assumed a two layer system with properties as

$$\tau = \begin{cases} \mu_1 \dot{y} \ , & |\tau| \geq \tau_y \\ \mu_2 \dot{y} \ , & |\tau| \leq \tau_y \end{cases} \tag{3.39}$$

where $\dot{y}$ is the time rate of shearing, $\frac{\partial u}{\partial z}$, and τ_y is the Bingham yield strength. Denoting the velocities in layer i (i=1,2) as

$$u_i(z,t) = \frac{\tau_o}{\mu_i} 2\sqrt{\nu_i t}\ U_i(\delta_s) \tag{3.40}$$

where τ_o is the imposed shear stress, ν_i, μ_i are the kinematic and dynamic viscosities and δ_s is the similarity variable.

$$\delta_s = \frac{z}{2\sqrt{\nu_i t}} \tag{3.41}$$

$U_i(\delta_s)$ is the similarity solution of Eqn. 3.34 given as

$$U_1(\delta_s) = \delta_s - (1-R_\tau)\left\{ \frac{\left[\delta_s \int_0^{\delta_s} e^{-z^2} dz + \frac{1}{2} e^{-\delta_s^2}\right]}{\int_0^{\delta_c} e^{-z^2} dz} \right\} \tag{3.42}$$

and

$$U_2(\delta_s) = R_\tau\{\delta_s - \frac{[\delta_s\int_{\delta_c'}^{\delta_s'} e^{-z^2}\,dz + \frac{1}{2}\,e^{-\delta_s'^2}]}{\int_{\delta_c'}^{\infty} e^{-z^2}\,dz}\} \qquad (3.43)$$

where $\delta_c = z_c(t)/2\sqrt{\nu_i t}$, $\alpha_\delta = \mu_2/\mu_1$ ($\alpha_\delta \to \infty$ for an ideal Bingham fluid), $\delta_s' = \delta_s/\sqrt{\alpha_\delta}$, $\delta_c' = \delta_c/\sqrt{\alpha_\delta}$, and $R_\tau = \tau_y/\tau_o$. Additionally, since the velocity field is continuous at $z = z_c(t)$ and is represented as

$$U_2(\delta_c) = \alpha_\delta\, U_1(\delta_c) \qquad (3.44)$$

a value for δ_c is determinable and consequently for $z_c(t)$. But, unfortunately, the inability to treat concentration variation with depth as was the case in approach A is still undesirable.

C. Variable Viscosity Steady Bingham Flow. Neglecting the obvious error involved with omission of the pressure gradient term, for the steady flow from applied shear stress of an ideal Bingham plastic with concentration dependent yield strength and viscosity, the constitutive equation is

$$\begin{aligned} \tau_o &= \mu(z)\,\dot{\gamma} && \tau_o \geq \tau_y \\ \dot{\gamma} &= 0,\ u(z)=0\ , && \tau_o < \tau_y \end{aligned} \qquad (3.45)$$

In the region where the yield strength is exceeded, the flow velocity is analogous to Couette flow with depth varying viscosity. For the region

where the shear strength exceeds the applied shear stress, no motion occurs (the mud behaves as a solid).

For a solution to Eqn. 3.34 for this case, a concentration relationship for the viscosity and yield strength must be specified. For example, one approximation for the viscosity/concentration relationship, based on data presented in Chapter 2 (see Figure 2-6), is of the form

$$\mu(C) = \mu_w(1 + \beta_\mu C)^{\alpha_\mu} \tag{3.46}$$

where μ_w is the viscosity of the suspending fluid (water), and β_μ and α_μ are empirical constants.

A power law expression for yield strength, τ_y, (also presented in Chapter 2, Figure 2-7) is

$$\tau_y = \beta_y C^{\alpha_y} \tag{3.47}$$

where β_y and α_y are empirical constants.

The boundary conditions are 1) an imposed shear stress at the upper interface, $\tau = \tau_o$ @ $z = Z_a$, and 2) no-slip at the lower yield elevation, $u = 0$ @ $z = Z_b$.

Additionally, for steady flow the depth varying shear stress, $\tau_y(z)$, is everywhere equal to the imposed interfacial shear stress, τ_o, down to the stationary interface, z_b, where $\tau_y = \tau_o$.

This approach has been presented for comparison only since the aforementioned error would be appreciable under quasi-steady flows in estuaries. The absence of time-dependence is also a drawback to this

approach. Depending on the depth of the fluid mud layer and the imposed shear stress, the velocity profile can take minutes to hours to reach steady state form. For imposed shear which is continuously changing, as is the case in tidal flows, steady flow is never reached.

The last two approaches offer the most promise in providing for realistic spatial and temporal variability of horizontal momentum diffusion into a fluid mud layer.

D. Variable Viscosity Rayleigh Flow. This approach describes unsteady flow of a fluid mud layer with depth varying viscosity initially subjected to horizontal motion at the upper interface, Z_a. The governing equation is still Eqn. (3.34) but no specification is made regarding the overall lower extent of the boundary layer, δ_{fm}. In general, a numerical solution is warranted. An explicit, finite difference approximation (with j time and i direction index), for example,

$$u_i^{j+1} = u_i^j + \frac{\Delta t}{\Delta z^2}\frac{1}{\rho_i}\{\bar{\mu}_i(u_{i+1}^j - u_i^j) - \bar{\mu}_{i-1}(u_i^j - u_{i-1}^j)\} \qquad (3.48)$$

where $\bar{\mu}_i = (\mu_{i+1} + \mu_i)/2$, gives an easily obtainable solution path. The boundary conditions are those given in A. Additionally, proper concerns for numerical stability and convergence must be addressed (i.e., $\Delta t \leq \Delta z^2\rho/2\mu_{max}$).

The last approach offers the most realistic simulation of rheological and temporal variability of the approaches presented thus far.

E. Variable Viscosity Unsteady Bingham Flow. A numerical solution of a form similar to Eqn. 3.48 above is employed for the region where the

mud is sheared. Additionally, the lower interface is tracked by considering the temporal response of the shear stress and yield strength at each layer. This is written

$$u(z) = \begin{cases} \text{Eqn. (3.48)} & \text{for} \quad \tau(z,t) \geq \tau_y(C,t) \\ 0 & \text{for} \quad \tau(z,t) < \tau_y(C,t) \end{cases} \tag{3.49}$$

The boundary conditions are the same as those of C. Comments concerning the numerical technique, stability and convergence mentioned in D, also apply for the shear layer here.

With regard to Bingham plastic vs. Newtonian fluid (with viscosity which varies with concentration) behavior, the data in Figure 2-7 suggest yield strengths which are sufficiently large to preclude flow under mild bed shear stress (e.g., C = 100 g/l corresponds to τ_y = 0.1 N/m^2). However, field and laboratory data used to verify the above approaches in Chapter 5 (Section 5.5) show evidence of relatively high flows under very mild imposed shear stress. For this reason, care must be taken in application of the above approaches using a functional relationship for yield strength such as Eqn. 3.47, that the empirical coefficients α_y and β_y fit a particular sediment behavior. It is suggested that non-Newtonian pseudo-plastic behavior (where viscosity is a function of shear rate) may be a more reasonable model than Bingham plastic for fluid mud flows. However, no further supporting arguments or discussion are made in this report since application of the Newtonian models showed reasonable results.

CHAPTER 4
LABORATORY EXPERIMENTS

4.1 Introduction

Laboratory experiments were conducted at the University of Florida's Coastal Engineering Laboratory. These experiments consisted of two flume tests and settling column tests. The flume tests were designed to evaluate the dynamical effects of wave action on a partially consolidated natural estuarine sediment bed. Bed erosion (by fluidization) and upper column suspension concentrations were measured. Settling tests were performed to obtain the concentration dependent settling properties of natural flocculating fine sediment. New settling column tests were devised to provide development and verification data needed for the vertical profile model.

4.2 Flume Study

4.2.1 Objectives

The objectives of the wave flume study were as follows:

1. To use advanced pressure sensor instrumentation to measure and document the effective stress breakdown (fluidization) in a partially consolidated cohesive bed subjected to wave loading.
2. To observe, record and determine factors characterizing fluid mud formation and stability (during wave erosion) presented in Chapters 2 and 3.

3. To measure wave resuspension concentrations related to hydrodynamical data (i.e., wave height, water depth, fluid mud and bed thickness) for the purpose of verification of the descriptive vertical transport model.
4. Investigate the role of wave resuspension in the overall sediment transport process in the prototype setting.

4.2.2 Mud Characterization

The estuarine sediment selected for use in the flume and settling column studies was mud from Tampa Bay, Florida. Collection was from a site adjacent to a Hillsborough Bay navigation channel. It was predetermined by a bay mapping study (City of Tampa, 1986) to be an area of predominately fine sediment (clay and fine silt) and relatively high sedimentation rates (0.3-1 m/year). Grain size distribution of dispersed free particles, obtained by standard ASTM hydrometer method, is shown in Figure 4-1. It can be seen that d_{50} = 2.6 μm, which indicates that ≈ 50% of the sediment sample was finer than the upper limit of clay size particles (2 μm). Furthermore, less than 10% by weight of the sediment sample was coarse silt to fine sand.

The flocculated sediment was pumped into 55 gallon drums in the field then to washing and storage tanks in the laboratory. The sediment was then mixed and decanted several times to equilibrate with tap water until a slight background salinity (1 ppt) remained. Details of this procedure can be found in Cervantes (1987). The slight salinity was sufficient to maintain the flocculated state of the cohesive (< 20μm) particles. Characterization tests were conducted at the University of

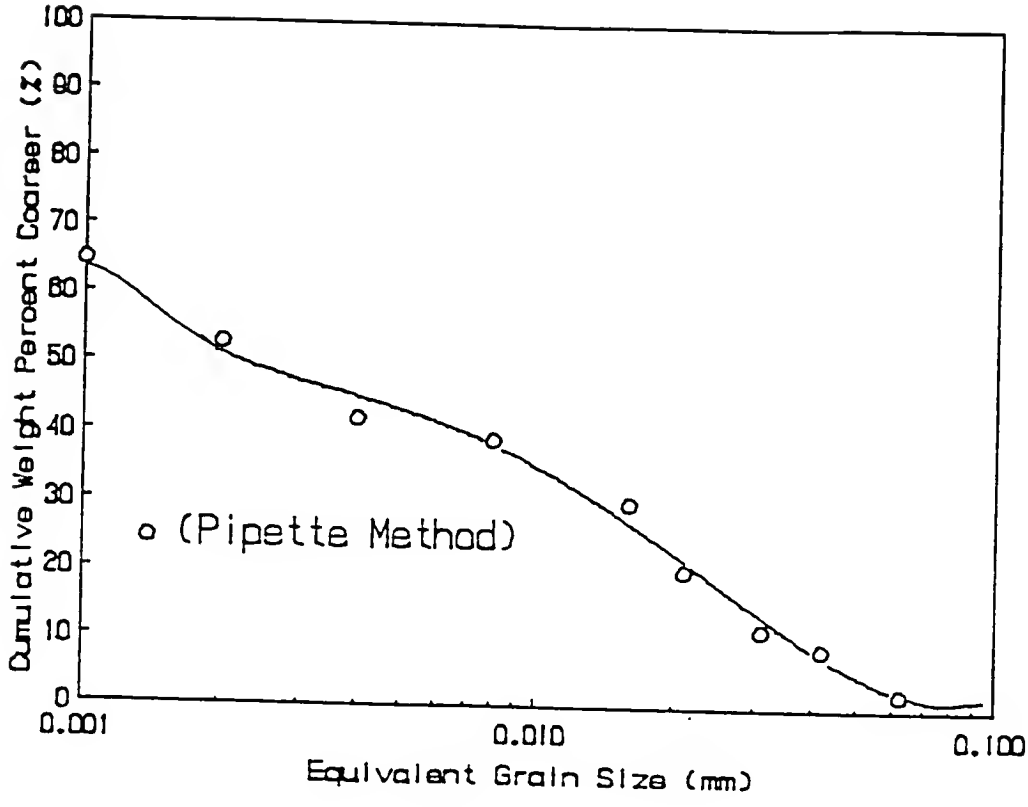

Figure 4-1. Grain Size Distribution of Hillsborough Bay Mud

Florida Soils Science Laboratory. X-Ray diffraction revealed that the clay size fraction was primarily made up of montmorillinite (91%) and very small amounts of kaolinite (4%) and quartz (5%). A cation exchange capacity (CEC) test reported 197.2 meq/100g (an unrealistic and suspected erroneously high value). Percent organic carbon content, determined by standard combustion technique (e.g., ASTM 500°C incineration) indicated that ≈ 5% by weight of the sediment sample was of detrital (organic) origin. Chemical composition of the fluid (tap water) can be found in Dixit (1982).

4.2.3 Equipment, Facilities and Techniques

Facilities. The flume was a 20 m long plexiglass tank fitted with a plunging type wavemaker at one end and a sloping beach at the other. The width and depth dimensions were 48.5 cm and 45 cm, respectively. The mud bed section was 8 m long with sloping sides to contain the mud during consolidation. The wave maker had a variable stroke from 5-20 cm and a variable period down to 0.8 seconds. Cervantes (1987) has presented a detailed description of the laboratory equipment and procedures used for the specific purpose of wave resuspension measurements. Figures 4-2a and 4-2b show the flume configuration for the two tests. The sediment trough slopes were reduced for the second test to help minimize boundary effects associated with a steep drop in depth (wave reflection and vortex generation). Vertical concentration profiles were taken at five locations labeled A-E. Supplemental data were collected to quantify hydrodynamic parameters, bed response to wave forces, and data pertinent to the temporal behavior and/or ultimate equilibrium form of the vertical suspension profile. These are described in detail in the following paragraphs.

Data Acquisition. Intensive simultaneous data collection of spatial and temporal variability of suspended sediment concentration, bed profile and density changes, flow and bed kinematics, bed dynamics including pore and total pressure profiling, spatial variability in wave height and length, and water temperatures down to the time scale of the wave period required sensitive data acquisition hardware and software. A sixteen channel Metrabyte DASH-16 analog to digital interface card installed in

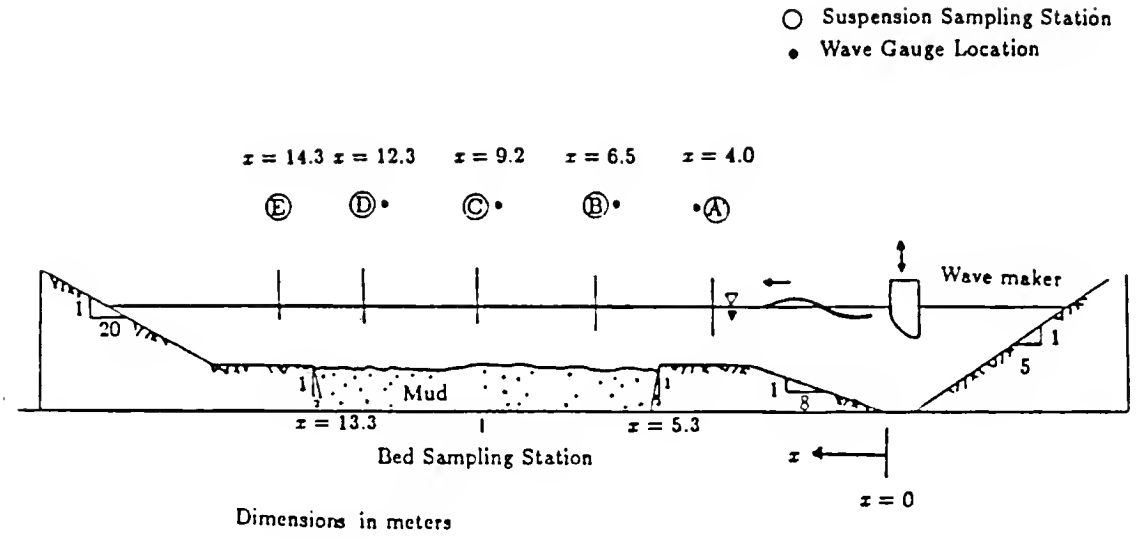

a. Run 1

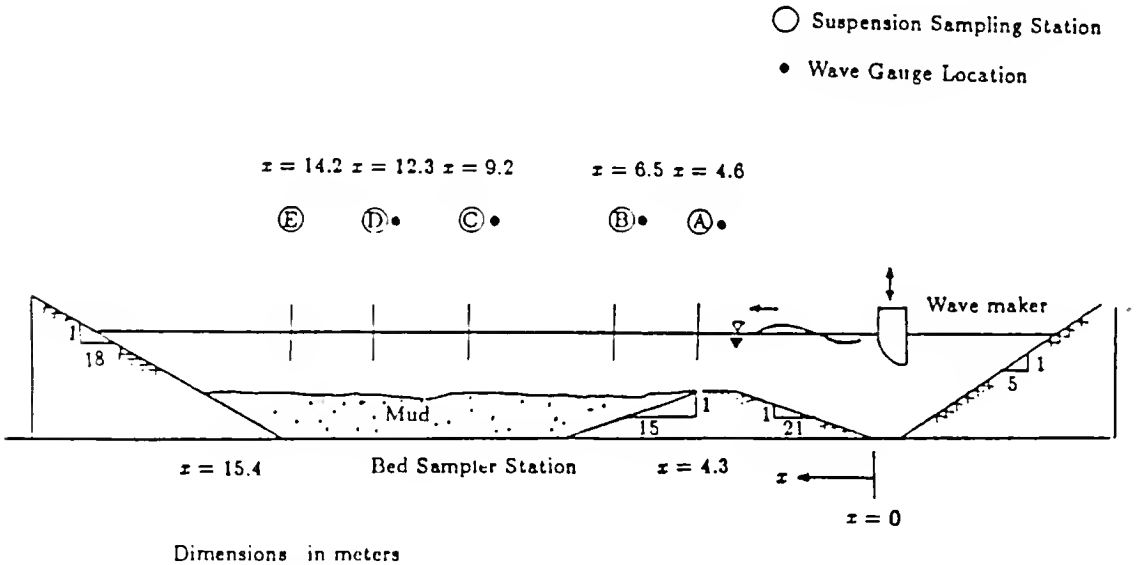

b. Run 2

Figure 4-2. Flume Configuration

an IBM personal computer (512k RAM) with interstitial R/C low pass filters met the requirement in an economical fashion. Maa (1986) has given details of the data acquisition system. For wave periods of one second, software was developed to read analog signals from the 16 channels every fifteen minutes for 30 second durations at a 20Hz frequency. For a ten hour laboratory test, this required more than 393,600 data points to be analyzed per run. Numerical filtering described by Kassab (1984) was used to minimize noise passed through the R/C hardware filter and to determine wave mean and rms amplitude values for each channel monitored. Pertinent data from the two flume studies are included in a reduced form in Appendix B.

Velocities. Horizontal and vertical velocities at three elevations (2, 6, 10 cm) above the bed were obtained with a Marsh McBirney (model 523) electromagnetic current meter. The meter was previously calibrated for time constant and system coefficient for oscillatory flow by Maa (1986). Care was taken to keep the transducer sufficiently far ($\approx$ 4 cm) from the mud bed, water surface and other instruments to prevent density interface and electromagnetic feedbacks from distorting the data.

Bed Pressures. Bed total and pore pressures were measured at various elevations below the mud surface so that effective stresses and bed elevation could be quantified. Pore pressures were measured with Druck model PDCR81 miniature pore pressure gauges with saturated ceramic stones with maximum pore diameters of 1 μm. The pore pressure gauges had a 15 mv per psi output voltage operation range. This was too low for the set range of the data acquisition system (±2.5 v). So, the gauges were fitted with specially designed 100x signal amplifiers. Total pressures

were measured at the same elevation as the pore pressure gauges using Druck model PDCR135/A/F total pressure gauges. These gauges come with built-in amplifiers and have a 1 v per psi operation range. The eight pressure sensors were installed 2, 4, 6, and 8 cm below the visual bed elevation at the start of each test. Because of installation and temperature sensitivity (nominally 0.1% full scale output per $^{o}_{c}$) calibration was obtained before and after each test in the tank using a slide-in plexiglass partition developed specifically for this purpose. The gauges were also checked before and after the tests in a calibration cylinder which contained depth variable distilled water graded with a 0.5 mm elevation scale. This allowed measurement of pressure sensitivities (in the 1 psi amplitude range) of 0.001 psi. An example of total and pore pressure gauge calibration curves is shown in Figure 4-3a and 4-3b. Due to the wide variability in offset voltages of the PDCR81 gauges, output (bit) adjustments are required in the linear regression calibration. For example, the zero offset for gauge 6 was 1000 bits higher than the desired range of (± 100 bits ~ 0.0 Pa).

Bed Densities. Bed elevations and densities were taken at selected locations and time intervals during the course of each test. Volumetric samples of 2 cm^3 were withdrawn at elevations 2, 4, 6, 8, 10 and 12 cm above the rigid bed adjacent to but sufficiently far as to not interfere with the pressure gauges using a hypodermic syringe. The dry densities (mass of sediment per volume of suspension) were obtained gravimetrically using procedures described by Lott (1986) and Yeh (1979). Bed elevations were measured to the nearest millimeter visually at 1 m intervals along the flume after variable time intervals (e.g., 0,5,15,30,60,...minutes).

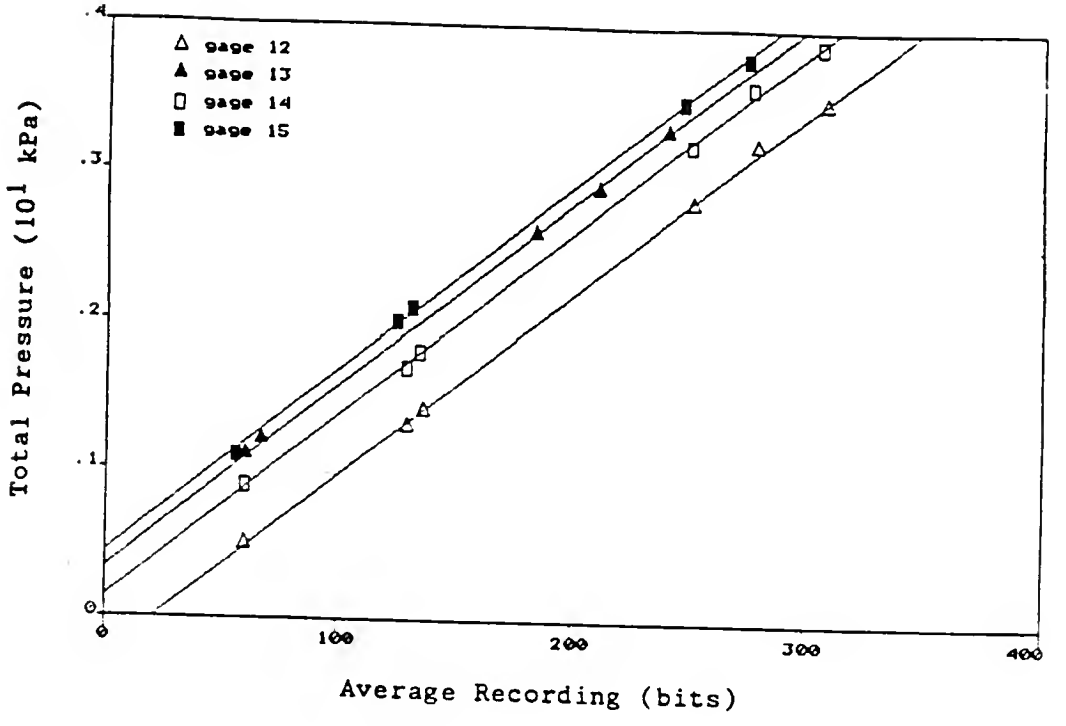

a. Total Pressure Gages

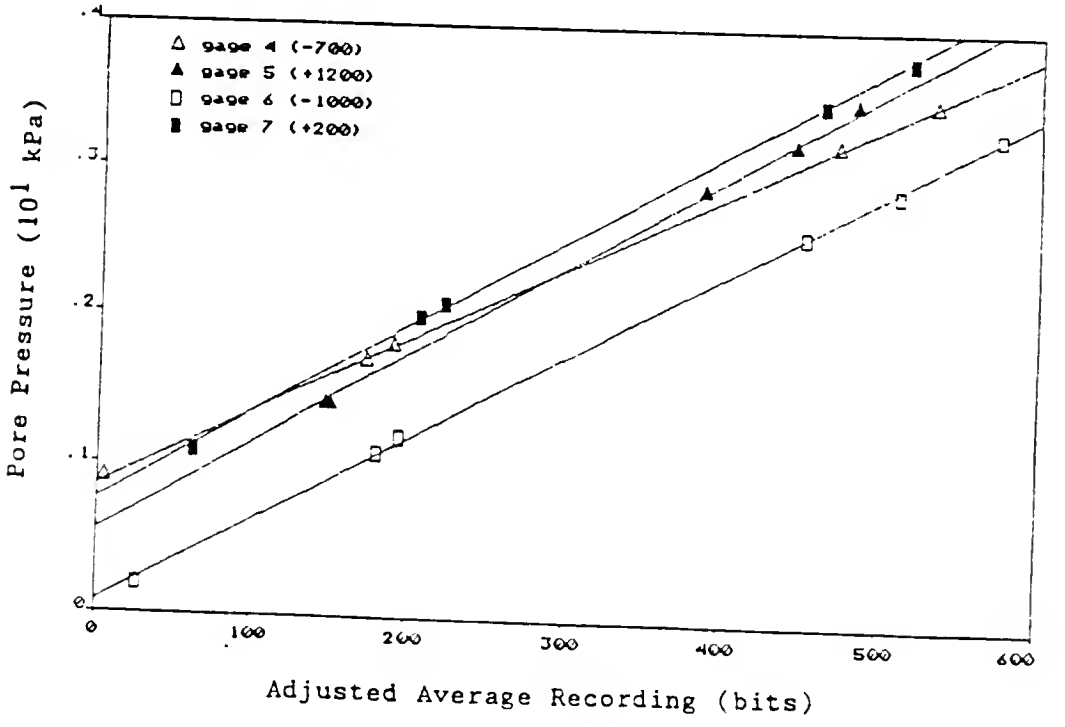

b. Pore Pressure Gages

Figure 4-3. Example of Pressure Gage Calibration

Wave Heights. Wave heights along the flume were recorded by a series of capacitance type wave gages. Calibration was conducted in the wave tank by variable height mounting brackets. Elevations were adjusted and correlated to output voltage. An example of a wave gauge calibration curve is shown below in Figure 4-4. One millimeter sensitivities were easily obtained.

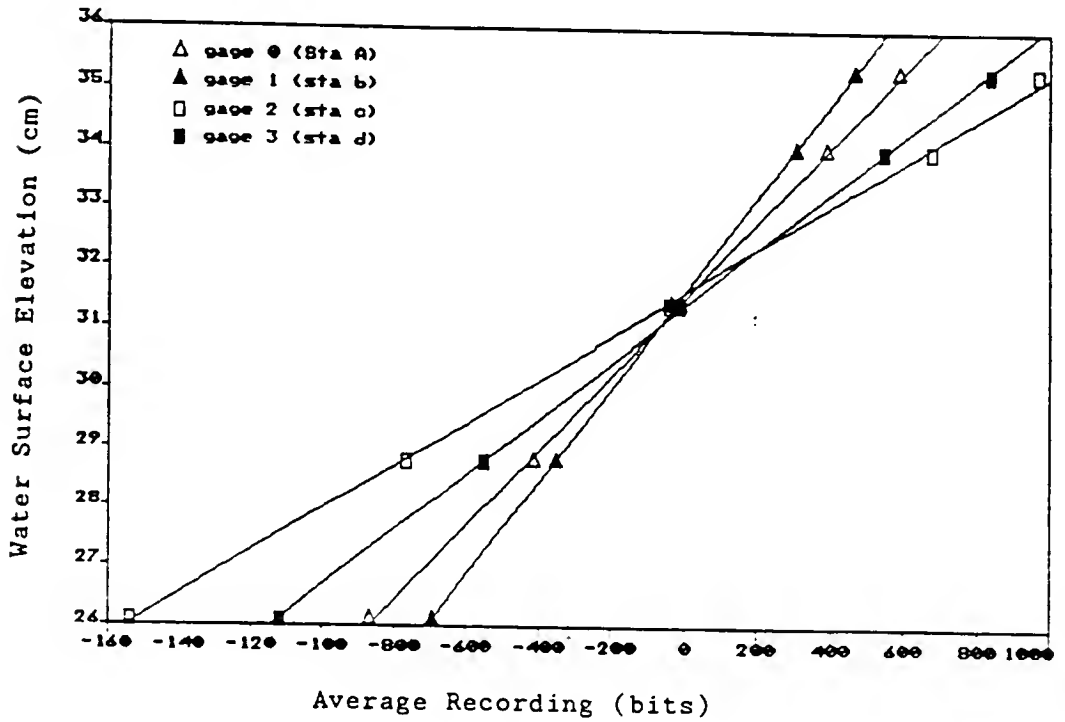

Figure 4-4. Example of Wave Gage Calibration

Suspension Concentrations. Wave averaged suspended sediment concentrations were taken using concentration samplers aligned with the flow. The concentration samplers consisted of five small (4mm diameter) copper tubes mounted vertically from which siphon samples were collected at various elevations above the rigid bed. Figure 4-5 shows a

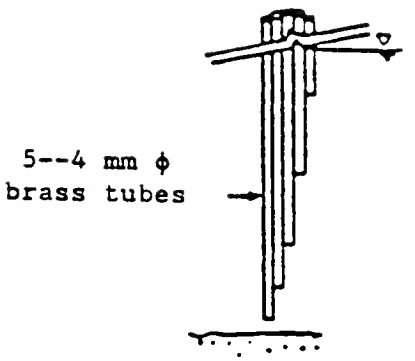

Figure 4-5. Suspended Sediment Siphon Sampler

typical configuration. Intake and tube velocities were 20-40 cm/s. Five stations along the flume (labeled A, B, C, D, E in Figures 4-2a and 4-2b) and five elevations (in Figure 4-5) provided adequate detail of total suspended sediment concentration. Samples were analyzed gravimetrically using Millipore vacuum filtration apparatus, 0.45 μm filters, 50 °C drying oven, and Metler precision (0.0001 g) balance (Yeh, 1979). Sample volumes were 50 ml which provided a 0.002g/l measurement accuracy.

4.2.4 Summary of Test Conditions

The flume configuration for Runs 1 and 2 were shown in Figures 4-2a and b. A summary of test conditions for Runs 1 and 2 can be found in Appendix B Table A-1.1 and A.2.1, respectively, For Run 1, the average

wave height, H, was 6.1 cm, period, T, was 1 sec., average water depth, h, was 31.4 cm and mud thickness, b, was 11.8 cm. The water temperature was 23 °C.

For Run 2, the water depth, h, was 31.7 cm, wave period and height, T and H, were 0.95 sec and 7.1 cm, respectively. The average mud thickness above the rigid bed was 13.0 cm. The flume water temperature was 21 °C.

4.2.5 Results

Bed. Figures 4-6a through 4-7d show wave averaged bed pressures recorded during the first and second runs at various times. The reference hydrostatic (dotted) line is obtained by integrating the density profile of the fluid, increased by suspended sediment, from the water surface down to the "visual" bed interface (the lowest observable lutocline, Z_{al}, in Figure 2-1) and assuming constant density (pore fluid) further downward to the rigid bed. This would be the pore pressure if the bed were composed of coarse porous material. The reference total pressure (dashed) line represents the integrated bulk density, $\rho_b(z)$, (see Eqn. 2.5) from z=0 (water surface) down to some elevation, z, as

$$P(z) = \int_z^0 \rho(z) g dz \qquad (4.1)$$

where g is the acceleration constant. It is seen that the pressure measured by the total pressure gauges adequately represents this line.

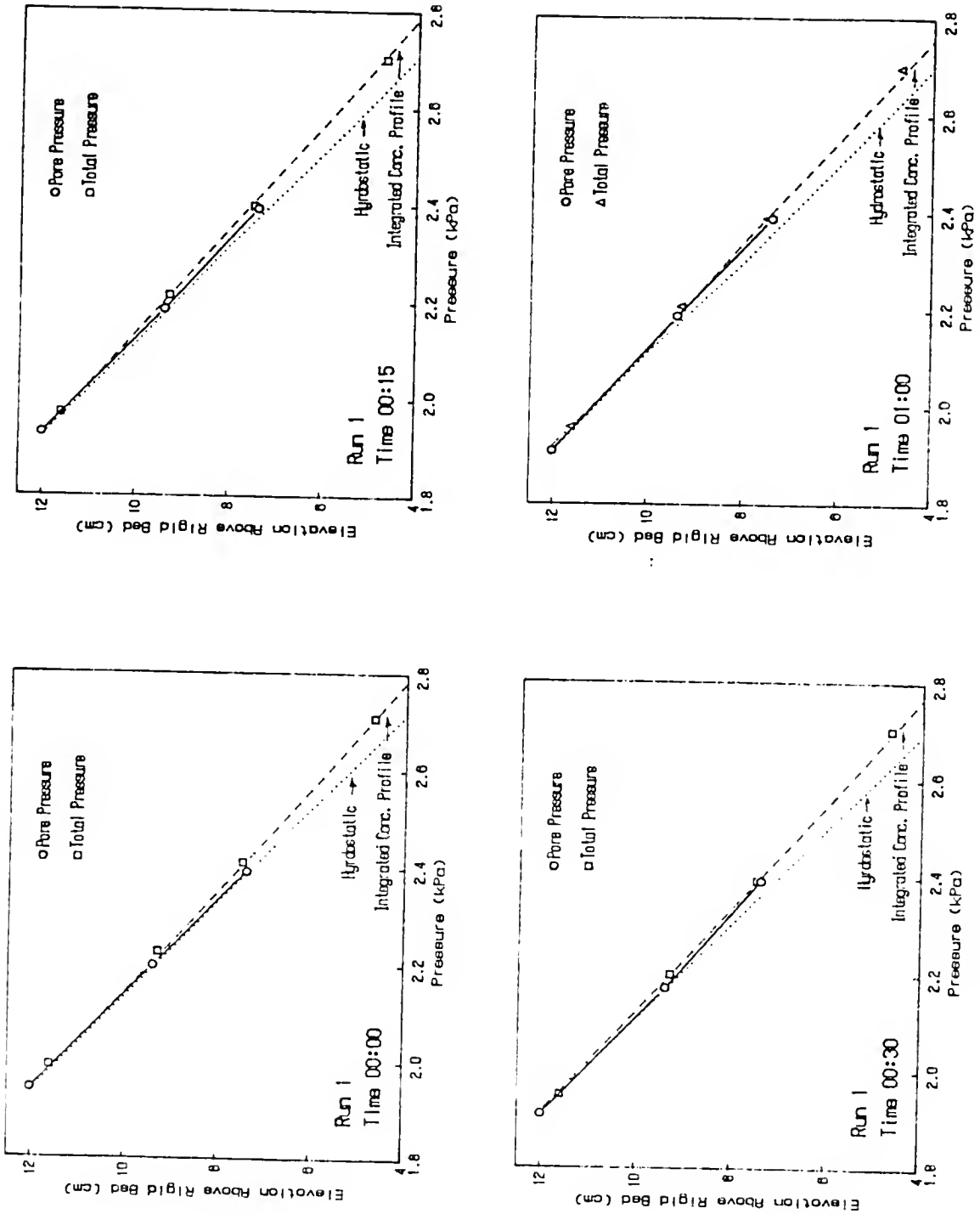

Figure 4-6. Wave-Average Bed Pressures At Various Times for Run 1

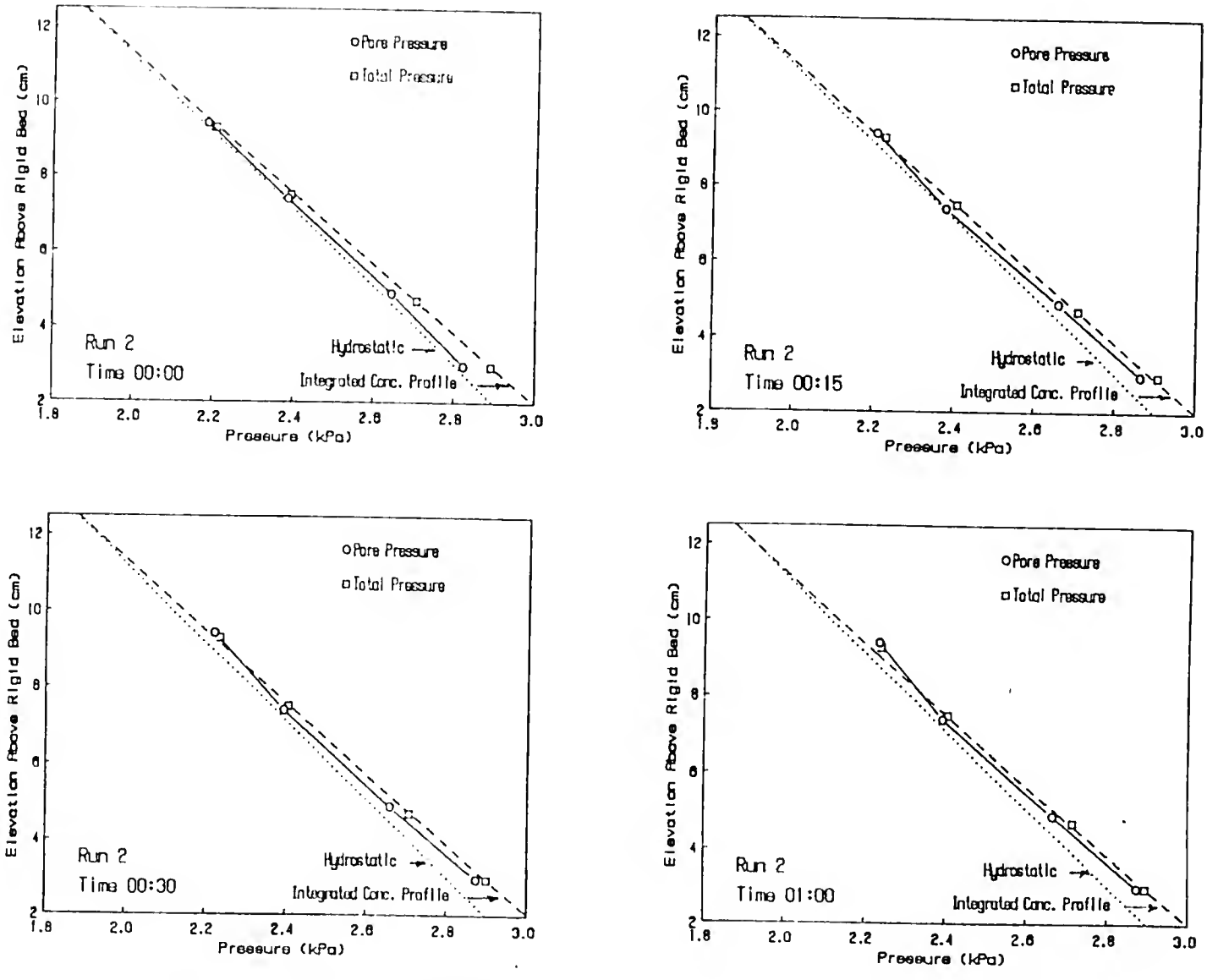

Figure 4-7. Wave-Average Bed Pressures At Various Times for Run 2

Figures 4-8 and 4-9 present bed effective stress time response for Runs 1 and 2 in a more direct manner. The most significant observation which can be made from these data is that the effect of wave oscillation has caused the initially weak but measurably apparent soil effective stress to deteriorate rapidly causing liquefaction of the bed material. If the upper level of the bed surface (Z_c in Figure 2-1) is assumed to be represented by the 0.001 kPa (absolute zero is too vague a definition) effective stress elevation (found from Figures 4-8 and 4-9), a plot of this level is depicted in Figures 4-10 and 4-11. Bed surface concentrations are shown in parentheses. Significant (40%) reduction in bed elevation is shown for the two tests. In one case Run 2 reduction of the structural bed follows the trend of the visual bed elevation, whereas in Run 1 the reduction in structural bed elevation is far more noticeable then the reduction in visual bed elevation.

In both cases the upper bed elevation concentrations were observed to be around 150-170 g/l. The significance of this is not clear however subtle discontinuities in bed concentration profile occur roughly corresponding to the $\sigma' = 1$ Pa elevation. Figure 4-12 shows the relative elevation of effective stress development in relation to these changes in concentration gradient for various times for both Run 1 and 2. The correspondence is seen to be much more apparent for Run 1.

It is also interesting to point out that the observed concentrations at which effective stress developed corresponded with the upper fluid mud concentration limit proposed by Krone (1962) (see Table 2-1). However, this may only be coincidental.

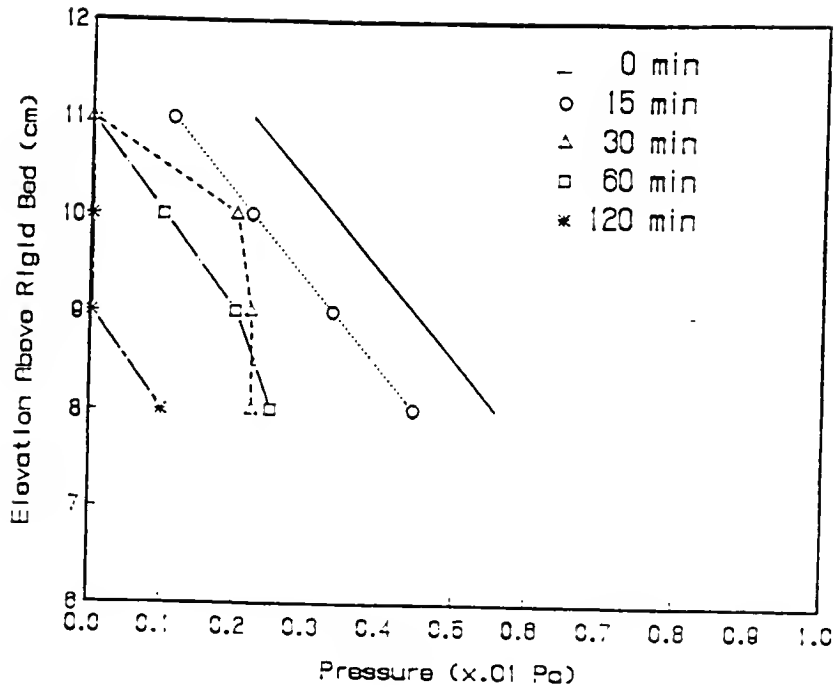

Figure 4-8. Temporal Response of Effective Stress for Run 1

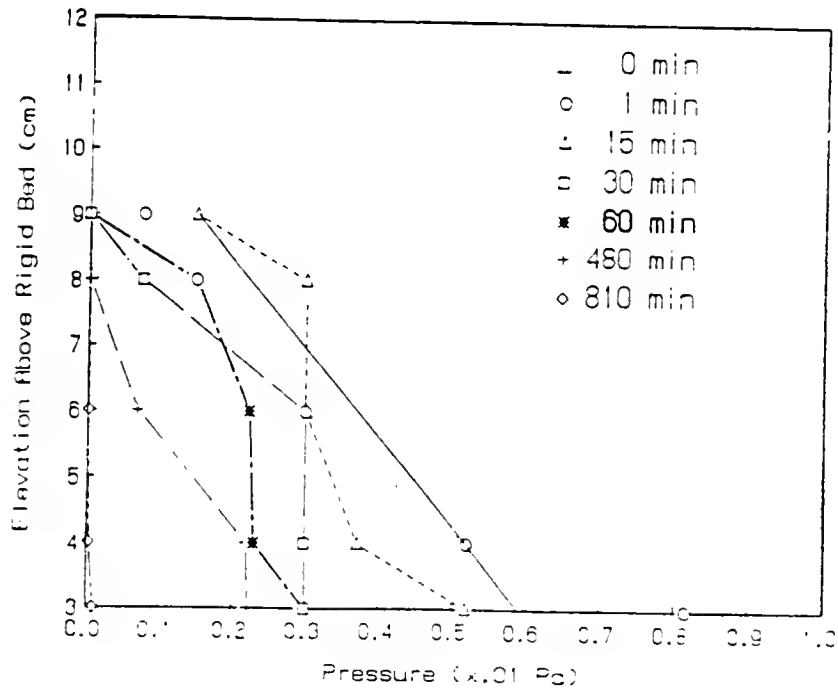

Figure 4-9. Temporal Response of Effective Stress for Run 2

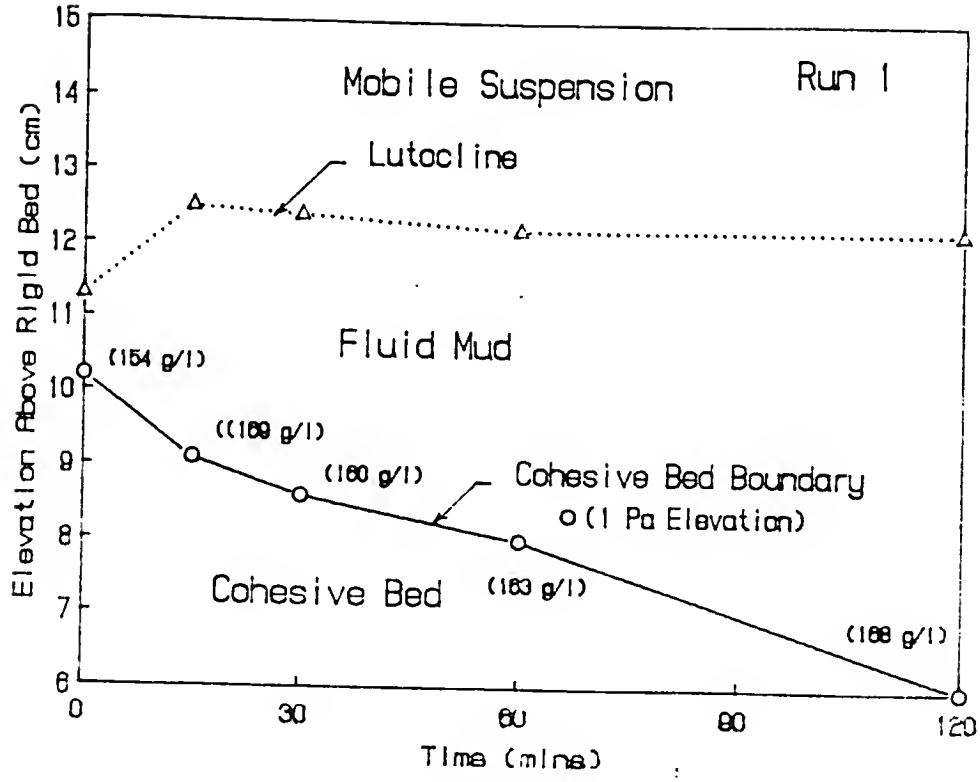

Figure 4-10. Structural and Visual Bed Elevations for Run 1

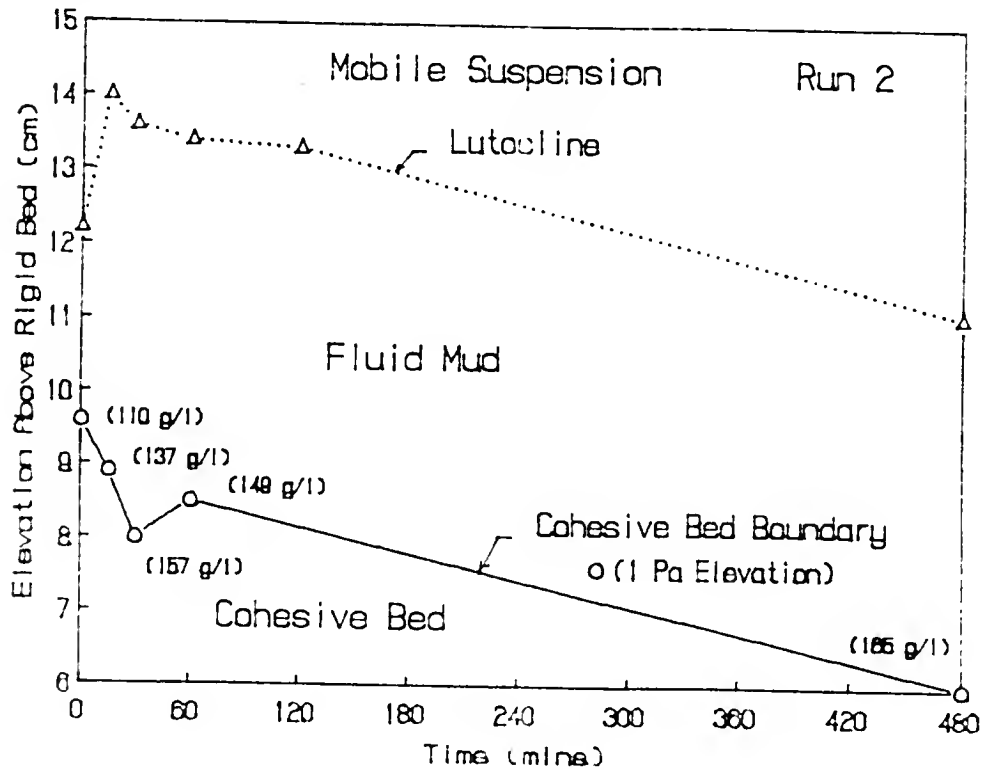

Figure 4-11. Structural and Visual Bed Elevations for Run 2

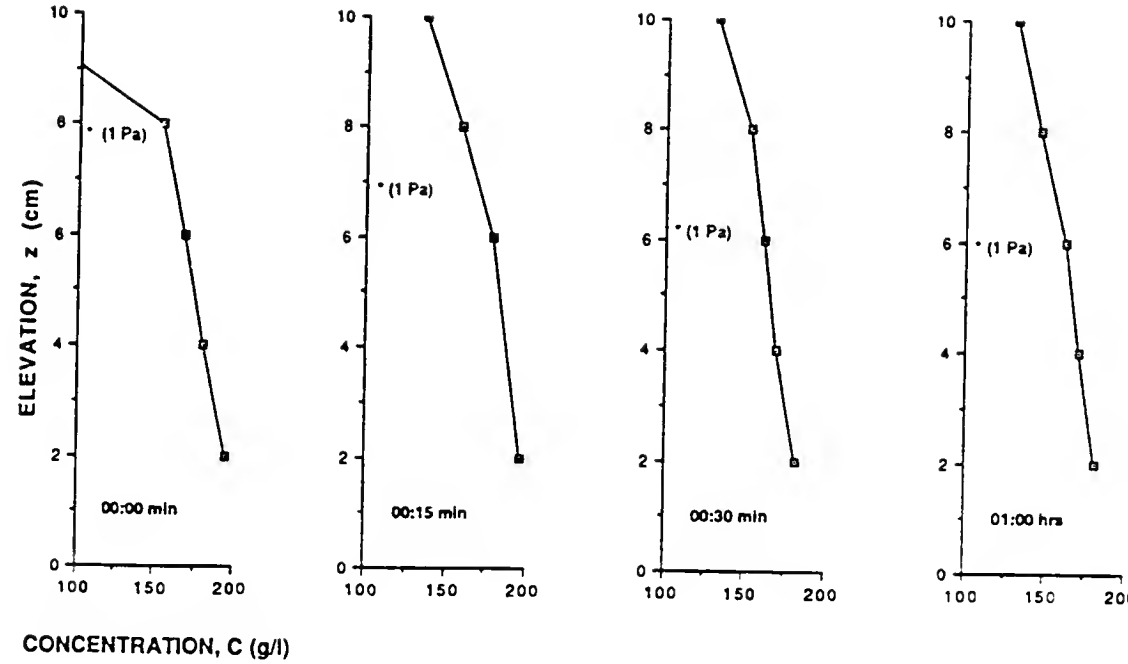

a. Run 1

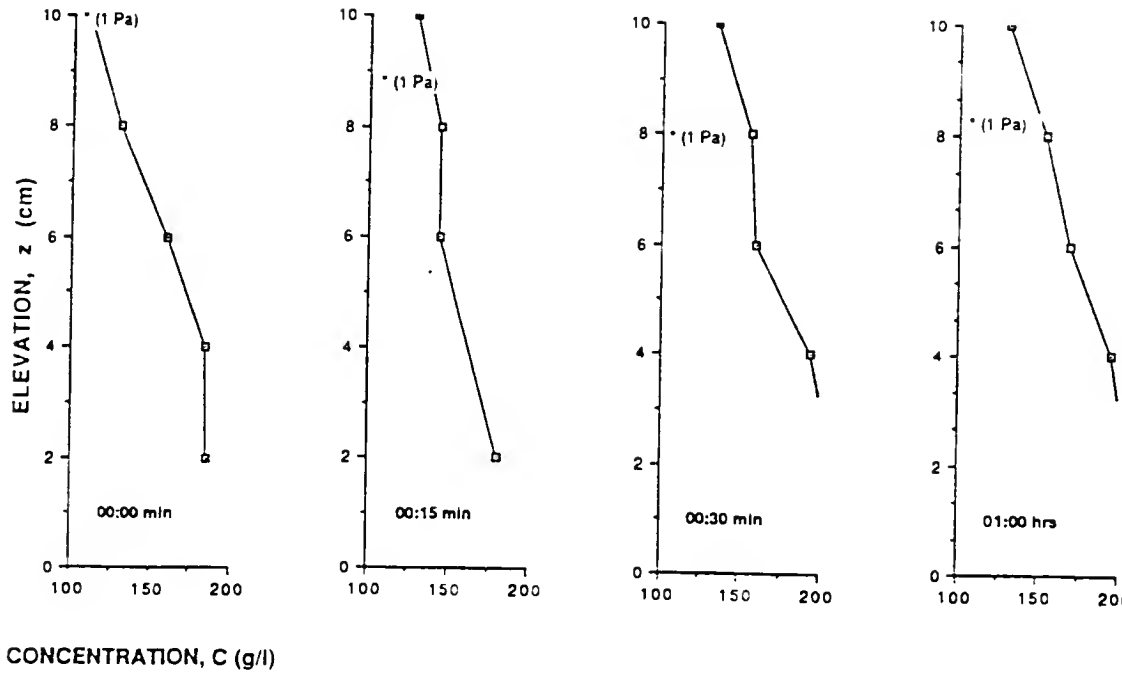

b. Run 2

Figure 4-12. Concentration Versus 1 Pa Effective Stress Elevation

Figure 4-13 shows the dry weight bed concentration profiles (bed here means with respect to the "visual" bed interface) for the first and second runs. It is observed that an apparent initial swelling and subsequent densification (concentration increase with bed elevation decrease) occurred. These two phenomena were characteristic of both tests. A similar observation was made by Maa (1986) in wave erosion studies using mud from Cedar Key, Florida and commercial kaolinite. The mechanism for this is also not clear; however, it may be due to weak aggregate destruction (to lower order aggregates) and crystalline restructure (edge to face bonds becoming face to face bonds) proposed by Krone (1962).

Some of the explanation can be attributed to horizontal fluid mud transport also observed in the tests. Figures 4-14 and 4-15 show "visual" bed elevations measured along the plexiglass side wall during the course of both tests. It is striking to see a rapid development of a sloping bed associated with the transport of a high concentration fluid mud layer towards the downstream section of the tank. This is believed to be caused by the non-linearity in the oscillatory velocities. An analytical treatment of this hypothesis is presented in Chapter 5 which results in a reasonable prediction of the net transport rate. Figures 4-16 and 4-17 show measured dynamic pressure amplitudes by the PDCR pressure gages in both runs. The pressure amplitudes are seen to increase after several hours of wave loading indicative of the fluidization process.

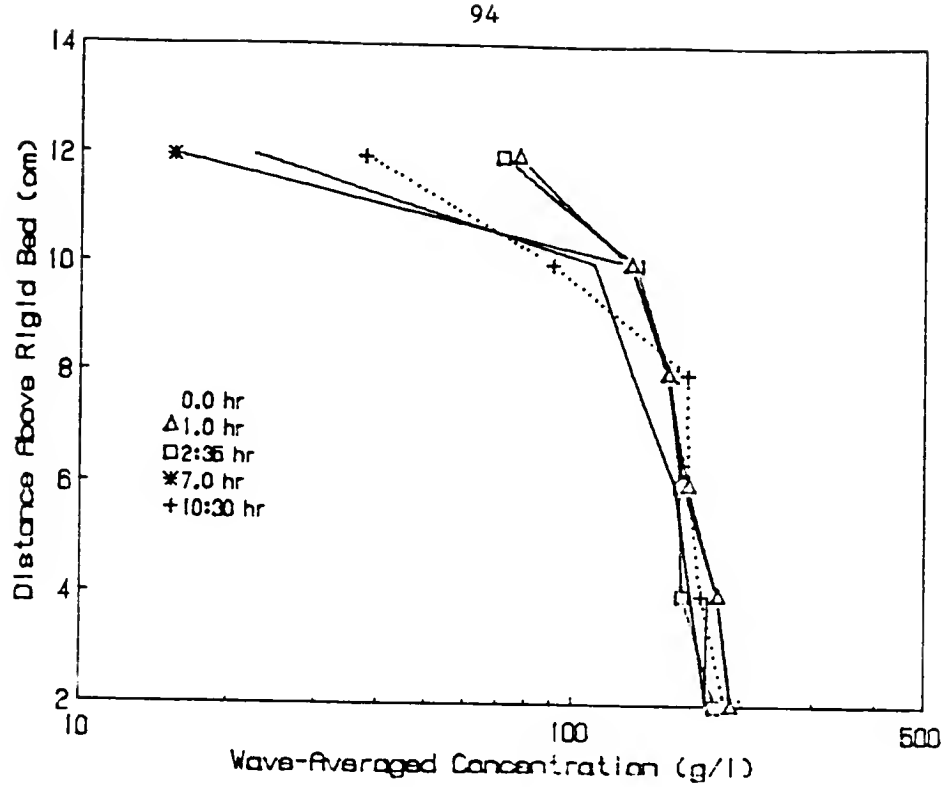

a. Run 1

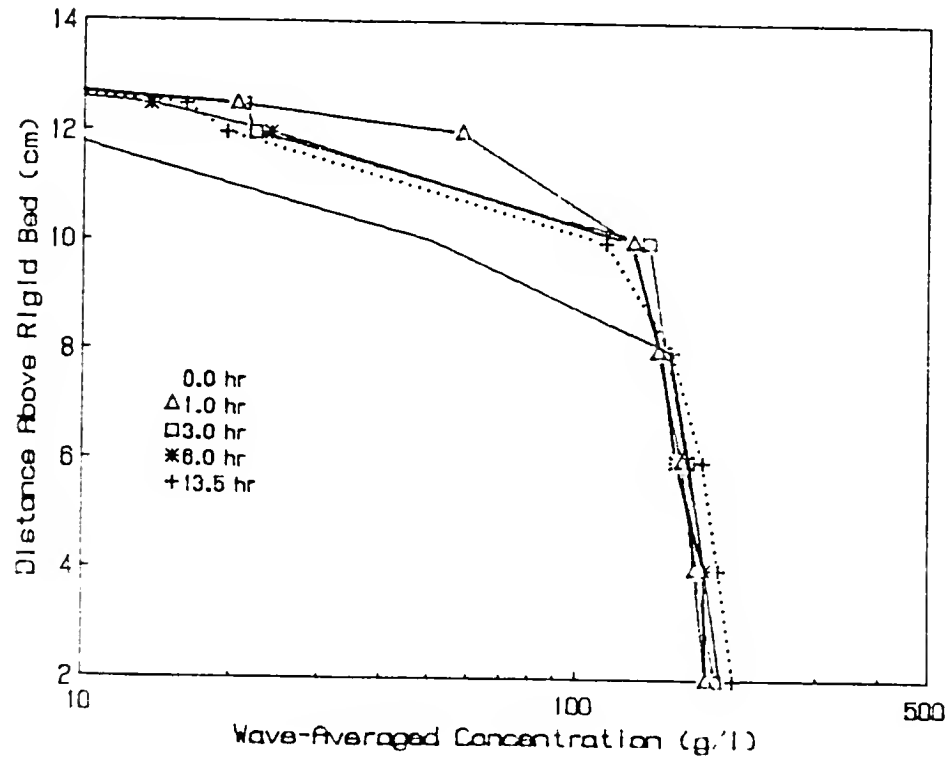

b. Run 2

Figure 4-13. Bed Concentration Variation With Time

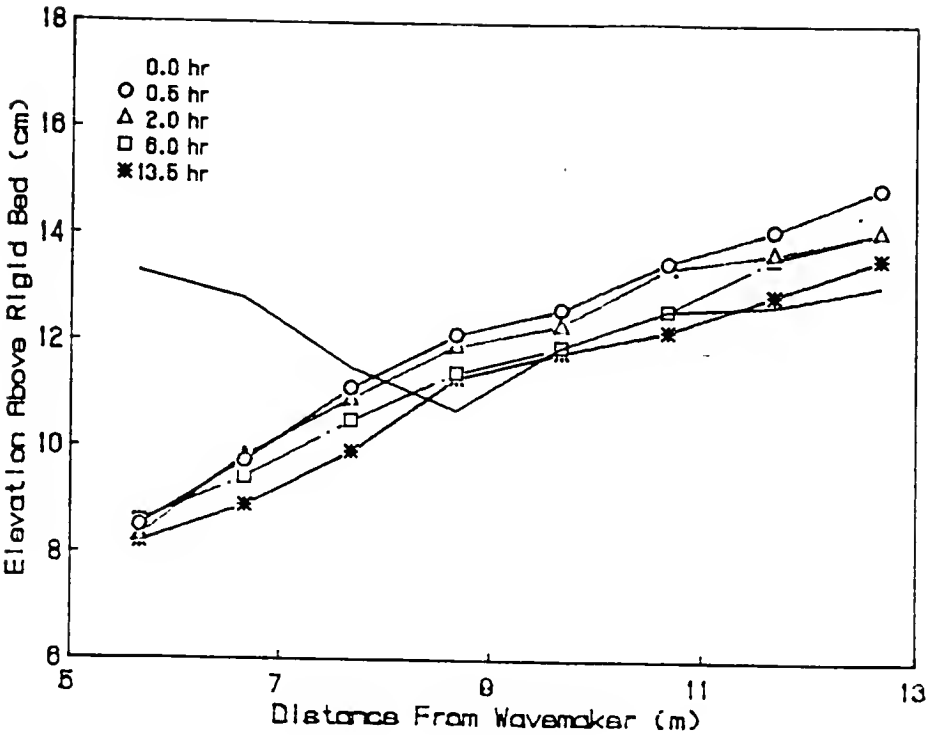

Figure 4-14. Visual Bed Elevation Variation with Time for Run 1

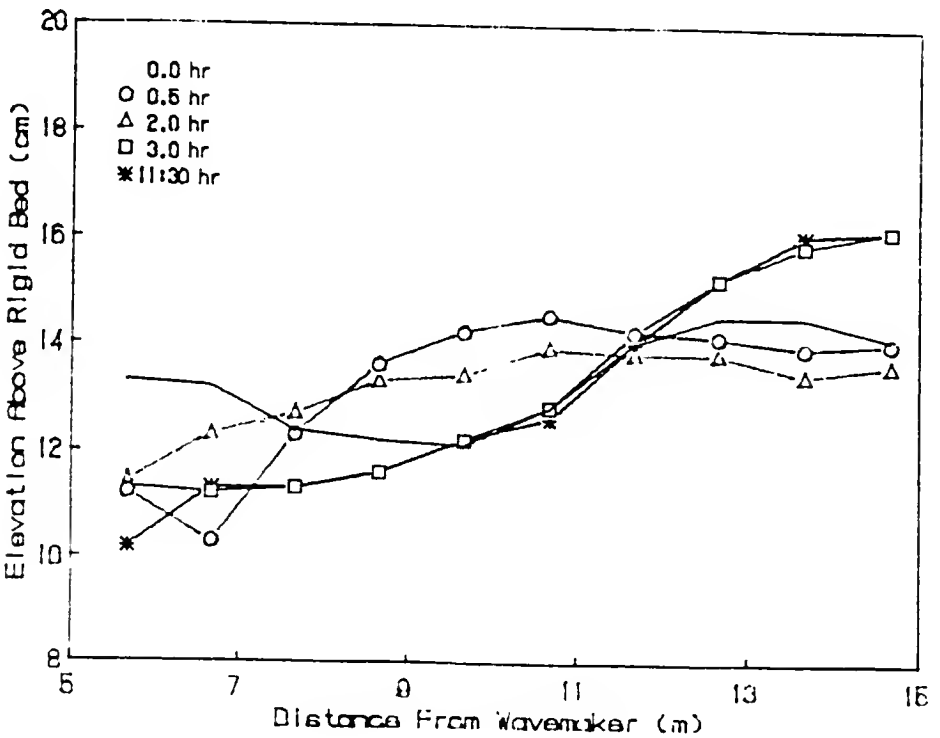

Figure 4-15. Visual Bed Elevation Variation With Time for Run 2

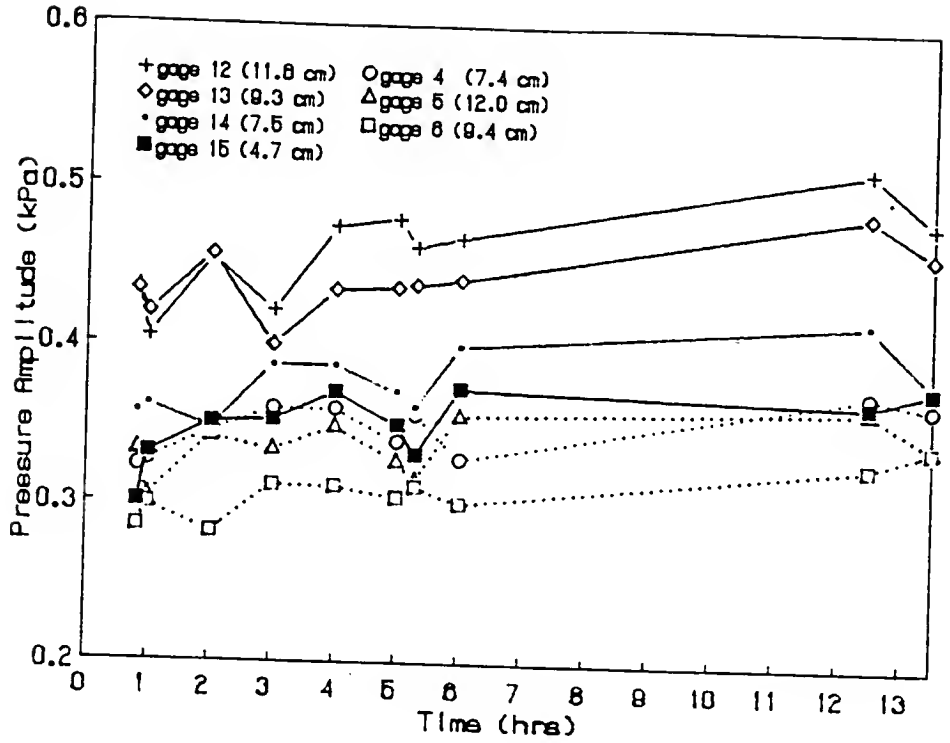

Figure 4-16. Bed Dynamic Pressure Amplitudes With Time for Run 1

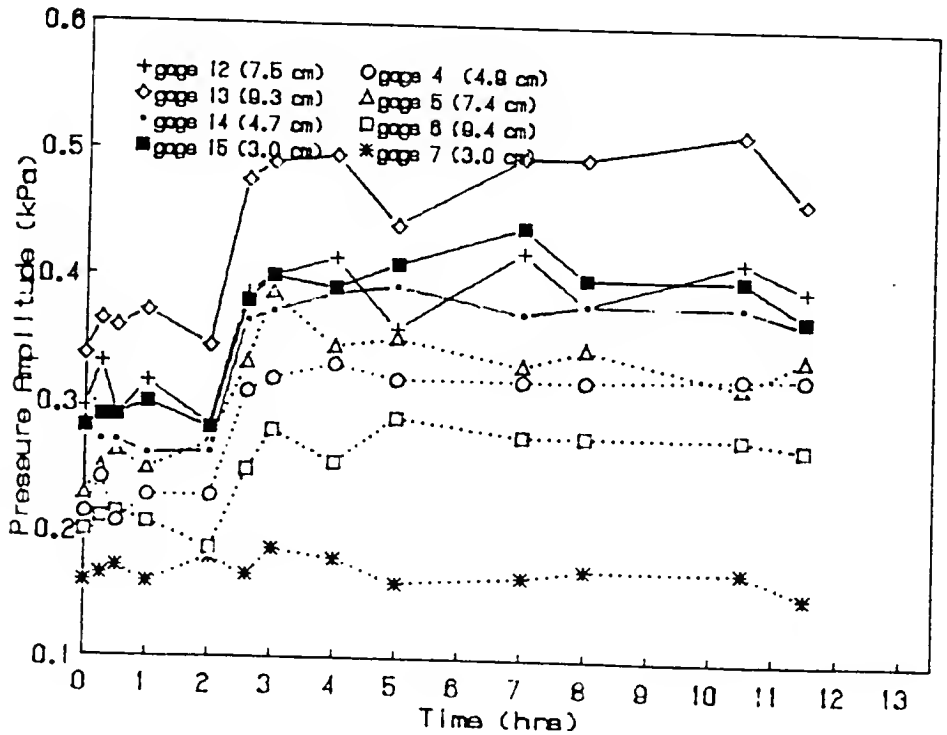

Figure 4-17. Bed Dynamic Pressure Amplitudes With Time for Run 2

Resuspension. Figures 4-18 and 4-19 show concentration profiles which developed over the middle of the mud bed section (station C) in runs 1 and 2. These profiles are observed to progress towards an equilibrium condition. An interesting observation concerns the resuspension potential of waves in the absence of unidirectional current. It was shown in Figures 4-10 and 4-11 that waves rapidly "resuspended" the bed material by the destruction of effective stress; however, in Figures 4-18 and 4-19 it is observed that vertical transport proceeded at a rather slow to moderate pace, and that "equilibrium concentrations" in the upper water column were relatively low (<300 mg/l). This is partly due to the relatively low turbulent mixing conditions prevalent in the runs characteristic of the relatively mild wave conditions--a limitation of the particular wave tank and generator used. For the more turbulent test (Run 2) the Wave Reynolds' Number ($R_w = u_b^2/\nu\sigma$; u_b= maximum near-bed orbital velocity, ν = kinematic viscosity of water, and σ = wave frequency) was only $R_w \approx 2 \times 10^3$. According to Kamphuis (1975) this is in the laminar to intermediate turbulent regime. Therefore, turbulence was not fully developed. In prototype conditions (with waves and currents) ambient turbulence from currents would undoubtedly lead to higher vertical transport rates (from high diffusivities) than under laboratory conditions with waves alone.

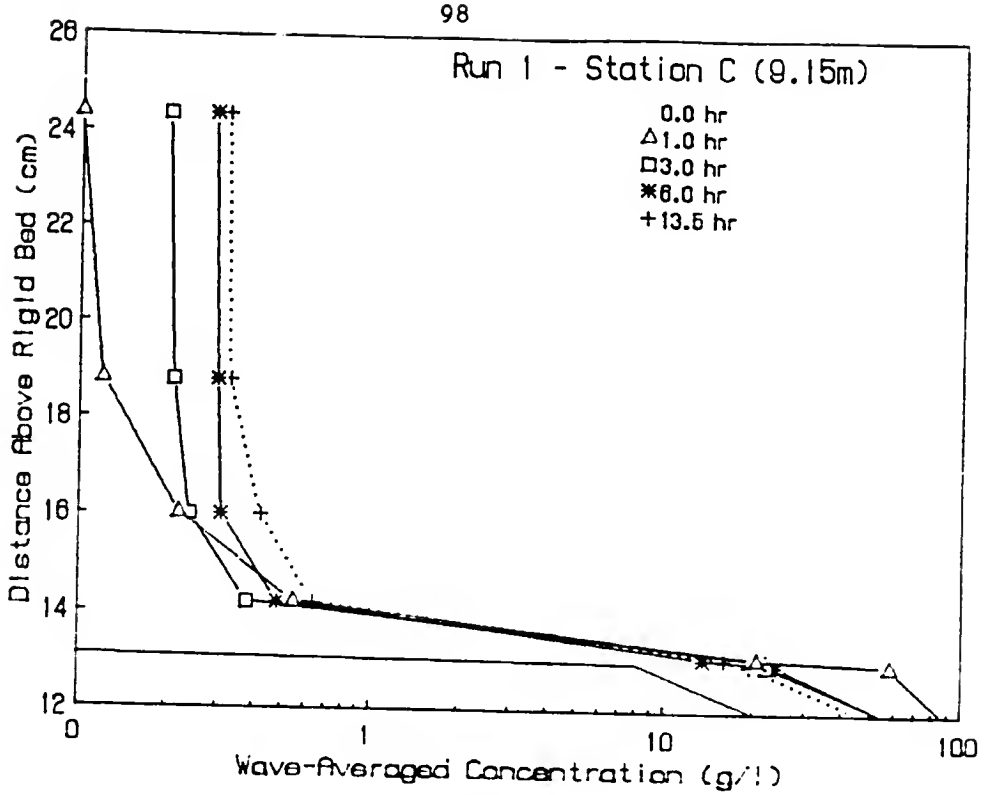

Figure 4-18. Concentration Profiles at Station C for Run 1

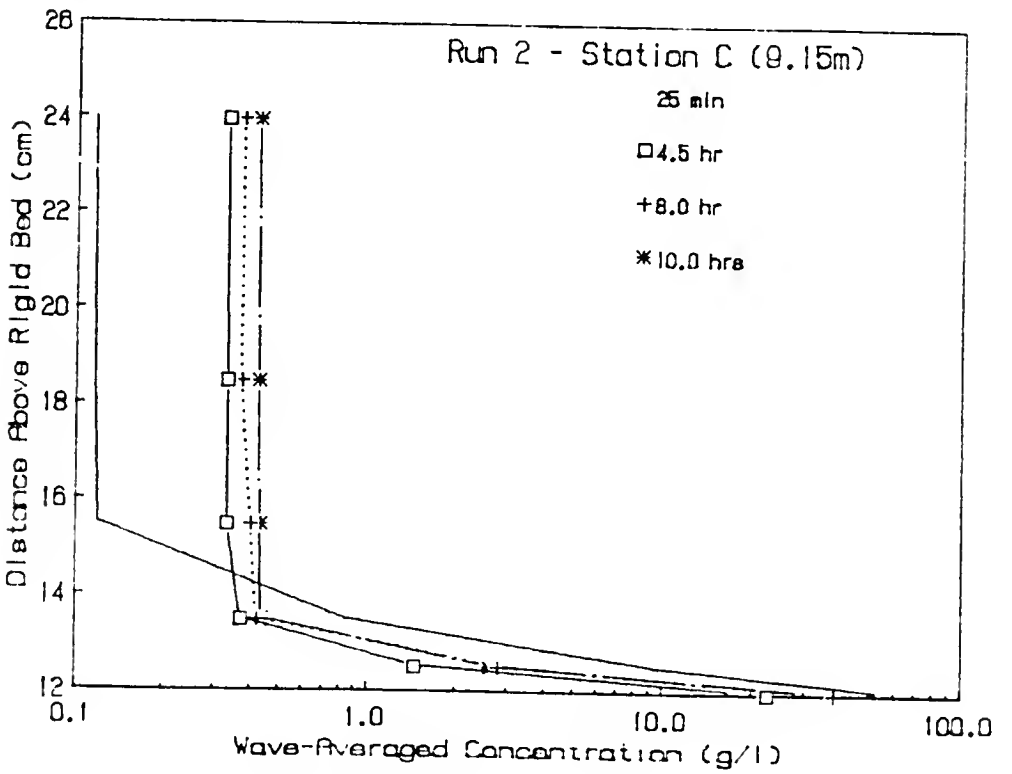

Figure 4-19. Concentration Profiles at Station C for Run 2

4.2.6 Discussion

The most significant contribution of wave/mud bed interaction is shown to be rapid fluidization of the structural bed, large fluid mud generating potential, and moderate upper column suspension concentrations. Wave oscillatory bed shear stress appears to be particularly effective in the destruction of poorly consolidated, weakly structured, bed deposits. There seem to be two mechanisms contributing to bed failure. They are conveniently labeled as "pumping" and "shaking" for lack of better descriptors. Pumping arises as a result of vertical pressure gradients at the bed causing inflow and outflow of pore fluid. Because the cohesive bed has a low permeability, excess pore pressures build up and reduce the effective stress. At the point when effective stress is no longer apparent, the mud/water mixture behaves as a high density fluid and dynamic wave pressures are more rapidly and readily transmitted (with depth). "Shaking" is the process by which oscillating bed shear stresses create oscillating shear strains which tend to break apart weak aggregate bonds. Moreover, oscillations (even when the bed behaves almost as an elastic solid) greatly enhance permeability in the same manner as shaking a coffee filter to allow for faster filtration. This may allow the "pumping" phenomenon to become more effective as initial increases in inflow and outflow of pore fluid into the bed matrix is achieved. In either case, wave erosion of cohesive beds is inherently different from that of unidirectional flows where erosion only proceeds to the bed shear stress-bed shear strength level with no significant effect on bed structure below this level. Yet, turbulent unidirectional flows allow for much greater vertical transport and, of course,

horizontal transport, which does not scour significantly under waves with nearly closed orbital paths. This is precisely why the combination wave/current transport potential is so great. Waves create significant bed erosion and fluid mud suspensions by the mechanisms described above. Unidirectional currents, having greater (generally) imposed interfacial shear stresses and greater mixing rates, lead to high mass transport rates.

4.3 Settling Column Tests

As pointed out in Chapter 3 (Sections 3.4.2 and 3.4.3), cohesive sediments in suspension have a settling velocity which is concentration dependent. This dependence can only be determined from observations of settling in quiescent conditions, or under non-quiescent conditions where the diffusion rates are quantifiable. The law which governs vertical mass settling in the absence of mixing is the one dimension mass conservation equation

$$\frac{\partial C}{\partial t} = - \frac{\partial F_s}{\partial z} \qquad (4.2)$$

This equation relates the time rate of change in suspended sediment concentration, $C(z,t)$, to the vertical gradient in settling flux, $F_s=w_sC$. Since the settling velocity, $w_s(C)$, varies with z, w_s cannot be taken directly out of the spatial derivative.

A brief review of previous field and laboratory approaches followed by a description of what is believed to be an improved settling column

method along with results for Tampa Bay mud are given in the following sections.

4.3.1 Historical Approaches

Several methods have been used to measure settling velocity of fine sediments in suspension. A review or previous studies and particular conditions for each can be found in Heltzel and Teeter (1987). Only a discussion of the methods is presented here.

Sediment settling velocity can be measured by direct or indirect means. Direct methods, e.g., by visual or photographic observations, measure the actual fall velocity of discrete particles or aggregates. Due to the non-uniformity in settling, success with this method is difficult to achieve. However, Chase (1979) used computer analyzed optical images to determine the settling characteristics of a natural marine sediment. One reason for his apparent success was his ability to analyze a large (reportedly over 1000) of aggregates.

More commonly, indirect methods are employed for determining "average" settling velocities of suspensions. Two such approaches are bottom accumulation, and point concentration (pipette) methods.

The accumulation method uses percent sediment mass settlement rate (out of suspension) and a characteristic distance (e.g., column height) to determine average particle settling velocity. The standard procedure (Owen, 1970) is to use a settling column of known dimensions, mix in a predetermined mass of sediment with water, and take time withdrawals of bottom deposits. After drying, the volume, weight, and times of the withdrawals together with the column height are used to obtain a settling

velocity distribution based on assumed vertically uniform concentration of suspension. An Oden curve is then obtained to determine percent settling. Among researchers to use techniques similar to this are Oden (Inter-Agency River Basin Committee, 1941, 1943), Owen (1970, 1971, 1976) and Lott (1987). Owen (1976) also developed a settling tube for field use based on this method. Lott (1987) used a procedure in which he measured time history of the suspension concentration profile to determine bottom settlement rate. An apparent problem with this procedure is that the settling velocity is related to depth averaged concentrations. However, order-of-magnitude or higher vertical variation in concentration is common in these columns. The settling velocity for the lower high concentration layers is much different than that in the upper column. Due to the non-linear variation in the settling velocity with concentration, the average settling velocity obtained in this manner typically may not correspond to the average concentration.

The pipette method measures concentration (through apparent density) at a point in a quiescent suspension. The change in concentration at a point of depth H below the surface over a period of time t is used to determine the average mass of sediment which has settled at a rate H/t, using the average concentration over that time as the reference concentration. Researchers who have used similar techniques include Krone (1962), Guy (1975) and Teeter (1986a). The problem with this method is that it measures concentration at only one point as a function of time C(t).

Uniform high concentration sediment suspensions settle with a sharp upper interface (Teeter, 1986b), and concentrations in the region below

the interface are fairly constant until they reach the hindered settling lower interface near the bottom. The interface grows upward until the flux of sediment across the interface diminishes. At that point the interface begins to drop (see Figures 5-4 and 5-11 for an illustration of this behavior. Point sampling in this region shows no change in concentration and by the above procedures no settling velocity. Clearly, this is not the case since the interface and the individual particles are settling at a finite velocity.

Comparing the two methods (pipette and accumulation) it can be seen that they are inherently different. The pipette method measures the temporal change in local concentration, thus $\partial C/\partial t$ is known at a particular point while accumulation records the temporal change in the actual mass flux, $w_s C$, at the bottom. Therefore, neither method provides a desirable means of directly obtaining w_s and C at a particular location and instant. A procedure which attempts to provide both settling velocity and concentration based on measuring the temporal history of the concentration profile is documented in the following section.

4.3.2 Concentration Profile Approach

A third method which can be used to measure the settling velocity of sediment suspensions in settling columns shall be called the concentration profile or multi-depth method. This approach uses the instantaneous vertical distribution of settling sediment tracked through time to determine the variation of settling velocity with concentration dependence, $w_s(C)$. In short, recorded observations of the spatial and temporal variations of the sediment suspension give a means of solving

for $w_s(C)$ from the settling equation (Eqn. 4.2) directly. Continuous x-ray, gamma-ray transmission (attenuation) or physical sampling at discrete elevations are the most common means for determining the concentration profile. Hince the terminology "multi-depth method" (McLaughlin, 1958).

McLaughlin (1958) used a procedure of this type to obtain the depth and time dependence of the settling velocity $w_s(z,t)$, of bentonite (655 mg/l) and alum [$Al_2(SO_4)_3.18H_2O$] (25 mg/l) suspensions in tap water. Concentrations were measured at 3 depths in a 1.2 m high settling column of 9.5 cm diameter. Gravimetric analysis of 20-40 ml withdrawn samples was used to obtain concentration profiles which were graphically integrated to quantify changes in suspension mass. Flocculation was shown to increase the average settling velocity with time to some maximum value which was depth and time dependent thereafter decreasing. This is shown in Figure 4-20. Note that the peak settling velocity increased with depth. Fitch (1957) presented multi-depth settling results for whiting [$CaCO_3$] (400 ppm) and ferrisul [$Fe_2(SO_4)_3.9H_2O$] (15 ppm) in water. He showed similar time and depth dependence of settling velocity as was observed by McLaughlin (1959). For Fitch's tests, the settling velocity was seen to reach a maximum after a relatively long period (1 hour) following test initiation. This probably occurred because the clay was in previously dispersed (stable) form requiring some time to react with the free hydrated metal ions before reduction of repulsive surface changes could occur. This is further supported by the fact that flocculation and floc growth are shown to occur very rapidly in previously destabilized fine sediment suspensions (Hunt, 1980).

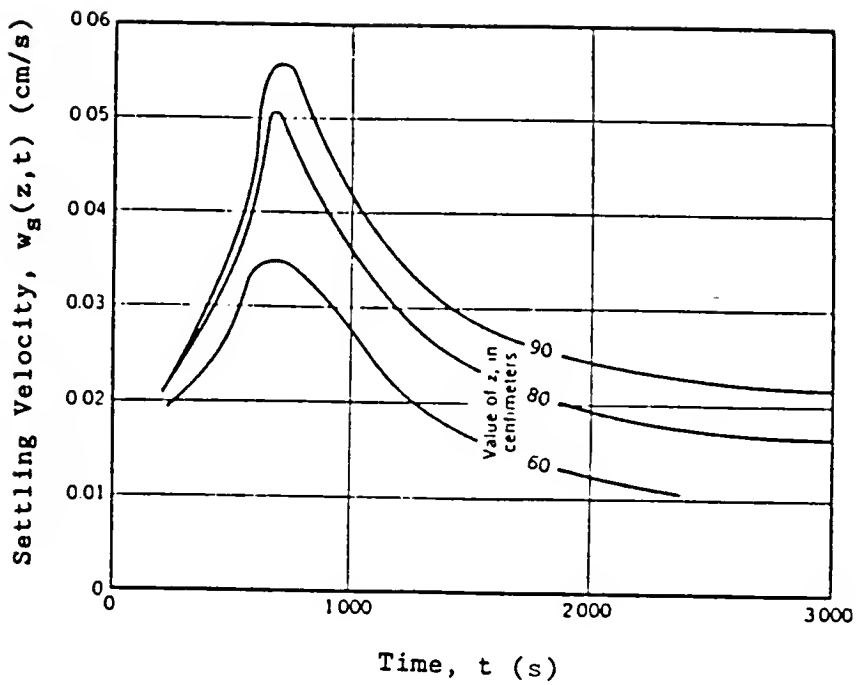

Figure 4-20. Local Mean Settling Velocity as a Function of Time for Bentonite Clay and Alum in Water (adapted from McLaughlin, 1958)

It is important to note that neither author related settling velocity to concentration directly.

An improved settling velocity measuring procedure (by concentration profile) is proposed. Multi-depth concentration sampling and numerical integration is used to determine effect of concentration on settling velocity dependence on concentration is presented together with results for Tampa Bay mud in the following pages.

Procedure. Settling velocity tests were carried out in a specially designed 2 m settling column at the University of Florida's Coastal Engineering Laboratory. The column, originally designed by Lott (1987), consisted of a 10 cm plexiglass tube fitted with 5 mm diameter siphon taps at nine elevations. Figure 4-21 is a scale drawing of the column

configuration. Tap hoses were 5 cm long and 5 mm diameter tygon tubes fitted with clamps.

For tests using Tampa Bay mud the following procedure was used:

1. High concentration sediment slurry was diluted with tap water to desired initial concentration and required volume (15.7 liter) to fill the settling column. Salt was added in some cases to achieve a 1 ppt ambient salinity. The suspension was then thoroughly premixed in a 20 liter carboy and allowed to equilibrate with time (a few hours to 1-2 days).
2. After preparation, the suspension was poured into the settling column and a vacuum bubbler tube was inserted. The suspension was further vigorously mixed for 2 minutes in the column.
3. The bubbler tube was then quickly removed and the first set of 20 ml samples were taken as fast as possible after the last bubbles reached the surface. Samples were collected in 50 ml glass bottles which were tightly capped, labeled, and set aside. Sampling then continued after time intervals of 5, 10, 15, 30, 60, 120, and 180 minutes. Water depth and temperature were recorded at each sampling time.Care was taken to flush the sampling tubes before each withdrawal.
4. Gravimetric analysis was used to determine concentrations of each sample. This provided concentration profiles at each sampling time.

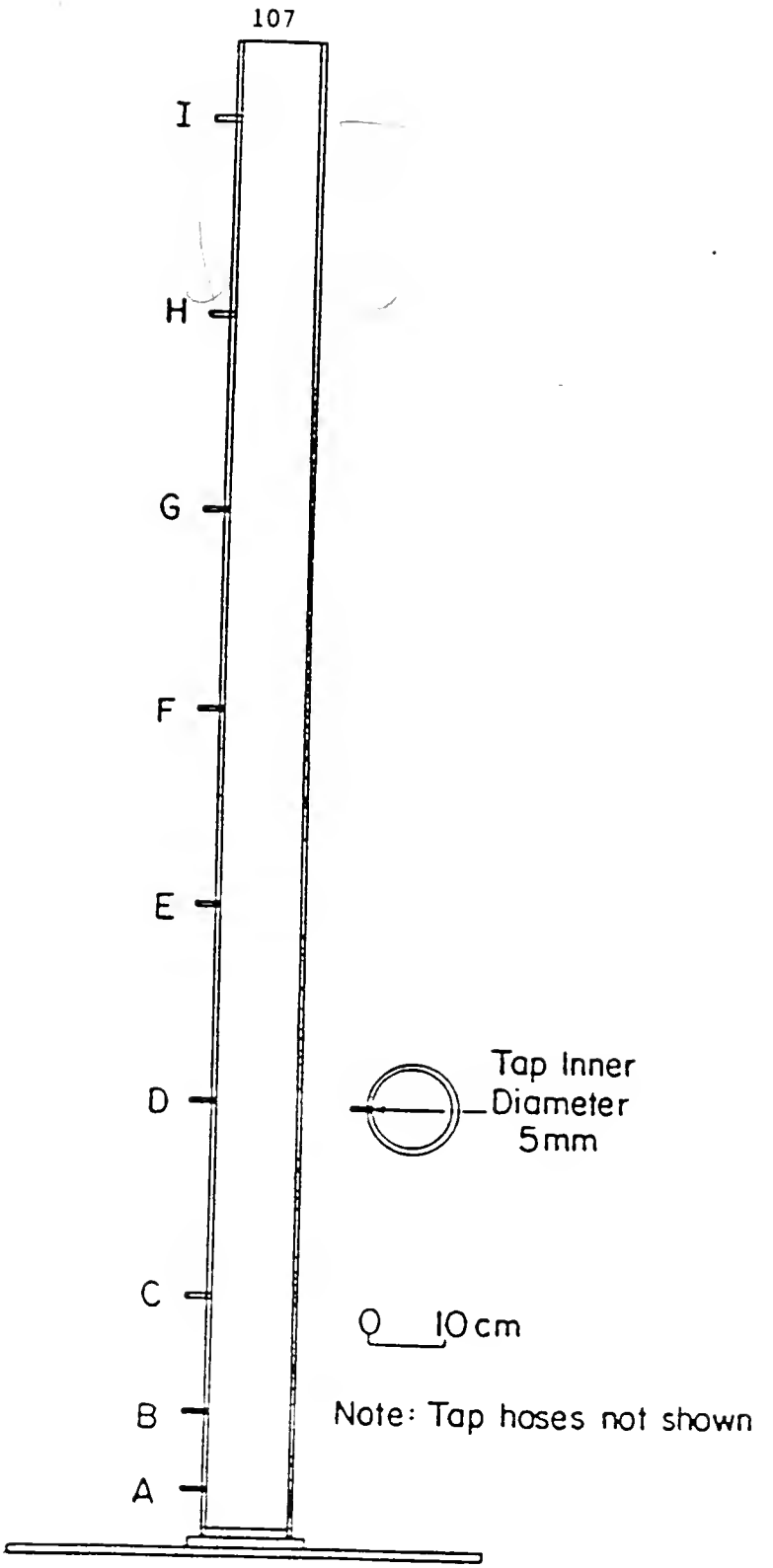

Figure 4-21. Scale Drawing of the Settling Column

5. The concentration data were then entered into an input data file to be used for a settling velocity calculation program described in the following paragraphs.

Analysis. A computer program was written to calculate sediment settling velocities at each elevation and time based on a finite difference solution of the settling equation (Eqn. 4.2). The difference equation chosen was as follows:

$$w_{s_i}^{j+1} = -\frac{1}{\chi_i^j}\frac{\Delta z_i}{\Delta t^j}\left[\chi_i^{j+1} - \chi_i^j\right] + \frac{1}{2}\left(w_{s_{i-1}}^j \chi_{i-1}^j + w_{s_{i-1}}^{j+1} \chi_{i-1}^{j+1}\right) \quad (4.3)$$

where χ_i^j is the log average of the sediment concentration and Δz_i is the vertical spacing between the i^{th} and $(i+1)^{th}$ sample elevation. The term, Δt^j, is the time increment and j is the time index. This is shown graphically in Figure 4-22. The log average concentration is defined as

$$\chi_i^j = e^{\{\frac{1}{2}(\ln C_{i+1}^j + \ln C_i^j)\}} \quad (4.4)$$

The boundary conditions are the no flux surface and bottom boundary conditions, $w_{s_i}^j \chi_i^j\Big|_{i=0} = 0$ and $w_{s_i}^j \chi_i^j\Big|_{i=n} = 0$, where n is the lowest tap number. The initial conditions are $w_{s_i}^j\Big|_{j=0} = 0$ and $C_i^j\Big|_{j=0} = C_o$, where C_o is the initial concentration. Note that the log average concentration is used as the mid-point concentration instead of the arithmetic average because

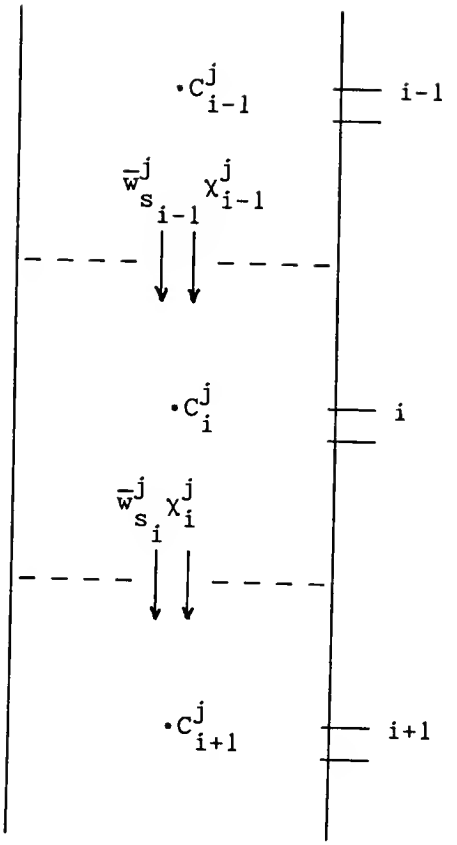

Figure 4-22. Grid Indexing used in the Settling Velocity Calculation Program

of the typical logarithmic shape of the concentration profile, i.e., it appears as a nearly straight line on semi-log paper.

The results from eight settling column tests using initial concentrations of between 1 and 20 g/l were used to determine the concentration dependence of the settling velocity of Tampa Bay mud. This is shown in Figure 4-23. Note that the data are quite scattered but clearly indicate an increasing velocity region due to flocculation effects and a decreasing velocity region due to hindered settling. It should also be noted that even though initial concentrations over a

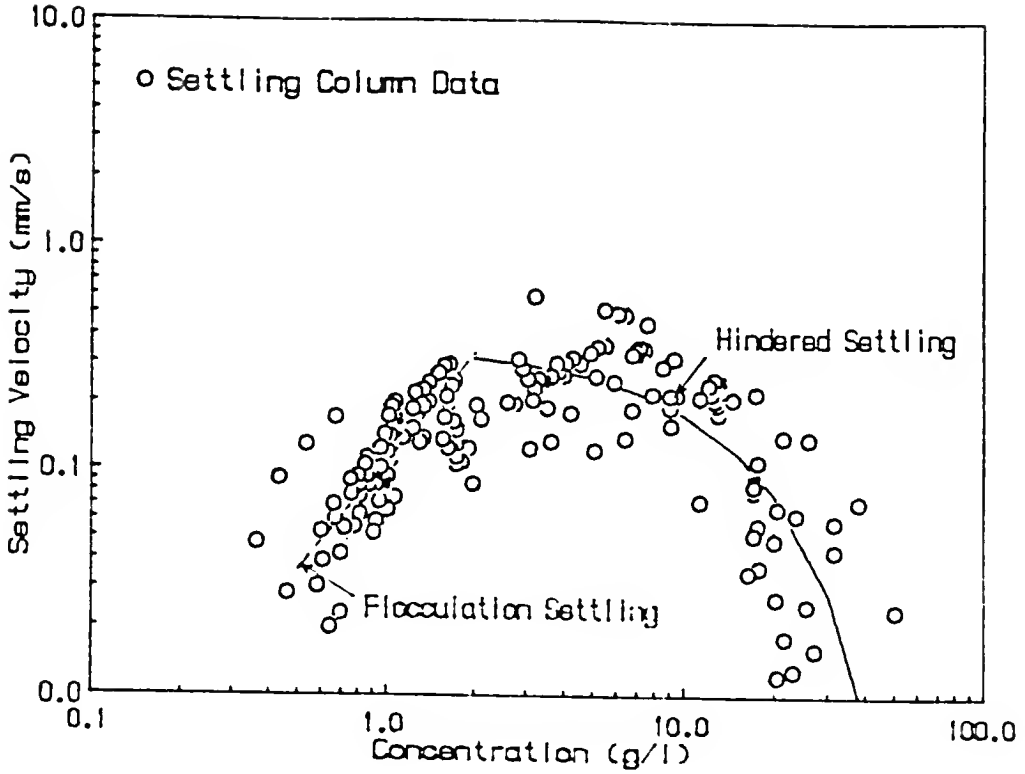

Figure 4-23. Settling Velocity Variation with Concentration of Tampa Bay Mud

relatively narrow range (1-20 g/1) were used, this method gives settling velocities over a much larger concentration range due to the suspension thinning in the upper column and the development of high concentration layers in the lower column.

The data in Figure 4-23 suggest a power law equation for settling velocity as a function of concentration in the flocculation settling range ($0.1 < C < 2$ g/1) of

$$w_s = 0.11\ C^{1.6} \qquad (4.5)$$

and in the hindered settling range ($2 \leq C \leq 70$ g/1),

$$w_s = 0.37\ (1 - 0.008\ C)^5 \qquad (4.6)$$

where w_s is in mm/sec and C in g/l.

The results (i.e., concentration profiles and settling velocity expression, Eqns. 4.5 and 4.6) of the individual settling column tests were used to test the settling velocity routine in the vertical transport model developed in Chapter 3. The comparisons between predicted and measured concentrations, treating the sediment as being made up of cohesive and non-cohesive components, are described in Section 5.2.1. Several interesting observations concerning the characteristics of natural estuarine fine sediment settling are also presented there.

Scatter in the data arose from many sources. One source was a slight time-variation in the settling velocity due to collision and flocculation which increase as settling proceeds. This time dependence has not been considered in this analysis. Another source of error occurs because the bubbler mixing procedure tends to cause initial aeration (by introduction of microscopic bubbles) which tend to increase effective buoyancy forces on sediment flocs. This seems to become less apparent shortly after the test is begun. Nevertheless, it is suggested that in future tests a mechanical agitator or other mixing device be used in lieu of the bubbler. Still another source of scatter did not become apparent until predictive modeling was carried out. As apparent from the concentration profiles shown in Section 5.2.1 (Figures 5-2 through 5-9), the sediment consisted of cohesive and non-cohesive constitutive fractions. Thus, while the settling velocity increased for the cohesive

fraction in the flocculation range, the non-cohesive sediment experienced hindered settling. Such interaction leads to a complex settling behavior which cannot easily be quantified. Furthermore, sorting is also experienced in the lower concentrations ($C < 10$ g/l) thereby greatly affecting the time-dependent settling behavior. Lastly, while an effort was made to keep the slurry, suspension and apparatus in a constant temperature environment, temperature changes of 2-4 °C were recorded. This change affects the settling velocity in a number of ways including Brownian collision frequency and viscosity changes. The mean temperature for the tests varied from 19-24 °C.

As a general note about settling tests (in columns or settling ponds), column height (or pond depth) affects resulting settling rates. As the height of the settling suspension (and sediment mass flux) increases, the resulting downward velocity decreases due to increased net upward flow velocity from displaced water from sediment settling below. The resulting "vertical diffusion" under quiescent net flow conditions has been treated analytically by Yong and Elmonayeri (1984). However, this effect would be expected to occur under flow conditions as well. Therefore the measured settling velocity represents a net settling velocity which is somewhat depth dependent but is acceptable within the accuracies involved. No further consideration of flow drag from displaced water was made in these analyses but it is a recommended area of further research.

CHAPTER 5
MODELING RESULTS AND DISCUSSION

5.1 Introduction

This chapter presents the results from comparisons of observed and simulated vertical concentration profiles, the applications of the vertical transport model, and calculations of fluid mud transport rates using the theoretical models presented in Chapter 3. It must be emphasized that this is a simple but useful application of available theoretical relationships to present and explain the behavior of vertical suspension concentrations of fine sediment in estuaries. This point is reflected by the relatively modest computational facilities which were required for simulations. The vertical transport model was written in M-S Basic and implemented on a 16 bit IBM-AT operating at 8 MHz. The program source code is included in Appendix C for reference. Normal simulation run times were on the order of 10-20 minutes except for the larger scale Severn Estuary runs which took up to six hours of CPU time.

5.2 Settling

In light of the differences previously pointed out by Owen (1976) and others between quiescent and turbulence-enhanced settling, it was desirable to test the settling routine in the model for both cases. A discussion of some of the differences and results from each application are presented in the following sections.

5.2.1 Quiescent Settling

Vertical concentration profiles resulting from quiescent settling column tests of Tampa Bay mud were useful in testing the settling routine of the vertical transport model before testing diffusion and settling combined. For cohesive sediments, it was concluded that two algorithms were required to calculate discrete settling fluxes at any particular point. As was pointed out by Teeter (1986b), discontinuities or steps in the concentration profile, such as at the interface between the increasing settling flux region (i.e., flocculation settling) and the decreasing settling flux region (i.e., hindered settling), complicate the numerical solution. Discontinuities of this type are associated with locations where the vertical flux gradient with respect to concentration is zero. Figure 5-1 shows mean curves for settling velocity, w_s, and flux $F_s = w_s C$ for Tampa Bay mud from settling column tests (Section 4.3.2).

For concentrations above the value (10 to 20 g/l) corresponding to the peak flux, settling is limited (hindered) from below and the potential settling flux at a point is greater than that below it, i.e.,

$$\left.\frac{\partial F_s}{\partial z}\right|_z < 0 \qquad (5.1)$$

(z is positive downward). This requires forward differences in the

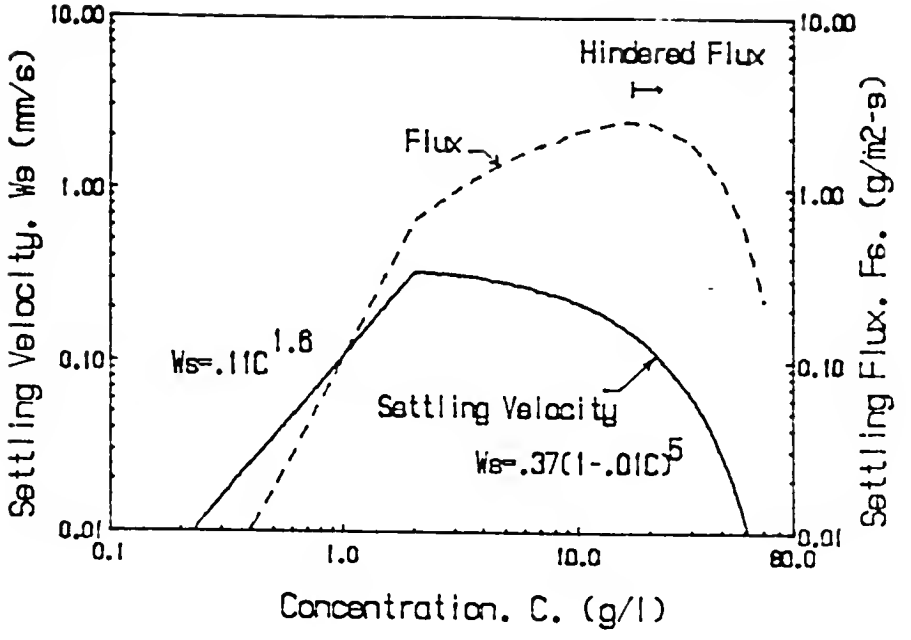

Figure 5-1. Settling Velocity and Flux Versus Concentration for Tampa Bay Mud

numerical solution of the settling equation (Eqn 4.2), i.e.,

$$\frac{\partial F_s}{\partial z} \approx \frac{w^j_{si+1} C^j_{i+1} - w^j_{si} C^j_i}{\Delta z_i} \qquad (5.2)$$

For concentrations below the peak flux, the flux increases with depth, and the flux at any particular point is limited only by the settling velocity and concentration at or above that level. This implies that a backward difference scheme is in order, i.e.,

$$\frac{\partial F_s}{\partial z} \approx \frac{w^j_{si} C^j_i - w^j_{si-1} C^j_{i-1}}{\Delta z_{i-1}} \qquad (5.3)$$

Therefore, for simulating settling from low to high concentrations, a logical test is required to switch from one differencing scheme to another. This allows for a simulation of discontinuities which develop in the transition region. A central difference scheme or a Lax-Wendroff scheme (Roache, 1972) is numerically unstable for this purpose. Similar procedures (with logical tests) have been used for numerical simulation of shock waves in compressible fluids (Roache, 1972).

For a typical natural sediment, non-uniformity in grain size (and associated cohesion) requires that the sediment be divided into multiple classes with representative settling characteristics. For a well mixed suspension subjected to quiescent settling conditions some degree of sorting will occur with large or dense particles settling faster than smaller or lighter ones. Therefore, each grain size (or floc) class must be treated separately to represent the overall settling behavior.

The Tampa Bay mud sample was separated into only two classes--a cohesive class C_1, and a non-cohesive class, C_2. The total sediment concentration, C_T, defined as the sum of individual class concentrations, C_i, measured at any time was thus,

$$C_T(t) = \sum C_i(t) = C_1(t) + C_2(t) \qquad (5.4)$$

In the settling tests, differential settling was immediately apparent in the lower, initial concentration tests (1-10 g/l) but, became less significant with increasing concentration. The latter is presumed to be reflective of the fact that higher concentrations settle "in mass"

(meaning all together) with less differential settling due to mutual interference. This supported the definiton of an upper concentration above which no sorting (and hence differential settling) could occur. This upper limit was arbitrarily set at 20 g/l and defined as the composite hindered settling concentration, C_{hT}.

For the non-cohesive class (C_2), which was 10% of the total sample by weight, (see Figure 4-1) the median grain size diameter, d_{50}, was 30 μm (see Section 4.2.2). Stokes' settling velocity (Eqn. 3.21) for individual particles of this diameter is $W_{so2} \approx 0.8$ mm/s. For moderate concentrations ($C_T < 10$ g/l), the settling velocity of this class is given by a Richardson-Zaki type expression of the form (described in Section 4.3.2).

$$w_{s2} = w_{so2}(1+\beta_i C_T)^{e_i} \qquad (5.5)$$

where β_i and e_i are constants and C_T is the total concentration (Eqn. 5.4). This is of course, a gross simplification of the physical process of multi-constituent hindered settling as the interaction between cohesive and small non-cohesive particles may include more than just an increase in hydrodynamic drag. This is reflective of the fact that β is expected to be different for different percentages of the constituents present.

For the cohesive class, C_1, flocculation settling was determined (Eqn. 4.5) to be given by an approximate relation of the form

$$w_{s2} = 0.11\ C_1^{1.6} \qquad (0.1 \leq C_1 \leq 2\ \text{g/l}) \qquad (5.6)$$

from settling column experiments. Note that in this expression the settling velocity is considered to be dependent only on the relative concentration of the cohesive fraction. However, this is also a simplification since, as would be expected, higher percentages of the non-cohesive fraction, C_2, would have a significant effect on the aggregate formation process as well as the increased interaction (e.g., small flocs falling behind large silt grains, etc.)

At and above the cohesive interference settling concentration, $C_{h1} \approx 2$ g/l, but below the composite hindered settling concentration, $C_{hT} \approx 20$ g/l, the average settling velocity for the flocs begins to diminish even though the average floc size may still be growing. This is due to hydrodynamic interference. The settling velocity for the non-cohesive partial concentration, C_1, is given by

$$w_{s1} = w_{so1} (1 - \beta_1 C_1)^5 \qquad C_{h1} \leq C \leq C_{hT}) \qquad (5.7)$$

where w_{so1} is a reference settling velocity (the settling velocity of the average floc size) and β_1 is the inverse of fully settled mud concentration.

The forward/backward difference scheme together was used with the settling velocity expressions (Eqns. 5.5 - 5.7) to simulate concentration profiles which developed in the quiescent settling tests (Section 4.3.2). Model results are compared with the measured data in Figures 5-2 through 5-9.

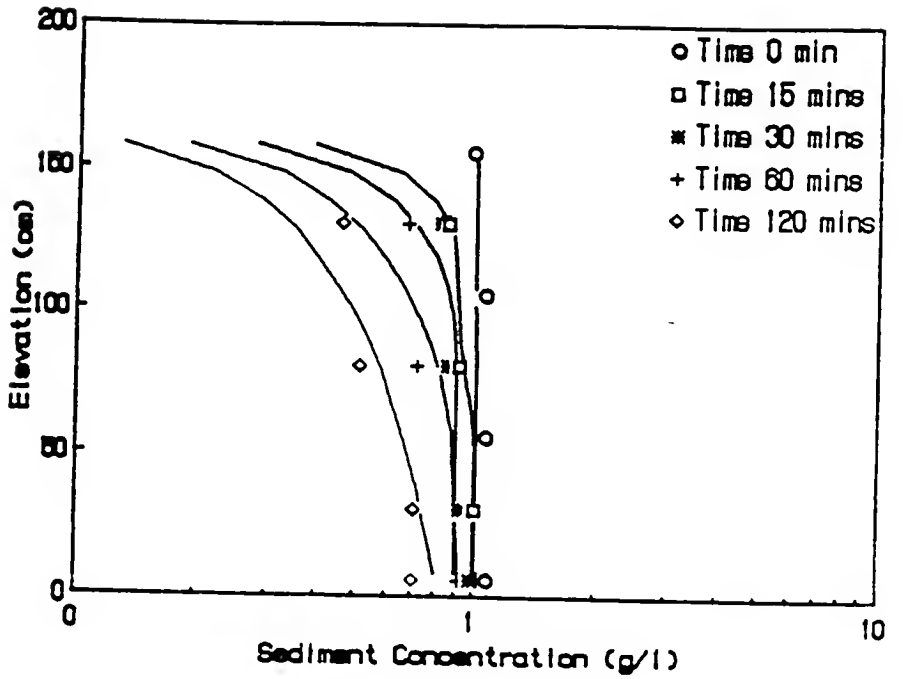

Figure 5-2. Model Simulated vs. Measured Settling Column Concentrations. Initial Concentration, C_o= 1 g/l.

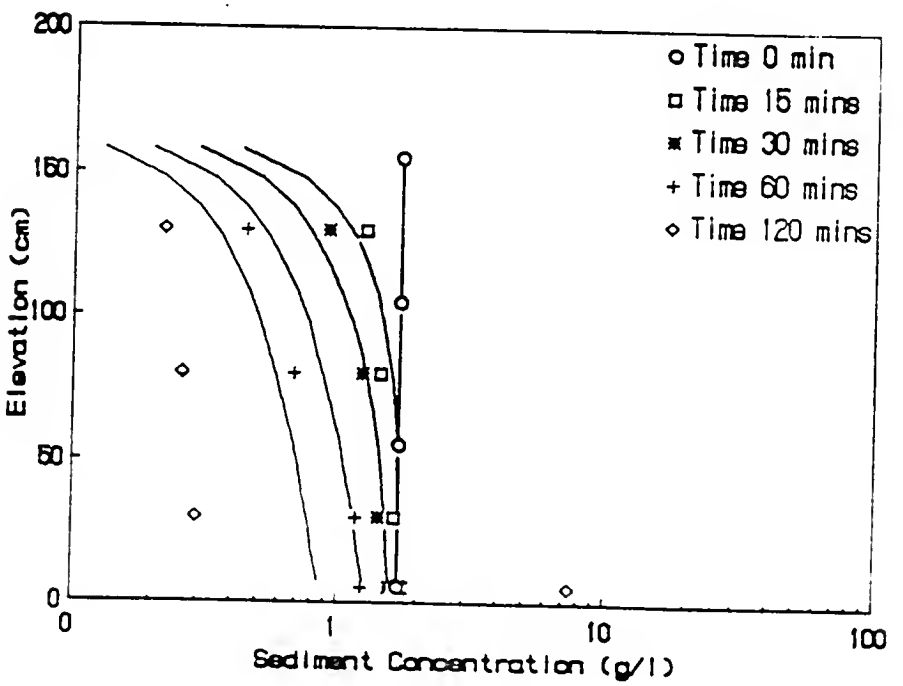

Figure 5-3. Model Simulated vs. Measured Settling Column Concentrations. Initial Concentration, C_o= 2 g/l.

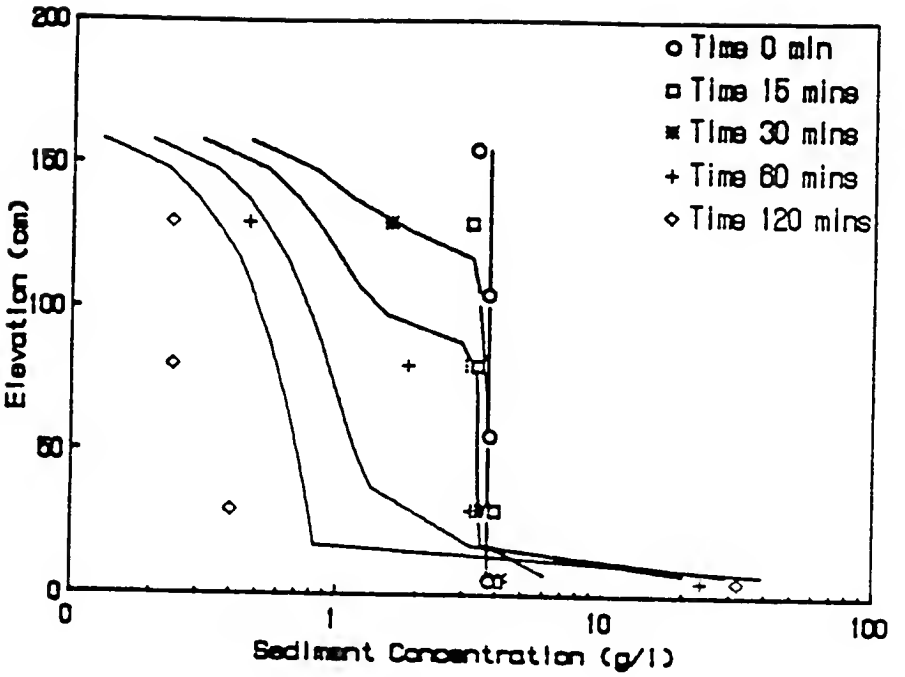

Figure 5-4. Model Simulated vs. Measured Settling Column Concentrations. Initial Concentration, C_o= 4 g/l.

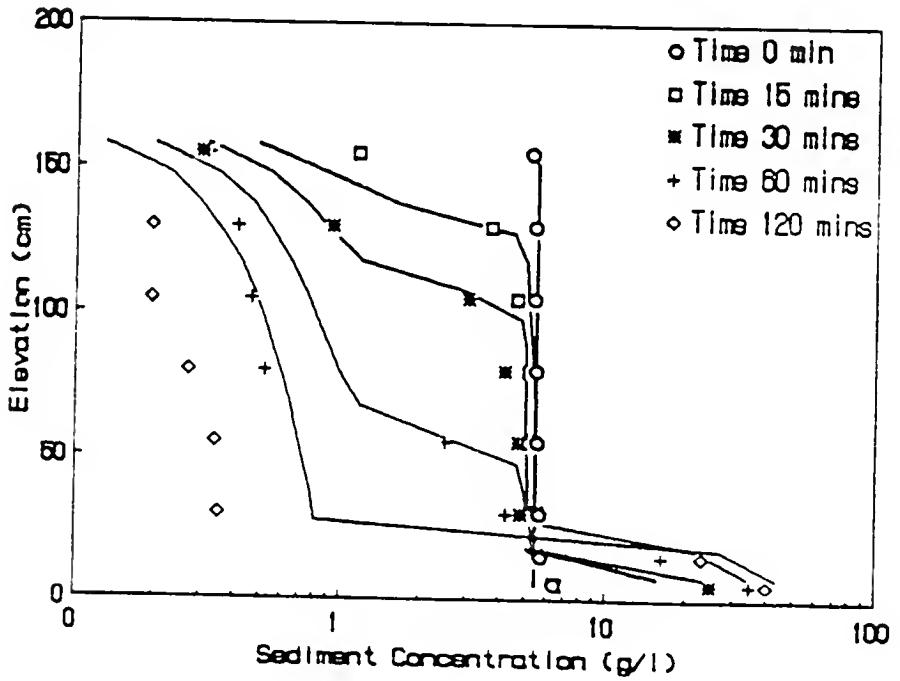

Figure 5-5. Model Simulated vs. Measured Settling Column Concentrations. Initial Concentration, C_o= 5.5 g/l.

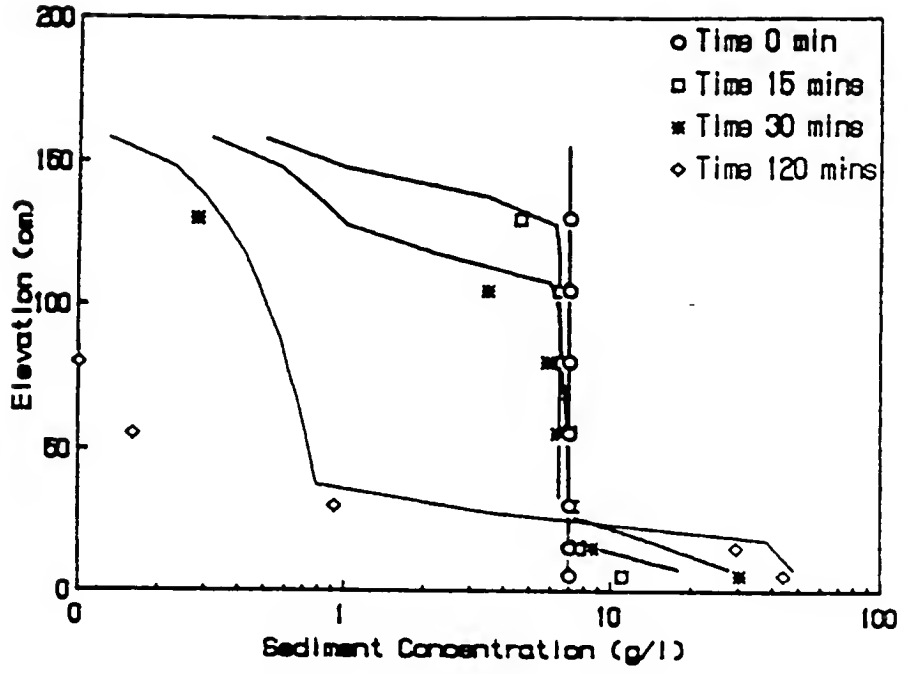

Figure 5-6. Model Simulated vs. Measured Settling Column Concentrations. Initial Concentration, C_o= 7 g/l.

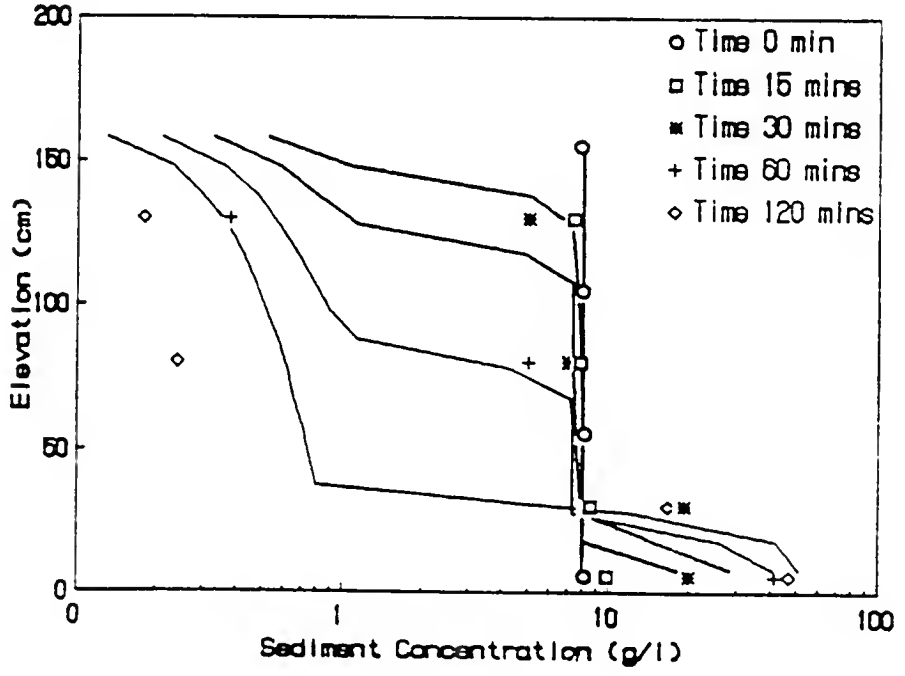

Figure 5-7. Model Simulated vs. Measured Settling Column Concentrations. Initial Concentration, C_o= 8 g/l.

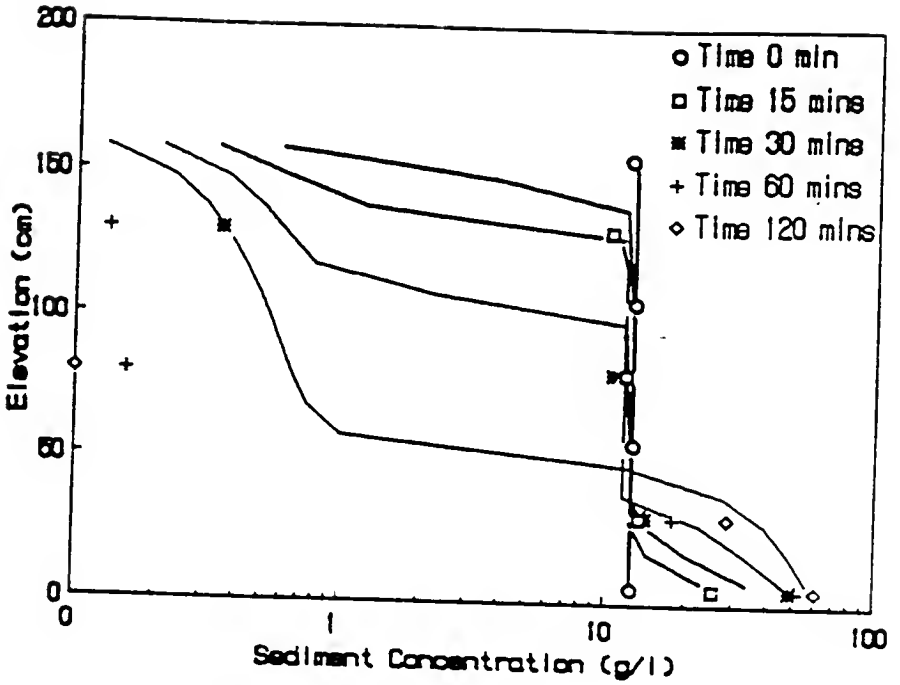

Figure 5-8. Model Simulated vs. Measured Settling Column Concentrations. Initial Concentration, C_o= 12 g/l.

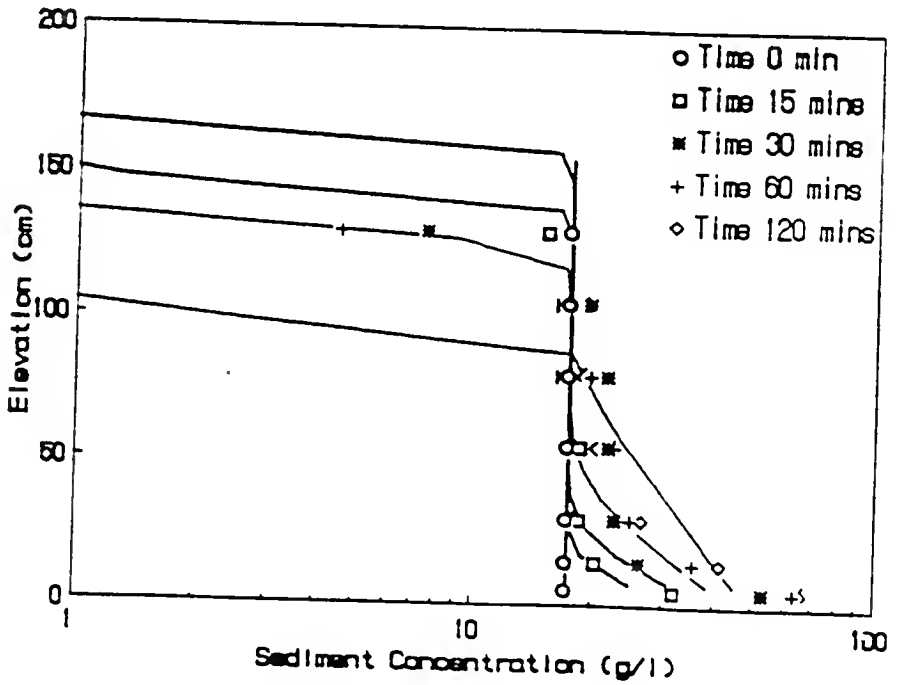

Figure 5-9. Model Simulated vs. Measured Settling Column Concentrations. Initial Concentration, C_o= 17 g/l.

In Figures 5-2 through 5-9 three distinct settling regimes are apparent; low, moderate and high concentration settling. The model can be seen to have greater success predicting the higher concentration ($C > 2$ g/l) settling regimes. This is because these regimes do not experience the overall sediment property changes from sorting that the low concentration (flocculating) regimes do. This observation is clarified below.

For settling with initial or final concentrations in the low to moderate range ($C_T < 2$ g/l) settling results in concentration "thinning." Suspension concentration decreases everywhere in the column except immediately at the bed. This is likely caused by aggregate sorting during the flocculation process. The more rapidly falling large aggregates collide with small individual particles or primary flocs which further adhere to the larger aggregates. These aggregates increase in size with depth of fall and accelerate because the velocity is proportional to the square of the aggregate diameter and overrides the fact that the aggregates' overall submerged density is decreasing slightly. The result is aggregate sorting--large aggregates depositing first followed by small ones. A conceptual sketch is given in Fig. 5-10. Time t_o is the time immediately after mixing when the concentration is seen to be nearly uniform. Concentration profiles at subsequent times ($t_1, t_2, \ldots$) are seen to be fairly log-linear away from the bed and decreasing with time.

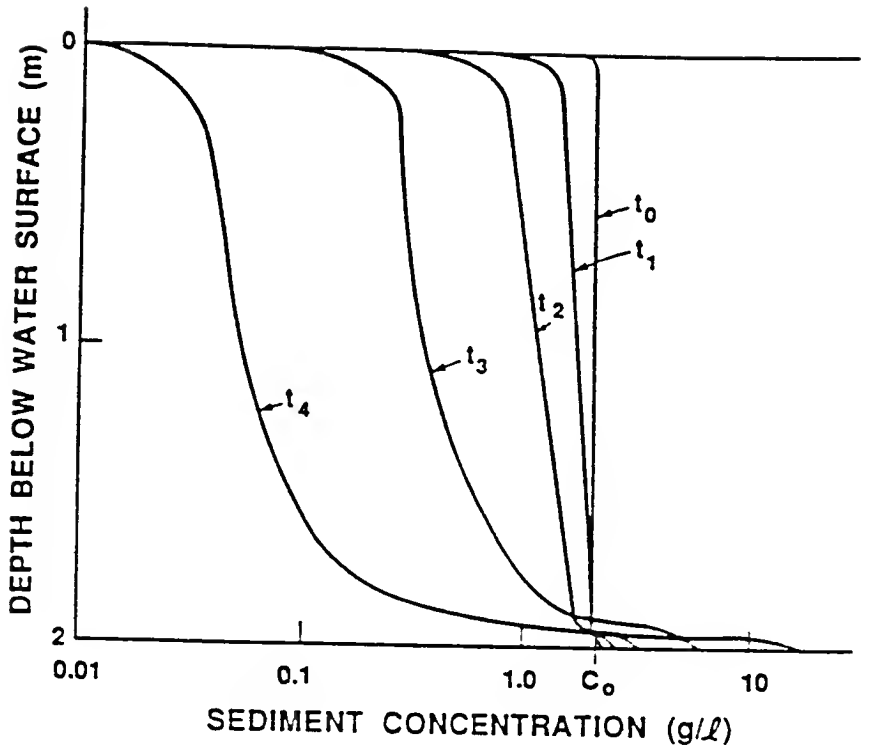

Figure 5-10. Conceptual Model of Concentration "Thinning" in Low Concentration Flocculation Settling.

It should be noted that the transition from low to high concentration settling occurs with no significant intermediate (moderate) concentration region.

In the moderate concentration range (2-20 g/l) the relationship between concentration and aggregate settling appears to be relatively constant with time. The sediment settles with two marked interfaces. Both interfaces converge with time. The upper interface separates the concentration "thinning" layer (above) from the constant settling layer (below). The lower layer interface represents the beginning of hindered settling and decreasing vertical flux rates. A conceptual sketch for settling in this regime is shown in Fig. 5-11.

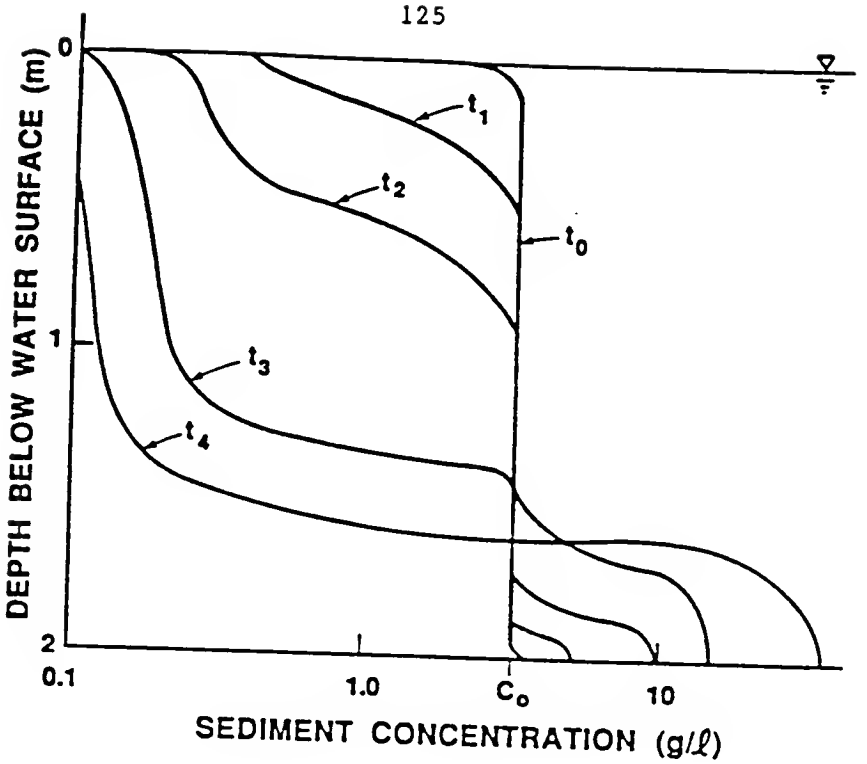

Figure 5-11. Conceptual Model for Constant Settling in Moderate Concentration Range of Flocculation Settling.

Again, time t_1 is shortly after initial mixing is stopped (t_o) and time t_4 occurs much later. Note that the actual settling velocity in the middle region (moderate settling) is not necessarily constant with time, but is locally spatially uniform.

The last regime is the high concentration (>20 g/l) hindered settling region. A characteristic feature is the decreasing sediment flux with increasing concentration. Concentration in this region is increasing everywhere with time. Flocs are closely spaced with little room for differential settling. Thus, the system settles in mass. This layer builds up as long as the flux from the intermediate and thinning layers exceeds the flux in the upper regions of this layer.

5.2.2 Turbulence-Enhanced Settling

Flocculation settling in the presence of turbulent shear, in most cases, results in larger aggregates and aggregates with higher densities than those under quiescent settling. Thus, the average settling velocity (see Section 3.4.2) is increased. The settling routine of the model was further tested for prototype settling using data reported by Odd and Roger (1986). As part of their report, concentration profiles were given of Parrett Estuary (a tributary of the Severn Estuary, UK) suspensions for seventy minutes during a high-water (HW) slack transition in the tide. Using data by Thorn (1981) for the concentration--settling velocity relationship (shown in Figure 2-8) for Severn Estuary sediment, the settling characteristics of a turbulent suspension profile during decelerating flow were simulated with the model. The results are presented in Figure 5-12.

The model predicts the evolution of the concentration profile with the exception of the slight smoothing of the developing fluid mud layer. This limitation may be attributed to near-bed measurement inaccuracies, horizontal effects (e.g., lateral non-uniformity) and/or model approximations.

One consequence of this particular finite difference solution is the smoothing of step changes (sharp concentration gradients) over one or two grids on either side of the location of the step. Since one-third meter vertical grids were the spatial discretization for this simulation, the upper fluid mud layer interface can appear to occur over up to a 1-2 m vertical scale. Further reduction in vertical discretization would

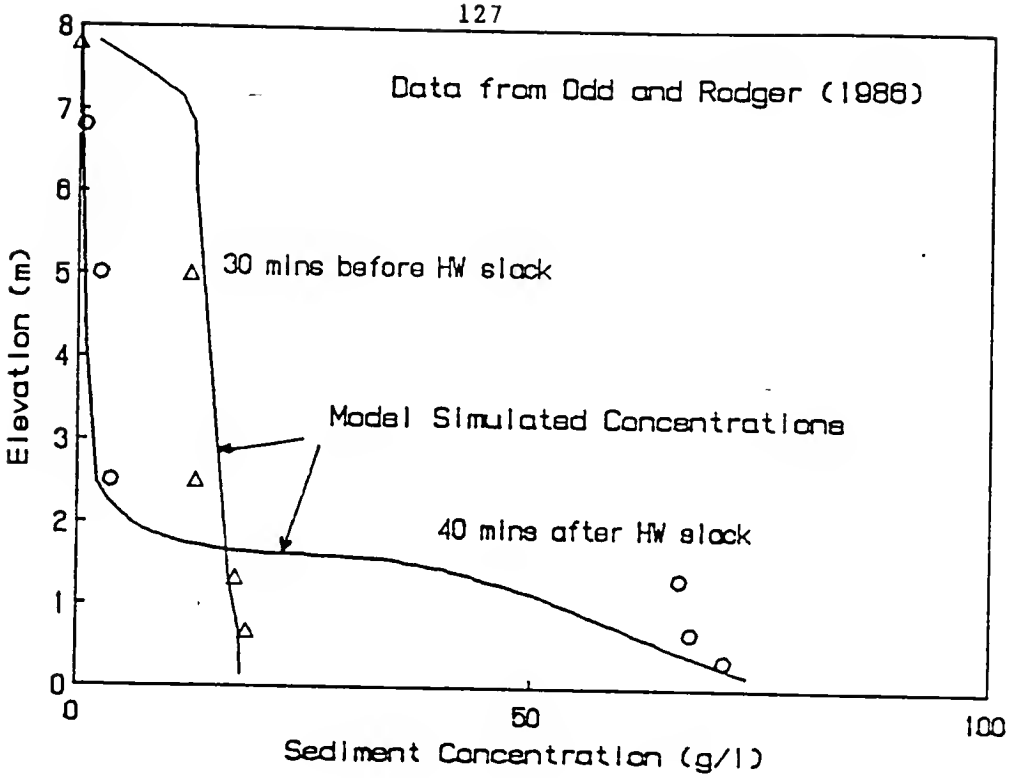

Figure 5-12. Simulated Field Settling of Parrett Estuary Suspensions.

"sharpen" interface appearance. Unfortunately, the result could be a loss in computational efficiency.

5.3 Wave Resuspension

Model simulation of the wave tank resuspension test results, described in Chapter 4, showed that a similar balance between settling and buoyancy stabilized mixing applies to vertical profiles under waves, as for unidirectional flows. However, the influence of stabilization was less significant for the wave case than the unidirectional flow case. The reasons are not clear but relevant discussion is presented in the following paragraphs.

The evolution of the vertical concentration profiles for conditions in the middle of the mud bed section (Station C, Figures 4.2a & b) were simulated for the two flume studies (Runs 1 and 2) described in Section 4.2. For model application the neutral diffusivity under waves was described by Eqn. 3.11, with $\alpha = 8.0 \times 10^{-4}$. Wave and flume characteristics for Runs 1 and 2 were summarized in Section 4.2.4 and given in Tables A.1.1 and A.2.1 respectively. The settling velocity expressions used were determined by settling column tests (Eqns. 4.5 and 4.6) and a buoyancy stabilization expression described by Eqn. 3.20 with $\beta' = 2.0$ and $\alpha' = -0.5$. Figures 5-13 and 5-14 show model simulated profiles compared with those measured during Runs 1 and 2. It can be seen that a reasonably good predictive ability of the model was achieved. The vertical mass diffusivity K_s, under waves, at least for the given conditions in the wave tank, appeared, after several trial and error simulations, to be inversely proportional to the square root of the local gradient Richardson number

$$Ks \approx R_i^{-1/2} \tag{5.8}$$

similar to what Munk and Anderson (1948) originally proposed for momentum diffusion (see Table 3.1). However, their analytical treatment towards this result was for unidirectional turbulent flow. The mass diffusivity α' constant they proposed (Eqn, 3.20) was -3/2. The reasonable predictions shown in Figures 5-13 and 5-14 with $\alpha' = -1/2$ suggest that wave mixing is less influenced by gravitational stabilization than

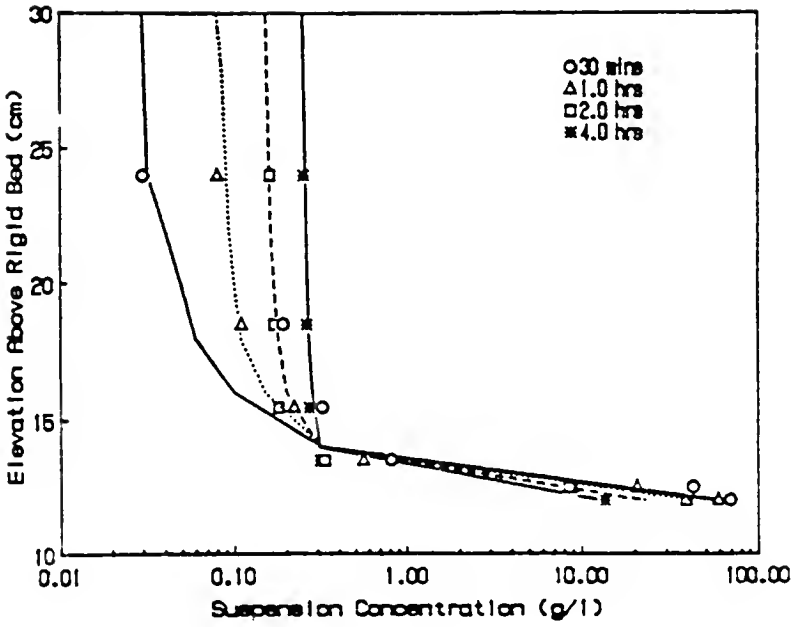

Figure 5-13. Model Simulated Versus Measured Concentrations -- Run 1.

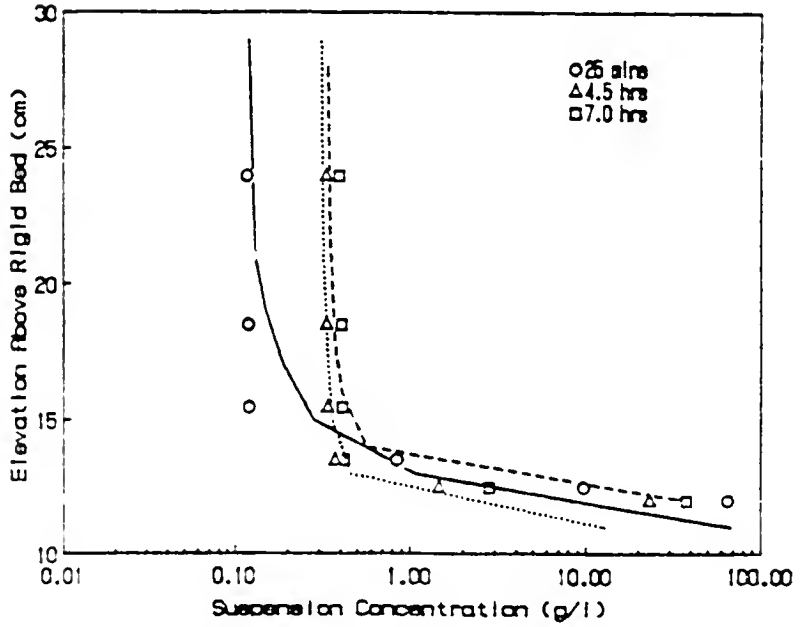

Figure 5-14. Model Simulated Versus Measured Concentrations -- Run 2.

unidirectional flows. This contrast may be due to the orbital nature of the interfacial velocities and the enhancement of instabilities at the interface (e.g., internal wave breaking, Kelvin-Helmholtz instabilities, etc.) from applied harmonic pressure gradients. More work in this area is required to further support this observation and before the exact mechanism(s) for destabilization can be quantified.

5.4 Lutocline Evolution in the Severn Estuary

The ultimate objective of the model development was to simulate high concentration vertical suspensions in the prototype environment, i.e., estuaries. While Section 5.2.2 showed predictive ability during prototype settling this section presents the results, followed by a discussion from the application of the model to a complete erosion, entrainment, settling and deposition cycle in a high sediment transport environment.

Some of the most comprehensive field measurements of estuarine fine sediment suspension dynamics have been obtained in the Severn Estuary (and tributaries), United Kingdom (Kirby, 1986; Kirby and Parker, 1977). Because of the high concentration fine sediment suspension environment typical of that estuary, interest in sedimentation and navigation concerns has been keen. With the large tidal energy (maximum tide range of 15 m) and abundance of suspendable fine sediment, sedimentation problems are periodic and significant. Particularly, the phenomenon of spring/neap cyclic resuspension is dominant.

Spring/neap cycling is the cyclic resuspension and deposition of sediment over periods of a fortnight. Large volumes of mobile suspension result during spring tides and high flow periods and lower magnitude suspension during weaker, neap tides. During the spring to neap part of the tide cycle, decreasing kinetic energy results in less resuspension. The process is net depositional. During the neap to spring sequence increasing energy levels gradually erode the newer deposits resulting in increasing suspension levels. Long term net deposition occurs where the balance is offset in favor of the spring/neap part of the cycle. In that case, deposits remain long enough to build a sufficient shear strength to resist the next maximum shear stress during the following spring tide.

Also characteristic of the Severn suspended sediment profile are the occurrences of lutocline and fluid mud layers. Kirby (1986) reported measurements of concentration profiles and lutocline formations taken during the 1982 study in the Severn Estuary, England. The predictive ability of the vertical transport model was further tested by using one set of Severn data. For this application the parabolic form of the neutral diffusivity (Eqn. 3.10) was used. A Munk and Anderson (1948) formulation for buoyancy stabilization, (Egn. 3.20) with $\beta'=10$ and $\alpha'=2.0$ was used and a settling velocity/concentration relationship (Eqn. 3.24) with coefficients previously reported for Severn sediment (Mehta, 1986), $k_1=0.51\times10^{-3}$ m/s, $n_1=1.3$, $w_{so}=0.26\times10^{-2}$ m/s, $k_2=0.80\times10^{-2}$, and $n_2=4.65$ (see Figure 2-8). Bed flux for erosion, F_e, (see Eqn. 3.26) parameters were $\alpha_1 = 2.0 \times 10^{-4}.\exp(-2.33 * \tau_o)$ and $\tau_s = 0.2$ n/m^2. For deposition bed flux, F_d, $\tau_{bm} = \tau_{cd} = 0.1$ N/m$_2$.

The simulation of the suspended sediment profiles showed the model to be capable of tracking lutocline formation, growth and decay.

Figures 5-15 shows the model predicted lutocline levels. Also shown in Figure 5-15 is the echo-sounder measured lutocline formations reported by Kirby (1986). Figures 5-16 through 5-20 show measured and simulated concentration profiles at particular times during the simulation.

It is observed that the lutoclines become less pronounced as they rise upwards during the accelerating periods of the tide. During the decelerating flows the interface(s) settles toward the bed, all the while becoming sharper until they reach fluid mud consistency. At that point the interfaces are influenced by dewatering (specifically the length of time for the pore fluid to escape upwards through the sediment matrix). The whole process is repeated during the accelerating tidal flows (flood or ebb) on the time-scale of hours. Similarly, the process is repeated in larger magnitude over periods of days through spring/neap transitions similar to spring/neap concentration cycling.

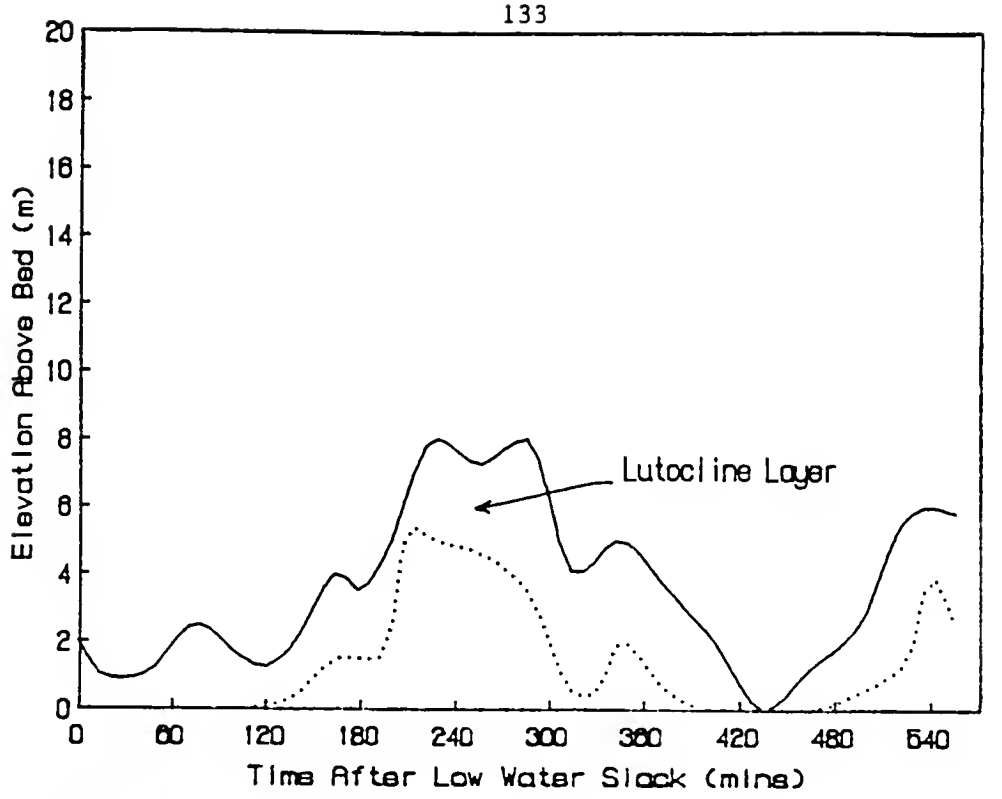

a. Measured Lutocline

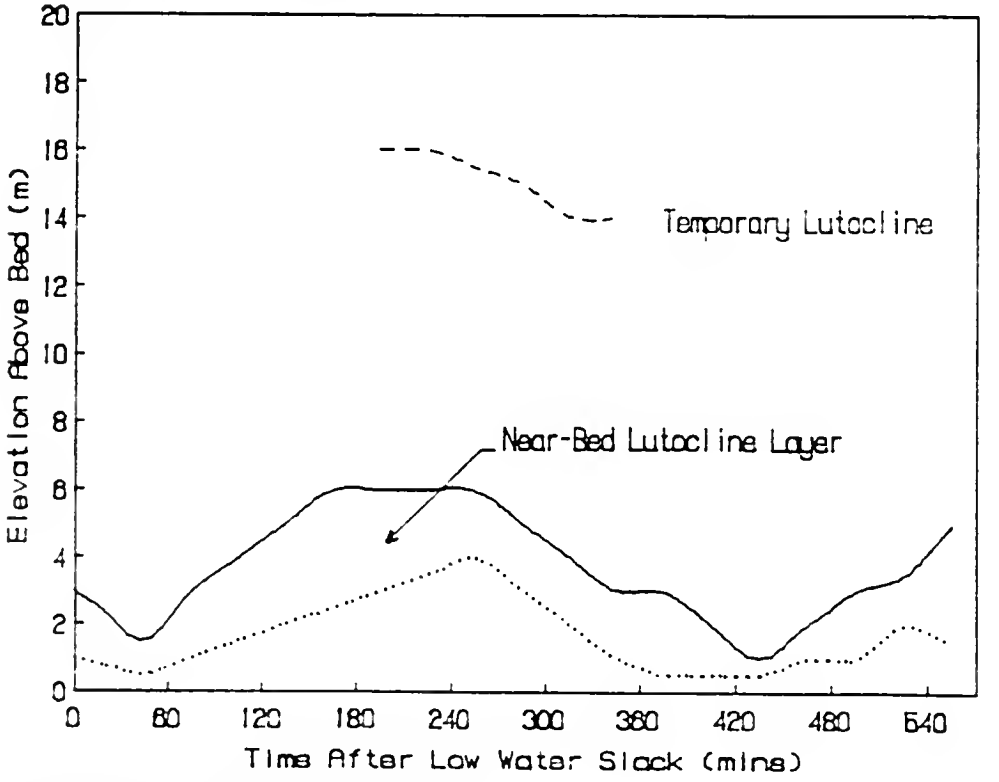

b. Model Simulated Lutoclines

Figure 5-15. Model Simulated and Measured Lutoclines -- Severn Estuary.

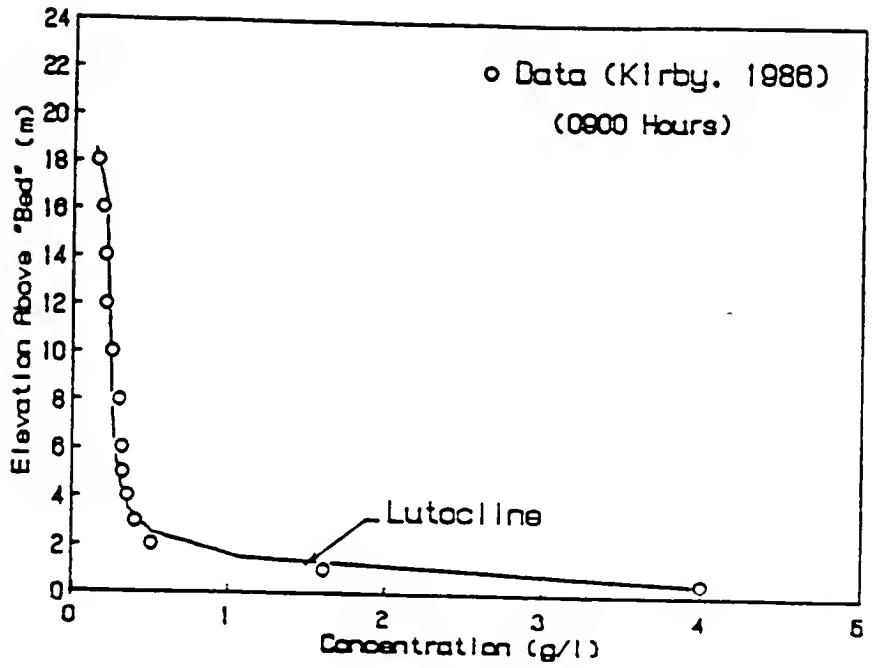

Figure 5-16. Model Simulated and Measured Concentration Profiles at 0900 hrs.

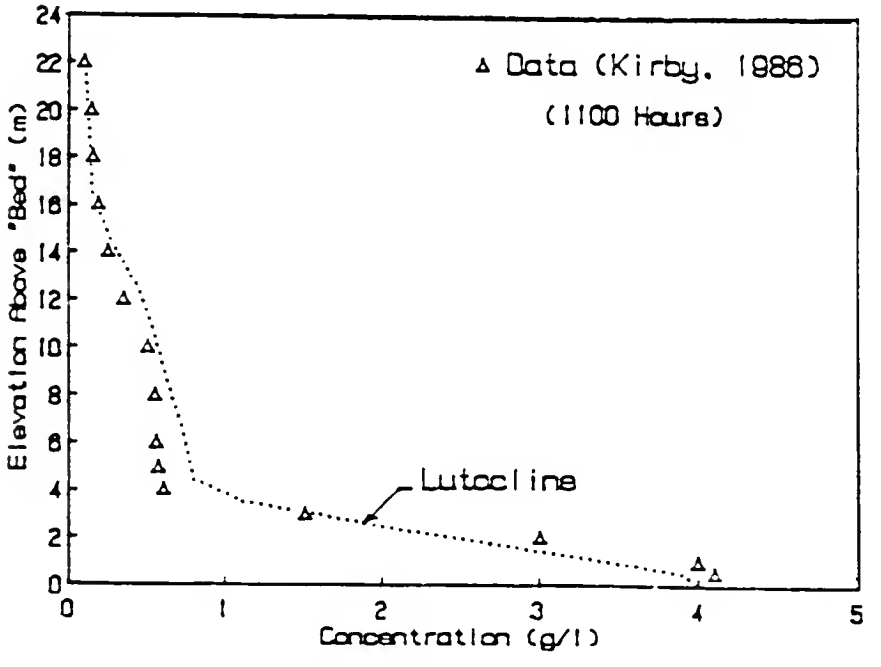

Figure 5-17. Model Simulated and Measured Concentration Profiles at 1100 hrs.

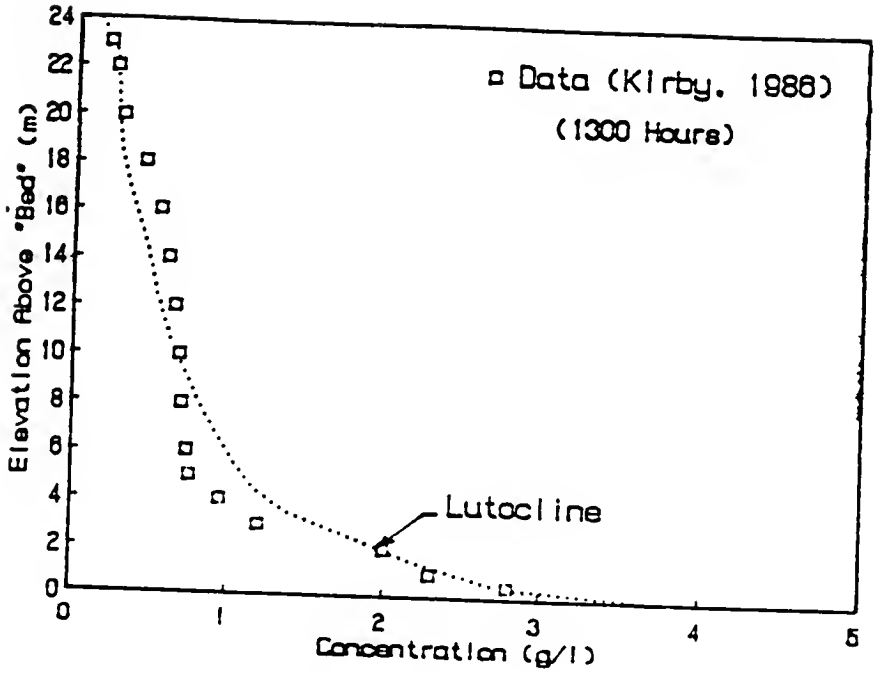

Figure 5-18. Model Simulated and Measured Concentration Profiles at 1300 hrs.

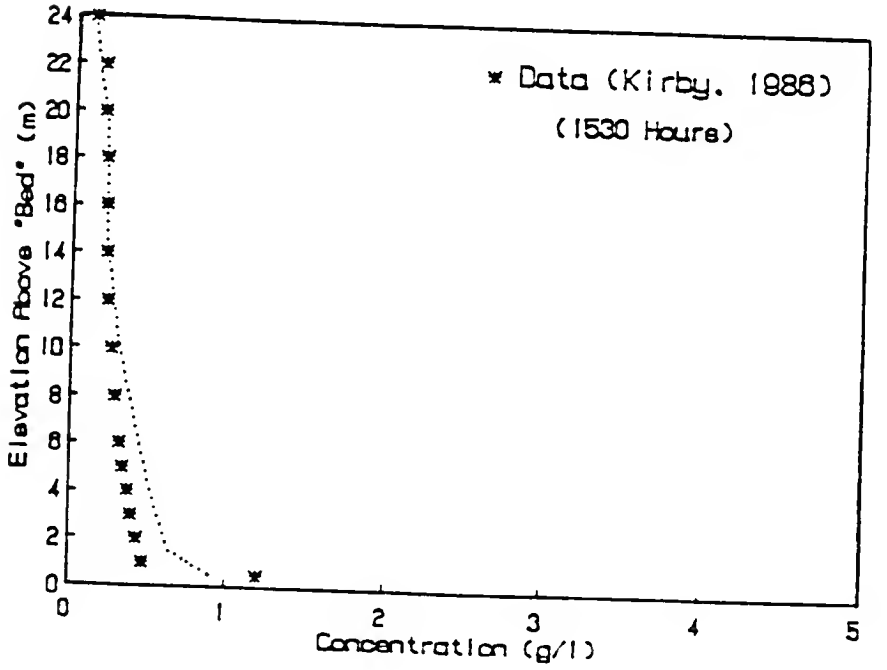

Figure 5-19. Model Simulated and Measured Concentration Profiles at 1530 hrs.

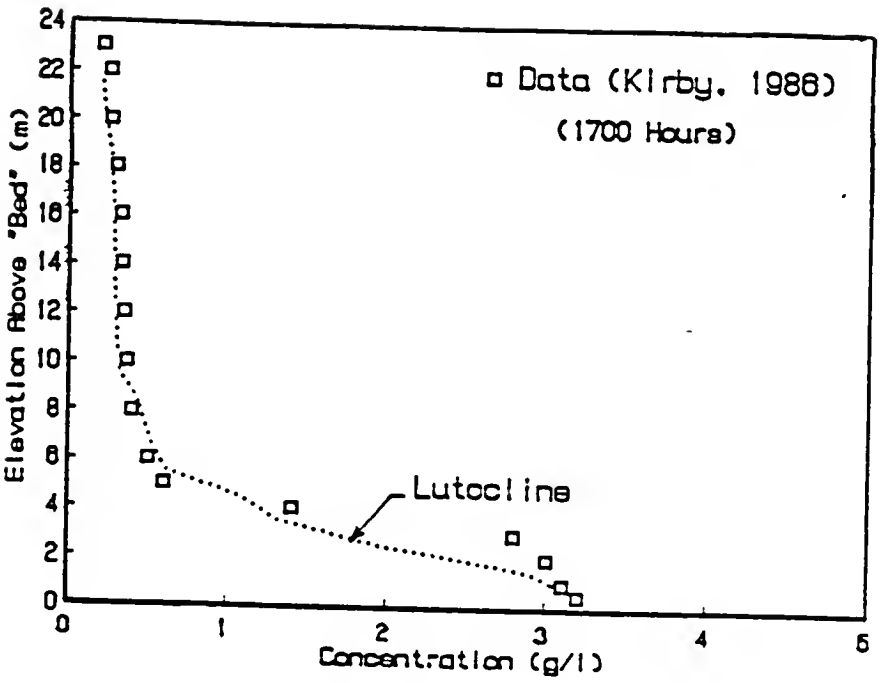

Figure 5-20. Model Simulated and Measured Concentration Profiles at 1700 hrs.

Finally, as a short addendum, an argument supportive of the use of a parabolic formulation for the vertical neutral diffusivity, K_n, can be made by noting the logarithmic shape of the velocity profiles from the Severn data (Kirby, 1986). Figure 5-21 shows six velocity profiles corresponding to the time and location of the concentration profiles already shown in Figures 5-16 through 5-20. By plotting u(z) versus ln(z), normalizing the slope by dividing by u_* and the intercept by subtracting by each intercept z_o, the data can be seen to fall on a straight line (on the semi-log graph). This indicates that the velocity profiles in the upper column, above the near-bed lutocline, represent fully developed turbulent open channel type flow (i.e., with a linear

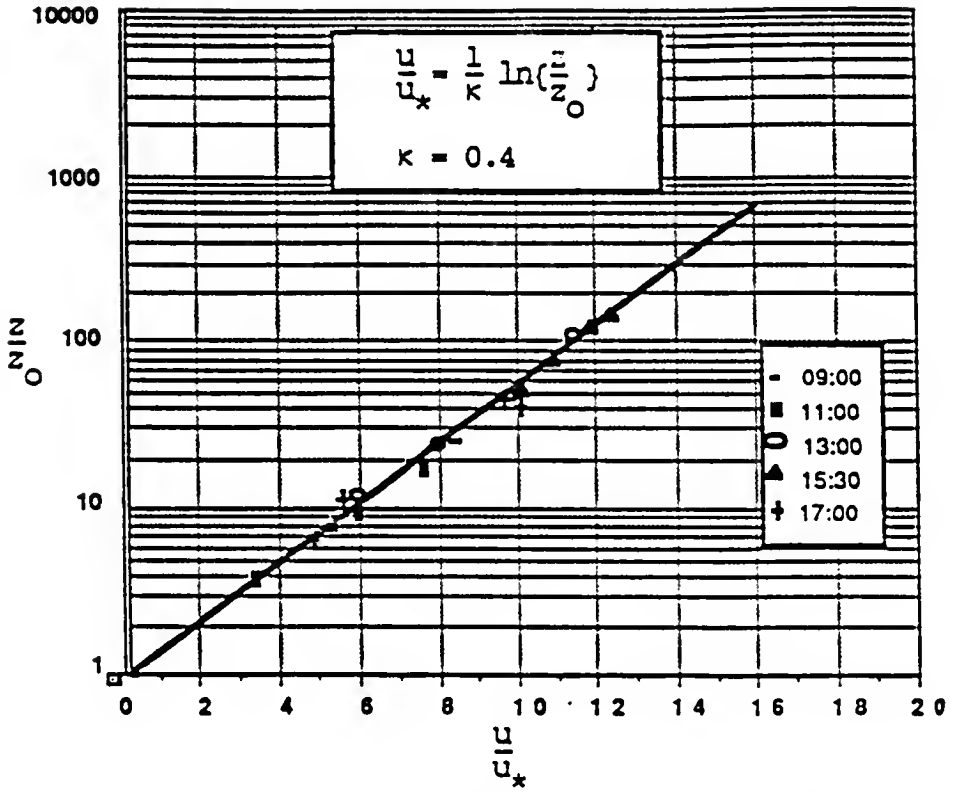

Figure 5-21. Normalized Velocity Profiles -- Severn Estuary (data from Kirby, 1986)

shear stress distribution), and thus supports the use of K_n given by Eqn 3.10.

5.5 Fluid Mud Transport

Horizontal transport in the fluid mud layers can be considered from several rheological and dynamical perspectives (examples are given in Section 3.7). As noted in Chapter 2, horizontal transport can account for order-of-magnitude higher transport rates than in the water column above. Field and laboratory data related to fluid mud flows in estuarine conditions unfortunately are sadly lacking--primarily due to the inadequacies in measurement equipment. Precise and simultaneous measurements of flow velocity and concentration profiles are required.

Many standard *in situ* means of obtaining these two measurements (e.g., with electromagnetic current meters and light attenuation photocell) while quite adequate in the upper water column, are totally inaccurate or unsuited for these near-bed, high concentration suspensions. An effort was made to quantify the mechanisms and rates of fluid mud transport in the wave tank experiments described in Chapter 4. A discussion of these results is provided in Section 5.5.1. In addition, calculations of transport rates compared to available field data (Kendrick and Derbyshire, 1985) are discussed in Section 5.5.2.

5.5.1 Wave Tank Fluid Mud Transport

Temporal changes in surface profile of the mud bed section after being subjected to wave action are shown in Figures 4-10 and 4-11. From the elevation view it is apparent that a net horizontal transport of bed material in the direction of wave propagation occurred relatively rapidly (≈ 5 min.). It is also apparent that an equilibrium profile was approached with an upward sloping form.

A crude estimate for the initial, average (over the first 5 min.) mass transport rate at the bed can be obtained by treating the bed density profiles as spatially (longitudinally) uniform with an average concentration of 120 g/l (120 kg/m^3) and by summing the volumetric quantity of material transported past the location where no change in bed elevation occurred (≈ 8 m). From Figure 5-22 the average is shown in the shaded area between 5 and 8 m from the wave maker. An average fluid mud mass transport rate of 3.6×10^{-2} kg/sec per meter width of bed is obtained.

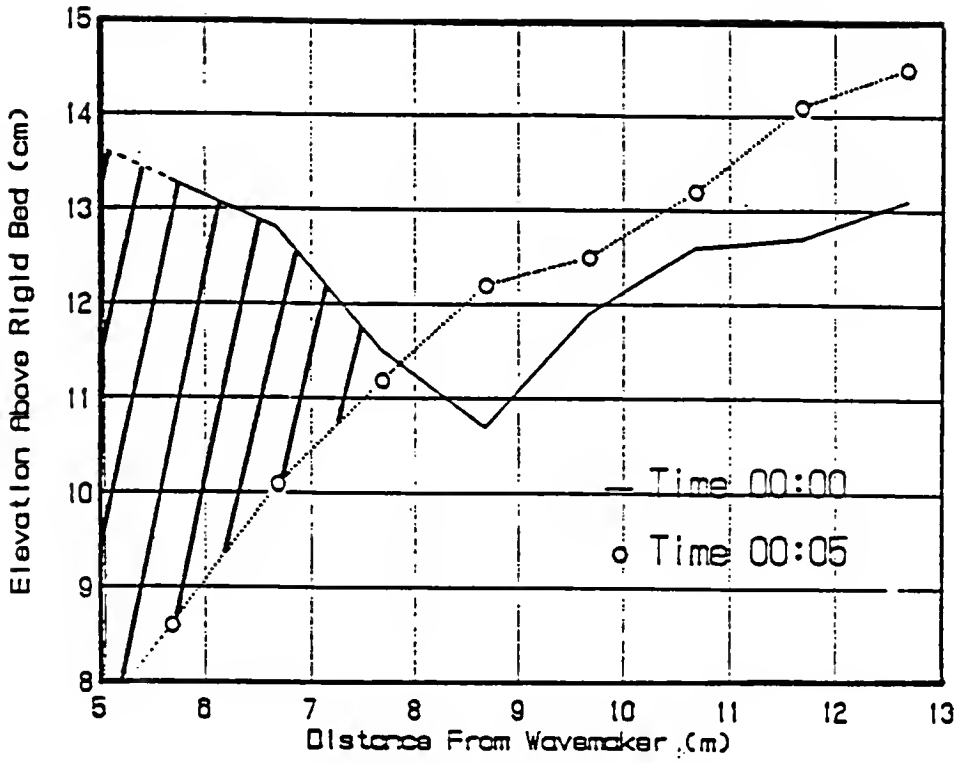

Figure 5-22. Total Fluid Mud Transport in Five Minutes - Run 1

This downstream transport in the wave tank is believed to have been driven by a wave-averaged, relatively small, imposed bed shear stress as a consequence of wave non-linearities resulting in mass transport velocities at the bed. Dean (1987) developed a graphical relationship for the wave-averaged bed shear stress from a non-linear wave theory, shown in Figure 5-23. By considering this non-linearity in the bottom velocity a rough estimate of the wave-averaged bed shear stress can be found with several crude assumptions. For conditions of the first run, i.e., wave height, (H) of 6.0 cm, water depth, (h) of 20 cm, 1 second period, (T), and equivalent deep water wave length (Lo) of 1.56 m, the wave steepness parameter (H/Lo) is 3.8×10^{-2}, and relative depth (h/Lo)

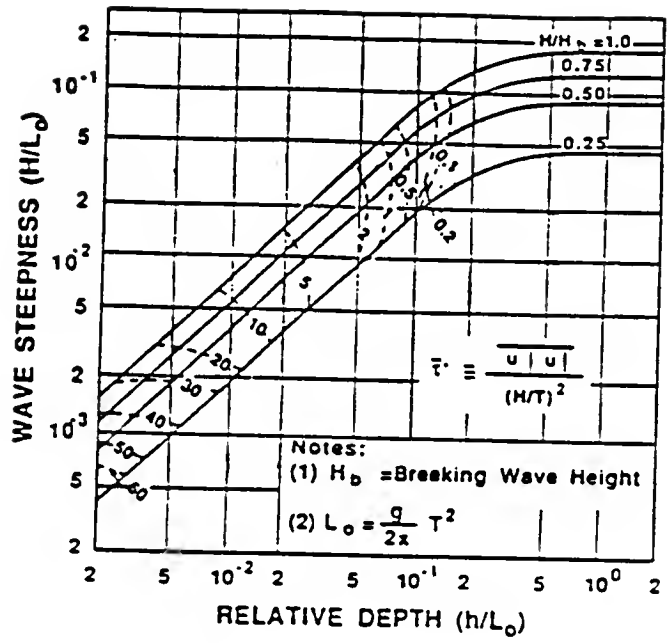

Figure 5-23. Non-Dimensional Bed Shear Stress (τ_b') Versus Wave Steepness (H/L_o) (reprinted with permission from Dean, 1987)

is 0.13. From Figure 5-23, the non-dimensional average bed shear stress,

$$\bar{\tau}' = \frac{\overline{u_b|u_b|}}{(H/T)^2} \qquad (5.9)$$

where u_b is the bottom water particle velocity. For purposes of simple calculation, using a friction factor, f=0.02, fluid density ρ=1010 kg/m^3, and wave height H=0.06 m, an average bed shear stress of approximately 0.9×10^{-2} N/m^2 is found. Using a simple first-order approximate relationship for viscosity versus concentration (Eqn. 2.6b) within the range of relationships presented in the literature (see Figure 2-6) with β_μ=0.2 and α_μ=1.0 and a depth variation in bed concentration shown in Figure 4-8, the wave-averaged velocity profile in the mobile fluid mud

layer can be found. By assuming that the horizontal pressure gradient is much less than the applied shear stress (a far reaching assumption discussed in Section 3.7), the variable viscosity Rayleigh flow model (case D, Section 3.7) can be applied with the specific boundary conditions and concentration profile determined for Run 1.

For the Run 1 data, the measured fluid mud concentrations below the visual bed (at 6 locations, n = 6, at 2 cm intervals, dt = 0.02 m), were (8, 51, 154, 168, 181, and 195 g/l). Imposing a 0.009 N/m^2 bed shear stress, the calculated velocity profile is shown in Figure 5-24.

For comparison purposes, summing the mass flux rates (uC) through each layer, i, a total transport rate of 3.3×10^{-2} kg/min is found. This qualitatively agrees with the average initial value observed (3.6×10^{-2} kg/min) in Run 1.

Because of the limiting length of the wave tank, the imposed wave-averaged shear stress is quickly balanced by gravitational effects (impending flow downhill), associated with the sloping bed. This is further supported by the fact that, upon completion of the test as the wave maker was turned off, the bed slowly (over 12-24 hrs.), crept towards a horizontal profile.

It is interesting to note that the depth of erosion in the upstream half of the bed section reached an equilibrium level (see Figure 4-10). It is speculated but no supporting evidence is presented here that this surface slope corresponds favorably with a longitudinally varying balance between the maximum bed shear stress and bed concentration dependent yield strength given by Eqn. (2.6). The downstream half of the tank was net depositional, predominantly representative of a balance between

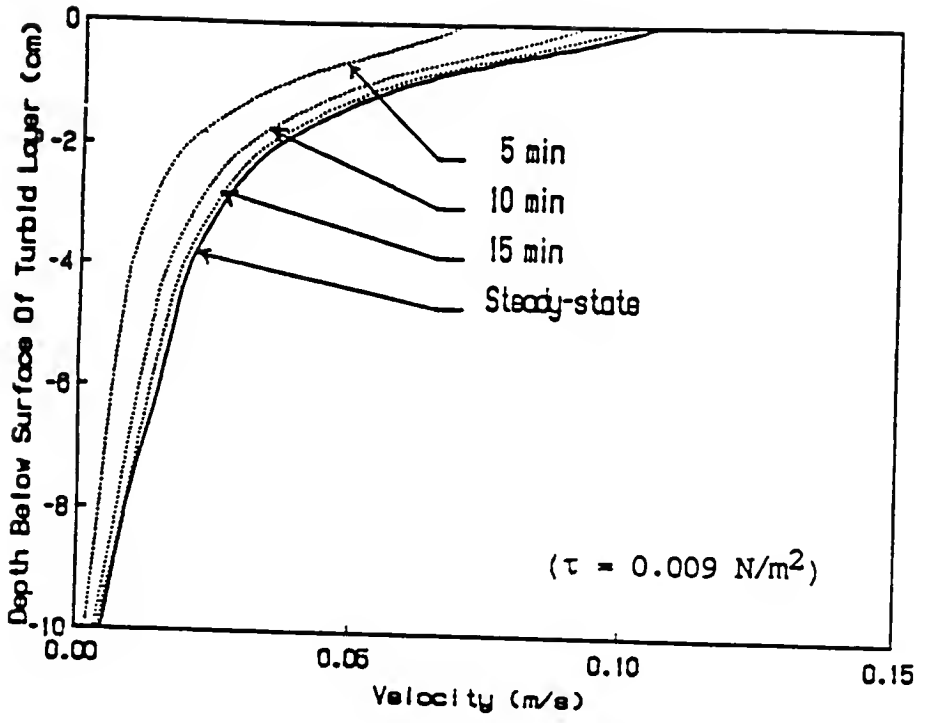

Figure 5-24. Calculated Fluid Mud Velocity Profile -- Run 1

imposed wave-averaged bed shear and gravitational body forces resulting from the sloping bed. However, a simple calculation, assuming an average ρ_m =1.06 kg/m^3 and bed slope $\Delta Z_a/\Delta x$ = 0.005 m/m yields a body force pressure gradient of 0.05 N/m^2 which is significantly higher than 0.009 N/m^2 given by the wave-averaged bed shear stress calculations. Therefore, in light of these in consistencies, further analysis was not attempted on the second set of data (Run 2).

5.5.2 Avon River Fluid Mud Transport

Kendrick and Derbyshire (1985) published results of field measurement of fluid mud flows in the Sea Mills Reach of the tidal Avon River near Bristol, United Kingdom. They used a field instrument array

capable of measuring the depth, density and velocity of the near-bed, fluid mud layer. The types of instrumentation included an underwater assembly which consisted of a 3 m-long streamlined rod fitted with a fin and suspended from an electro-mechanical cable. At the lower end of the rod a gamma-ray transmission probe was attached in a horizontal orientation. An electro-magnetic current meter probe, mounted at the same elevation, provided density and velocity data. A pressure transducer and compass were installed at the top of the rod to provide relative depth and velocity direction measurement. By raising and lowering the probe from the survey vessel, continuous profiles of fluid mud data (e.g., velocity, concentration, thickness) were recorded.

Figure 5-25 shows the measured concentration profile and the observed velocity magnitudes for a near-slack water condition from the Kendrick and Derbyshire (1985) data. The profiles depict nearly exponentially decaying velocity and linearly increasing concentration with depth. Also plotted (dotted line) is the resulting depth variation in horizontal flux (u(z).c(z)). Note that the maximum flux ($\approx$ 6.0 kg/m^2-s) occurs well below the surface of the turbid layer where the velocities are relatively low ($<$ 0.1 m/s). This is an order of magnitude higher than the flux that would be expected under near-slack conditions with, for example, u = 0.5 m/s and c = 1 kg/m^3 resulting in a horizontal flux, F_h = 0.5 kg/m^2-s in the upper water column (mobile suspension layer).

In light of the appreciable importance of the transport capacity of the fluid mud layer, the data of Kendrick and Derbyshire (1985) provide a means of testing the horizontal transport models presented in Chapter 3 (Section 3.7). One calculation approach, the unsteady depth variable

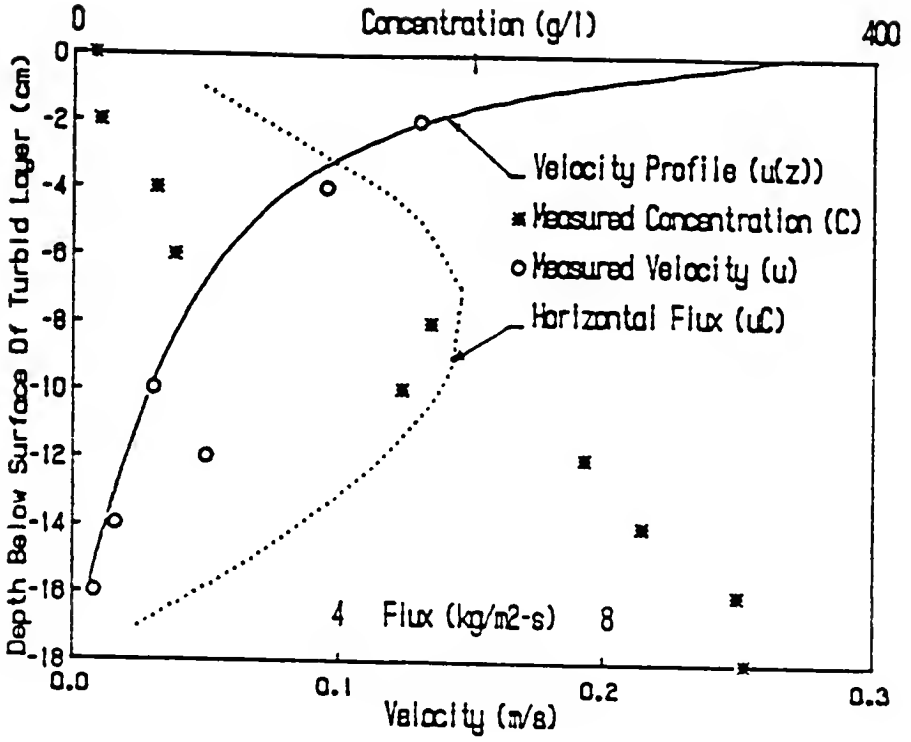

Figure 5-25. Measured Fluid Mud Concentration, Velocity and Horizontal Flux -- Avon River (data from Kendrick and Derbyshire, 1985)

viscosity solution (case D, Section 3.7) proved useful in estimating transport rates and momentum diffusion depth.

For the numerical solution of Eqn. 3.34, physical and numerical conditions specified for case D were required. First, a concentration dependent viscosity relation, as presented in Chapter 2 (Eqn. 2.6b), with β_μ and α_μ equal to 0.2 and 1.0 respectively was assumed valid (for justification see Section 2.4.1). Second, a constant interfacial shear stress was applied. In this regard, it must be pointed out that the report by Kendrick and Derbyshire (1985) did not present upper column flow conditions from which the exact magnitude of the interfacial shear stress could be determined. For this reason only a crude estimate for this value was used (τ_b = 0.02 N/m^2). For differencing, the number of

grids used was 9 with vertical increment of .02 m and the time step was 4 s. Concentrations in each grid were 10, 35, 75, 120, 165, 210, 255, 305, and 355 g/l, respectively. The no-slip velocity boundary condition was applied at the lowest grid boundary.

Figure 5-26 shows the results for the 0.02 N/m^2 applied shear stress. It is noted that qualitative agreement in form is achieved. One important observation from these results is that a very small applied shear stress (order 10^{-2} N/m^2) resulted in appreciable (order 1-10 cm/s) horizontal velocities in this layer. What is not known from this approach is the relative length of time to achieve these relatively large velocities because the exact definition of τ_o was unknown.

Finally, it was desired to calculate the total horizontal transport (per unit width) rates, T_h, given as,

$$T_h = \int F_h(z).z.dz \qquad (5.10)$$

summed over time, $\int T_h.dt$, for both the upper mobile suspension layer ($0 \leq z \leq Z_a$) and the mobile fluid mud layer ($Z_a \leq z \leq Z_b$), over a tide cycle. For an assumed water depth of 10 m, average sediment concentration of 0.3 kg/m^3, 24 hour (diurnal) tide cycle, and maximum upper column velocity (averaged over depth) of 1.3 m/s, the average mass transport over the first 6 hours of positive flow velocities was 50.7 x 10^3 kg/m.

In comparison, for the concentration profile data shown in Figure 5-25, and calculated velocities from the unsteady model (case D, Section 3.7), the total transport contribution from the mobile fluid mud layer

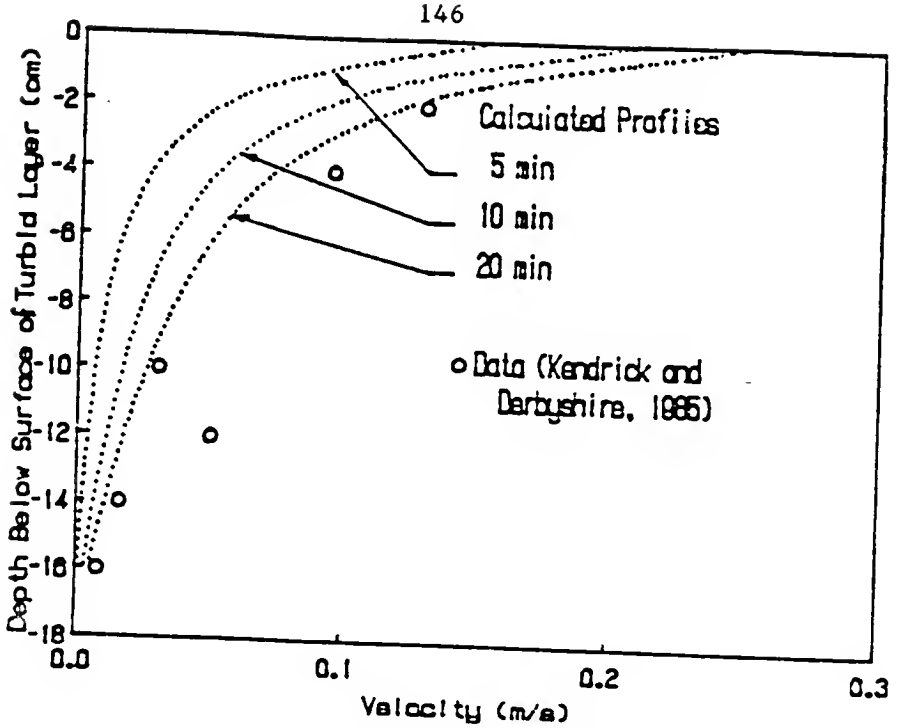

Figure 5-26. Calculated and Measured Horizontal Fluid Mud Velocities

(assuming concentrations and thickness remained constant) was 59.9 x 10^3 kg/m. The above calculation, while quite qualitative, illustrates the importance of transport in the mobile fluid mud layer. In this example, less than 2% of the flow depth (the mobile fluid mud layer) contributed more than 50% of the horizontal mass transport. For a fluid mud layer which becomes thicker under erosion (e.g., as in the Severn Estuary), the contribution to the horizontal mass transport would be expected to be greater.

CHAPTER 6
CONCLUSIONS AND RECOMMENDATIONS

6.1 Conclusions

The vertical concentration profile of estuarine fine sediment suspensions is governed by the vertical gradient of both upward mass diffusive (mixing) flux and downward gravitational settling flux. It is also dependent on the sediment flux across the bed boundary. Characteristics of the profile include lutocline layers (regions of sharp concentration gradients) in the upper column and near bed fluid mud (see Chapter 2, Section 2.1 for definitions).

In order to better understand the mechanisms which influence the vertical structure, a one-dimensional vertical mass transport (diffusion) equation was used to solve for C(z,t). Parametric relationships between settling velocity, w_s, and concentration, C, and between diffusivity, k_z, and concentration gradient, $\partial C/\partial z$, were used in the analysis. Application to data from settling column tests, wave flume resuspension tests and field investigations provided reasonable predictive agreement.

The horizontal, viscous shear flow equation, solved numerically, was used to provide estimates for the relative mobility and sediment transport potential of the fluid mud layer relative to that of the upper column suspension.

The following specific conclusions can be drawn from this study:

1) Lutoclines are formed as a result of the non-linearity between diffusive flux, F_d, and concentration gradient, $\partial C/\partial z$. A lutocline layer, the region over which $\partial C/\partial z$ is maximum, is a region over which vertical mixing is minimal. Buoyancy stabilization, turbulence dampening caused by a large potential energy gradient (arising from a large density gradient), reduces the diffusivity, k_z, locally to very small values. Expressions for buoyancy stabilization, originally developed for thermal and salinity stratification, as a function of gradient Richardson number, Ri (Eqn. 2.11), in the Munk and Anderson form as

$$\frac{K_s}{K_n} = \varepsilon(1 + \beta' Ri)^{-\alpha'} \qquad (6.1)$$

are quite useful in quantifying diffusion dampening from large suspended sediment concentration gradients. Because Ri is a function of $\partial C/\partial z$ and assuming Fickian diffusion where, $F_d = K_z\, \partial C/\partial z$, for $K_z = K_s$, the relationship between F_d and $\partial C/\partial z$ ($F_d(\partial C/\partial z)$) is highly non-linear. This was shown for two commonly used forms of Eqn. 6.1 in Figure 3-1. The effect of sediment settling tends to further stabilize the lutocline layer thereby making lutoclines much more persistent in high energy environments than other types of pychnoclines (e.g., haloclines). Because fine sediment settling velocity is a function of concentration, generally increasing velocity in the flocculation settling range ($0.1 < C < 3$ g/l) (e.g., Eqn. 3.24) results in increasing downward settling flux across the lutocline, in turn decreasing the net upward entrainment and

"sharpening" the interface. This results in a further decrease in vertical diffusivity and an increase in lutocline stabilization.

2) Near bed fluid mud results from rapid deposition or erosion (or fluidization). During deposition, if the rate of deposition, $F_p = Pw_sC$, exceeds the rate at which sediment develops structural integrity (effective stress), fluid mud will form. This is nearly always the case for cohesive sediment at relatively high suspension concentrations because hindered settling results in decreasing settling flux with increasing concentration (i.e., $C \geq 20$ g/l). The concentration (at which bed formation occurs) being high (e.g., 200 g/l) causes sediment to "bunch up" near the bed.

For fluid mud formation by rapid erosion (or fluidization) the rate at which bed material loses structural integrity must be greater than the rate at which sediment is entrained into the upper well mixed mobile suspension layer i.e., $F_e(Z_c) > F_d(Z_a)$. For example, wave action has been shown to result in fluid mud formation by rapid destruction of bed effective stress resulting in fluidization with little vertical entrainment (Section 4.2.5). Measured total and pore pressures and concentrations under wave loading in a laboratory flume showed that destruction of effective stress occurred with little change in near bed concentration. While no unique concentration was found to correspond to the development of effective stress it was noted that effective stress generally occurred for concentrations usually > 170 g/l. This transition corresponds, crudely, to discontinuities in concentration profile which developed with time after wave loading (Figure 4-12).

3) Pertaining to the structure of the fluid mud layer, several important points can be made. First, the upper interface of the fluid mud layer, Z_a in the definition Figure 2-1, was found to correspond to the hindered flux (from settling) concentration, C_h, (in quiescent settling), and to the maximum net downward flux (sum of settling and diffusive fluxes) when mixing occurred. The hindered settling concentration, C_h, for Severn Estuary and Tampa Bay muds was found to be $\approx$ 20 g/l (see Figures 2-9 and 5-1). This concentration, which was observed at the upper fluid mud layer in both settling column tests (Figures 5-4 through 5-9) and wave flume tests (Figures 5-13 and 5-14) using Tampa Bay mud is indicative of the very low vertical mixing characteristic of both types of tests. In data from the Severn Estuary (Kirby, 1986), under turbulent tidal flows with a maximum flow velocity $>$ 1.0 m/s, considerable reduction in C_h was observed (e.g., $1 \leq C_h \leq 4$ g/l, as a lower limit, see Figures 5-16 through 5-20). Furthermore, high concentration gradients associated with the upper fluid mud interface were found to greatly dampen the vertical entrainment of eroded or freshly deposited bed material in the Severn Estuary runs (Section 5.4). The Munk and Anderson (Eqn. 6.1) form for buoyancy stabilization of turbulent diffusivity proved adequate in concentration predictions in both upper column mixing and near bed fluid mud entrainment.

4) The kinematics of the mobile fluid mud layer, for a particular set of assumptions, were found to be reasonably well represented by the unsteady shear flow equation (Eqn. 3.34) with concentration dependent viscosity (Section 3.7, case D). While the exact magnitude of the imposed interfacial shear stress was unknown for the data of Kendrick and

Derbyshire (1985), for a shear stress of 0.02 N/m^2 (a reasonable near slack tide value), the resulting velocity profile after twenty minutes seemed to fit the measured velocity data (Section 5.5). Therefore, where calculations of the lower limit of horizontal momentum diffusion (and the zero velocity mobile/stationary interface elevation) for unsteady fluid mud flow under an imposed shear is the objective, numerical solution of Eqn. 3.34 with appropriate formulation for $\mu(C)$ may be valid. Through calculation of the horizontal velocities, the importance of horizontal advective transport of the mobile suspension layer was shown. With the assumption of a sinusoidal variation in interfacial shear stress and no dissipation (from entrainment), the total horizontal sediment transport for the mobile fluid mud layer was (conservatively) shown to be of the same order as the transport in the mobile upper column suspension layer. Under other conditions it could be orders of magnitude greater than the upper column transport.

In regards to laboratory studies presented in this report, two contributions to procedure and understanding stand out.

First, a laboratory procedure designed to measure bed effective stress during dynamic wave loading provided insight into the mechanisms of bed fluidization from waves. Sensitive commercially available miniature pore pressure gages (Druck model PDCR81) and total pressure gages (Druck model PDCR135A/F) mounted side by side at multiple depths below the "visual" bed allowed measurement of the effective stress profile. Interpolation between elevations with zero and non-zero measured effective stress provided estimation of the bed elevation as defined in Chapter 2 (beginning of effective stress, see Section 2.3). It

is speculated (but no supporting analysis is provided) that bed liquefaction (fluidization) under waves occurs from two mechanisms--termed "shaking" and "pumping". Shaking is the action of oscillatory shear stress applied at the bed/suspension interface which transmits to elastic or viscoelastic motion within the bed resulting in structural failure. Pumping is the buildup of excess pore pressure due to gradients in hydrodynamic pressures under waves and the impermeable nature of cohesive fine sediment beds.

Second, a new procedure for measuring settling velocity characteristics of fine sediment suspension has been proposed which provides a direct measure of concentration and settling velocity variation with time and depth. From discrete $C(z,t)$ measurements in a settling column, numerical solution of the settling equation (Eqn. 4.3) for $w_s(z,t)$ can be carried out. Large quantities of data are provided from relatively few tests providing adequate averaging of $w_s(C)$ from which functional relationships for concentration enhanced (e.g., Eqn. 3.24) and concentration hindered settling (e.g., Eqn 3.25) can thus be found.

Finally, it was an early objective of this research to determine a precise definition for fluid mud based on concentration (or density). Ideally, it would be convenient to define concentrations, C_a and C_c, for the upper and lower extremes of fluid mud applicable to typical estuarine fine sediment or, at most, related to sediment properties alone. However this was shown to be impractical since the role of flow properties in fluid mud formation and transport were found to be of first order importance. Rather than totally abandon this goal an "operational" or

rule-of-thumb definition is instead proposed based on empirical results which at best should only be considered to be of order of magnitude accuracy. First, since the upper interface has been shown to correspond to the hindered settling flux concentration, C_h, which seems to occur between 10 to 20 g/l, a reasonable estimate for the lower density range is then $\rho_{fm} \geq 1.01$ kg/m^3. Second, because structural properties (effective stress) were observed in Tampa Bay mud for both tests in concentrations above 170 g/l and because Been and Sills (1981) found non-zero effective stress in all of their experiments in concentrations only slightly higher than the above value ($\approx$ 200 g/l), the operational upper density is proposed as $\rho_{fm} \leq 1.1$ kg/m^3. Thus a crude rule-of-thumb density range fluid mud is $1.01 \leq \rho_{fm} \leq 1.1$ kg/m$_3$ which can be seen to be exactly what Krone (1962) proposed (see Table 2-1) 26 years ago (but with little physical justification).

6.2 Recommendations

The dynamic formation, growth and dissipation mechanisms of fluid mud and lutocline layers under waves and currents are far from being fully understood. Simple relationships for entrainment from (and buoyancy stabilization of) the upper fluid mud interface, Z_a, (or across any lutocline) as a function of gradient (or bulk) Richardson number (e.g., Eqn. 3.20 or 3.31), while adequate for first order approximations, are quite simplistic. Much of the physical process of interfacial instability has been omitted. For instance, surface waves may enhance instabilities in conjunction with uni-directional currents resulting in higher entrainment rates. Promise is shown in the area of turbulence

modeling where better definition of $K_z(z)$ can be made by calculating ensemble averages for turbulent fluxes (u'c').

Functional relationships for sediment mass flux from the bed surface (i.e., erosion or deposition flux) and the physics from which they are based, previously defined for mobile suspension/bed interfaces (with no fluid mud layer), may not be adequate for the inverse condition (with fluid mud layer). The stationary fluid mud layer may act to either buffer hydrodynamic forcing (e.g., bed shear stress) by turbulence dampening thereby diminishing erosional bed flux or accentuate erosive conditions because of the added mass density.

Lastly, it is strongly felt that transport modeling of fine sediment environments, where erosion and deposition are important, must include better definition of the time and depth variation of the bed. Sediment that is deposited during decelerating flow conditions slowly consolidates with structural properties dependent on the properties of the sediment (e.g., composition), flow (e.g., turbulent shear), and consolidation history (e.g., overburden). The transition from suspension (which could be stationary fluid mud) to structured bed varies with time and depth (with respect to some fixed datum). Depending on the degree of severity of the next erosion phase, the applied bed shear stress can mobilize all or part of the previous deposit. For example, during the spring to neap part of the tide the near bed is net-depositional as deposition and consolidation exceed erosion rates because of the decreasing (averaged over one cycle) tidal energy. During neap to spring the process is reversed as erosion rates exceed deposition and previously consolidating sediment is resuspended. A dynamic fluid mud through consolidating bed

transition model, along the lines proposed by Schiffman et al. (1986) for quiescent settling, would allow layering of this region with better refinement in quantifying mobile fluid mud layer growth and decay, transition in the mobile/stationary fluid mud interface (elevation Z_b) and transition in the stationary fluid mud/bed interface (elevation Z_c), as well as depth variation in bed properties.

APPENDIX A
DIMENSIONAL ANALYSIS OF TRANSPORT EQUATION

The sediment transport equation for sediment suspension concentration, C, (Eqn. 3.1) in cartesian (x,y,z) coordinates, averaged over the time scale of turbulence (see Section 3.2), is written

$$\frac{\partial C}{\partial t} + u\frac{\partial C}{\partial x} + v\frac{\partial C}{\partial y} + w\frac{\partial C}{\partial z} = \frac{\partial C}{\partial z}(w_s C) + \frac{\partial}{\partial x}(K_x\frac{\partial C}{\partial x}) + \frac{\partial}{\partial y}(K_y\frac{\partial C}{\partial y}) + \frac{\partial}{\partial z}(K_z\frac{\partial C}{\partial z}) \qquad (A.1)$$

where u,v,w are velocity components in x,y,z direction, w_s is the sediment settling velocity, and K_x,K_y,K_z are turbulent mass diffusivity components.

For the purpose of determining the relative importance of lateral (x,y) versus vertical (z) advective and diffusive fluxes, it is convenient to use non-dimensional scaling arguments for the two-dimensional form (x,z) of Eqn. A.1. Order of magnitude analysis is then made of the horizontal and vertical terms for a typical estuarine condition.

For estuarine flow, averaged over the time scale of turbulence, the advective velocity w is negligibly small and is henceforth omitted from analysis. The two-dimensional form of Eqn. A.1 is,

$$\frac{\partial C}{\partial t} + u\frac{\partial C}{\partial x} = \frac{\partial C}{\partial z}(w_s C) + \frac{\partial}{\partial x}(K_x\frac{\partial C}{\partial x}) + \frac{\partial}{\partial z}(K_z\frac{\partial C}{\partial z}) \qquad (A.2)$$

Defining non-dimensional (primed) variables as

$$C' = \frac{C}{C_m} \quad , \quad t' = \frac{t}{t_o} \quad , \quad u' = \frac{u}{u_o} \quad , \quad x' = \frac{x}{L} \quad , \quad z' = \frac{z}{H} \quad ,$$

$$w_s' = \frac{w_s}{w_{sm}} \quad , \quad K_x' = \frac{K_x}{H^2}\, t_o \quad , \quad K_z' = \frac{K_z}{H^2}\, t_o \qquad \text{(A.3)}$$

where the symbols with m or o subscripts are characteristic maxima and thus each primed variable is of order 1. The factors L and H are the estuary length and depth dimensions, respectively. The term t_o is a reference time scale defined below.

Substituting conditions posed by A.3 into Eqn. A.2 gives

$$[\frac{C_m}{t_o}]\frac{\partial C'}{\partial t'} + [\frac{u_o C_m}{L}]u'\frac{\partial C'}{\partial x'} = [\frac{w_{sm} C_m}{H}]\frac{\partial C'}{\partial z}(w_s'C') + [\frac{C_m H^2}{t_o L^2}]\frac{\partial}{\partial x}(K_x'\frac{\partial C'}{\partial x}) + [\frac{C_m}{t_o}]\frac{\partial}{\partial z}(K_z'\frac{\partial C'}{\partial z})$$

(A.4)

where all terms not in brackets, [ ], are order 1. Multiplying Eqn. A.4 through by $[\frac{t_o}{C_m}]$ gives,

$$[1]\frac{\partial C'}{\partial t'} + [\frac{u_o t_o}{L}]u'\frac{\partial C'}{\partial x'} = [\frac{w_{sm} t_o}{H}]\frac{\partial C'}{\partial z}(w_s'C') + [\frac{H^2}{L^2}]\frac{\partial}{\partial x}(K_x'\frac{\partial C'}{\partial x}) + [1]\frac{\partial}{\partial z}(K_z'\frac{\partial C'}{\partial z})$$

(A.5)

for a reference time scale, t_o, equal to the maximum sediment settling time, H/w_{sm}, Eqn. A.5 becomes

$$[1]\frac{\partial C'}{\partial t'} + [\frac{u_o H}{L w_{sm}}]u'\frac{\partial C'}{\partial x'} = [1]\frac{\partial C'}{\partial z}(w_s'C') + [\frac{H^2}{L^2}]\frac{\partial}{\partial x}(K_x'\frac{\partial C'}{\partial x}) + [1]\frac{\partial}{\partial z}(K_z'\frac{\partial C'}{\partial z})$$

(A.6)

and the relative importance of each term (since all the primed terms are

order 1) is given by the numerical value of the bracketed term.

For an estuary, the depth is much less than the length and therefore $1/L^2 << 1/H^2$ and $H^2/L^2 << 1$. Thus the horizontal diffusivity gradient is negligible for first order calculations. For the horizontal advective flux gradient to be < order 1,

$$[\frac{Hu_o}{w_{sm}L}] < 1 \qquad (A.7a)$$

or

$$[\frac{H}{w_{sm}}] < [\frac{L}{u_o}] \qquad (A.7b)$$

For a typical estuary, $L = 10 \rightarrow 10^2$ km, $H = 10^0 \rightarrow 10^1$ m, $u_o \approx 10^0$ m/s, and $w_{sm} = 10^{-3} \rightarrow 10^{-2}$ m/s. The numerical mid-range value for

$$[\frac{Hu_o}{w_{sm}L}] \text{ is } 10^{-1} \rightarrow 10^{-2} \qquad (A.8)$$

which satisfies the condition given by Eqn. D.7.

Note that H/w_{sm} is a characteristic time of settling, ts, and L/u_o is the advective travel time, t_l, through the estuary. Eqn. A.7 holds true when the travel time through the estuary is greater than the time of settling i.e, $t_l > t_s$. Under these conditions

$$\frac{\partial C}{\partial t} = \frac{\partial}{\partial z}(w_s C + K_z \frac{\partial C}{\partial z}) \qquad (A.9)$$

applies.

APPENDIX B
DATA ON WAVE RESUSPENSION TESTS

A.1 Run #1 Data -- 7/30/86

Table A-1. Wave Data (Period, Length, Height and MWS Elevation), Run 1

Wave Data	Time (hrs:mins) 00:00	00:15	00:30	01:00	02:00	03:00	04:00	05:00	06:00	13:30
	Gage #0 (Location 4.14m)									
H_{rms}(cm)	0.1	8.1	8.1	8.6	8.1	8.1	8.4	8.0	8.3	8.4
MWS (cm)	31.8	31.8	31.8	31.9	31.8	31.8	31.8	31.8	31.8	31.9
	Gage #1 (Location 6.19m)									
H_{rms}(cm)	0.2	5.3	5.6	6.9	7.1	7.6	7.4	7.4	7.5	8.3
MWS (cm)	31.7	31.6	31.5	31.5	31.4	31.4	31.4	31.4	31.3	31.1
	Gage #2 (Location 8.67m)									
H_{rms}(cm)	0.1	4.7	5.2	5.8	6.1	6.4	5.9	6.2	6.3	6.1
MWS (cm)	31.8	31.6	31.5	31.4	31.4	31.3	31.4	31.4	33.3	31.4
	Gage #3 (Location 12.0m)									
H_{rms}(cm)	0.1	2.9	3.4	3.9	4.8	5.3	4.7	4.5	4.9	4.5
MWS (cm)	31.8	31.6	31.6	31.5	31.5	31.5	31.5	31.5	31.4	31.5
	Bed-Averaged Values									
T_*(sec)	1.5	1.1	1.1	1.0	1.0	1.0	1.0	1.0	1.0	1.0
L^* (m)	2.02	1.42	1.44	1.34	1.34	1.31	1.34	1.38	1.38	1.31
H (cm)	0.1	4.4	4.9	5.6	6.0	6.4	6.0	6.1	6.3	6.3
h (cm)	31.8	31.6	31.5	31.5	31.4	31.4	31.4	31.4	31.3	31.3

L^* - Wavelength measured between wave gages 1 and 2.

Table A-2. Visual Bed Elevations (cm), Run 1

Location (m)	Time (hrs:mins) 00:00	00:15	00:30	01:00	02:00	03:00	04:00	05:00	06:00	13:30
12.7	13.1	14.9	14.9	14.6	14.1	14.2	14.0	14.1	14.1	13.6
11.7	12.7	14.4	14.1	14.0	13.7	13.6	13.4	13.4	13.6	12.9
10.7	12.6	13.5	13.5	13.4	13.4	12.8	12.9	12.7	12.6	12.2
9.7	11.9	12.7	12.6	12.4	12.3	12.2	12.2	12.1	11.9	11.8
8.7	10.7	12.3	12.1	12.0	11.9	11.7	11.8	11.7	11.4	11.3
7.7	11.5	10.9	11.1	11.3	10.9	10.8	10.7	10.8	10.5	9.9
6.7	12.8	9.3	9.7	9.8	9.8	9.8	9.7	9.6	9.4	8.9
5.7	13.3	8.4	8.5	8.3	8.3	8.4	8.5	9.0	8.6	8.2
AVG	12.3	12.1	12.1	12.0	11.8	11.7	11.7	11.7	11.5	11.1

Table A-3. Wave-Averaged Bed Pressures (kPa), Run 1

Gage #	(cm)	Time (hrs:mins) 00:00	00:15	00:30	01:00	02:00	03:00	04:00	05:00	06:00	13:30
		Pore Pressure Gages									
4	7.4	3.47	3.47	3.37	3.36	3.36	3.37	3.36	3.46	3.44	3.43
5	12.0	2.82	2.80	2.77	2.77	2.75	2.77	2.76	2.76	2.76	2.75
6	9.4	3.19	3.17	3.15	3.17	3.16	3.15	3.17	3.18	3.14	3.13
7	-	-	-	-	-	-	-	-	-	-	-
		Total Pressure Gages									
12	11.6	2.89	2.86	2.83	2.84	2.82	2.83	2.82	2.82	2.81	2.81
13	9.3	3.23	3.21	3.19	3.20	3.18	3.16	3.16	3.16	3.16	3.15
14	7.5	3.50	3.48	3.47	3.47	3.46	3.46	3.45	3.43	3.43	3.42
15	4.7	3.93	3.92	3.92	3.93	3.92	3.92	3.91	3.89	3.89	3.87

Table A-4. Dynamic Pressure Amplitudes (0.1 kPa), Run 1

Gage #	(cm)	Time (hrs:mins) 00:00	00:15	00:30	01:00	02:00	03:00	04:00	05:00	06:00	13:30
		Pore Pressure Gages									
4	7.4	-	4.4	4.7	4.7	4.8	4.9	5.2	4.9	4.7	5.3
5	12.0	-	4.6	4.8	4.4	4.9	4.8	5.0	4.7	5.1	4.9
6	9.4	-	3.8	4.1	4.3	4.1	4.5	4.4	4.4	4.4	4.9
7	-	-	-	-	-	-	-	-	-	-	-
		Total Pressure Gages									
12	11.6	-	6.0	6.3	5.9	6.6	6.1	6.9	6.9	6.8	7.0
13	9.3	-	6.1	6.3	6.1	6.6	5.8	6.3	6.3	6.4	6.6
14	7.5	-	5.1	5.2	5.1	5.0	5.6	5.6	5.6	5.8	5.5
15	4.7	-	3.9	4.4	4.8	5.1	5.1	5.4	5.1	5.4	5.4

Table A-5. Sediment Bed Concentrations (g/l), Run 1

Elevation (cm)	Time (hrs:mins) 00:00	00:15	00:30	01:00	02:00	03:00	04:00	05:00	06:00	13:30
12.0	8.0	65.0	68.5	58.3	38.5	22.3	13.5	13.1	24.0	19.5
10.0	51.0	136.	132.	130.	127.	140.	139.	131.	128.	114.
8.0	154.	159.	153.	146.	140.	151.	150.	147.	148.	155.
6.0	168.	179.	162.	163.	155.	167.	171.	163.	158.	179.
4.0	181.	155.	170.	172.	168.	174.	182.	180.	180.	192.
2.0	195.	197.	182.	182.	185.	190.	185.	194.	182.	205.
AVG	150.	149.	145.	142.	136.	141.	140.	138.	137.	144.

Table A-6. Sediment Concentrations Station A (g/l), Run 1

Elevation (cm)	Time (hrs:mins) 00:00	00:15	00:30	01:00	02:00	03:00	04:00	05:00	06:00	13:30
26.0	0.00	0.16	0.14	0.22	0.30	0.35	0.38	0.39	0.29	0.64
20.3	0.00	0.15	0.16	0.22	0.30	0.34	0.38	0.40	0.44	0.62
17.6	0.00	0.18	0.22	0.21	0.28	0.33	0.35	0.39	0.41	0.62
15.8	0.00	0.20	0.24	0.23	0.29	0.34	0.38	-	0.42	0.60
14.7	0.02	0.56	0.98	0.21	0.30	-	0.35	0.38	0.42	0.63

Table A-7. Sediment Concentrations Station B (g/l), Run 1

Elevation (cm)	Time (hrs:mins) 00:00	00:15	00:30	01:00	02:00	03:00	04:00	05:00	06:00	13:30
26.2	0.00	0.02	0.11	0.31	0.29	0.25	0.30	0.33	-	0.60
20.6	0.00	0.02	0.30	0.34	0.29	0.27	0.34	0.33	0.36	0.65
17.8	0.00	0.42	0.29	0.34	0.31	0.29	0.33	0.35	0.37	0.64
15.9	0.04	0.47	0.30	0.36	0.28	0.26	0.36	0.32	0.34	0.64
14.7	0.14	0.49	0.32	0.34	0.28	0.28	0.32	0.32	0.36	0.72

Table A-8. Sediment Concentrations Station C (g/l), Run 1

Elevation (cm)	Time (hrs:mins) 00:00	00:15	00:30	01:00	02:00	03:00	04:00	05:00	06:00	13:30
24.0	.00	0.03	0.07	0.08	0.16	0.20	0.26	0.29	0.29	0.32
18.5	.00	0.22	0.19	0.11	0.17	0.21	0.25	0.30	0.30	0.33
15.5	.00	0.38	0.32	0.22	0.16	0.24	0.26	0.29	0.31	0.42
13.5	.04	2.39	0.80	0.55	0.33	0.38	0.31	0.32	0.48	0.64
12.5	.05	42.1	41.8	20.5	8.43	21.1	8.78	2.97	13.7	16.2

Table A-9. Sediment Concentrations Station D (g/l), Run 1

Elevation (cm)	Time (hrs:mins) 00:00	00:15	00:30	01:00	02:00	03:00	04:00	05:00	06:00	13:30
26.1	0.00	0.02	0.01	0.07	0.18	0.29	0.31	0.37	0.32	0.32
20.6	0.00	0.03	0.08	0.14	0.22	0.30	0.34	0.39	0.34	0.30
17.7	0.01	0.23	0.22	0.34	0.44	0.41	0.50	0.44	0.40	0.29
15.9	0.01	5.96	1.74	2.25	1.06	0.88	0.90	0.72	0.51	0.36
14.7	0.13	56.1	30.0	27.0	3.87	3.77	3.40	1.82	1.73	1.65

Table A-10. Sediment Concentrations Station E (g/l), Run 1

Elevation (cm)	Time (hrs:mins) 00:00	00:15	00:30	01:00	02:00	03:00	04:00	05:00	06:00	13:30
25.8	-	0.00	0.01	0.13	0.35	0.53	0.58	0.66	0.69	0.54
20.4	-	0.33	0.52	0.60	0.80	0.86	0.77	0.84	0.76	-
17.6	-	0.55	0.71	0.94	1.27	1.42	1.17	1.06	0.94	0.70
15.7	-	0.84	1.26	1.38	2.07	2.56	2.59	2.22	1.65	0.82
14.7	-	3.42	4.29	3.75	4.42	5.60	7.18	4.3	3.22	1.4

A.2 Run #2 Data -- 3/5/87

Table A-11. Wave Data (Period, Length, Height and MWS Elevation), Run 2

Wave Data	Time (hrs:mins) 00:00	00:15	00:30	01:00	02:00
	Gage #0 (Location 4.14m)				
H_{rms}(cm)	3.3	3.3	3.3	3.4	3.4
MWS (cm)	31.8	31.6	31.6	31.7	31.7
	Gage #1 (Location 6.19m)				
H_{rms}(cm)	3.1	3.2	3.3	3.3	3.4
MWS (cm)	31.7	31.6	31.6	31.6	31.6
	Gage #2 (Location 8.67m)				
H_{rms}(cm)	2.5	2.6	2.7	2.7	2.8
MWS (cm)	31.6	31.6	31.6	31.6	31.6
	Gage #3 (Location 12.0m)				
H_{rms}(cm)	1.6	1.8	1.8	1.9	1.9
MWS (cm)	3.15	31.6	31.5	31.5	31.5
	Bed-Averaged Values				
T_*(sec)	2.10	2.10	2.15	2.20	2.20
L^* (m)	2.91	2.98	2.98	2.96	2.96
H (cm)	2.45	2.58	2.61	2.66	2.70
h (cm)	31.6	31.6	31.6	31.6	31.6

L^* - Wavelength measured between wave gages 1 and 2.

Table A-11 (Cont.). Wave Data (Period, ...,etc.)

Wave Data	Time (hrs:mins) 02:35	03:00	04:00	05:00	07:00	08:00	10:30	11:30
	Gage #0 (Location 4.14m)							
H_{rms}(cm)	9.1	8.7	8.7	8.6	8.7	8.8	8.7	8.6
MWS (cm)	31.7	31.7	31.8	31.8	31.6	31.7	31.7	31.8
	Gage #1 (Location 6.19m)							
H_{rms}(cm)	8.1	8.6	8.1	8.8	7.9	8.3	8.5	8.3
MWS (cm)	31.8	31.7	31.7	31.8	31.9	31.8	31.8	31.8
	Gage #2 (Location 8.67m)							
H_{rms}(cm)	6.4	7.2	7.3	7.5	7.5	7.9	7.8	8.0
MWS (cm)	31.7	31.7	31.7	31.8	31.8	31.8	31.7	31.8
	Gage #3 (Location 12.0m)							
H_{rms}(cm)	3.9	4.3	4.6	4.7	5.0	4.5	4.8	4.4
MWS (cm)	31.6	31.7	31.6	31.7	31.7	31.7	31.7	31.7
	Bed-Averaged Values							
T_* (sec)	0.95	0.98	0.98	0.98	0.95	0.98	1.00	1.00
L^* (m)	1.35	1.31	1.35	1.35	1.27	1.35	1.34	1.42
H (cm)	6.19	6.83	6.83	7.12	6.97	7.15	7.21	7.19
h (cm)	31.7	31.7	31.7	31.7	31.7	31.7	31.7	31.7

L^* - Wavelength measured between wave gages 1 and 2.

Table A-12. Visual Bed Elevations (cm), Run 2

Location (m)	Time (hrs:mins) 00:00	00:15	00:30	01:00	02:00
14.7	14.1	14.2	14.0	13.3	13.6
13.7	14.5	13.9	13.9	13.5	13.4
12.7	14.5	14.2	14.1	13.9	13.8
11.7	14.0	14.3	14.2	14.0	13.8
10.7	12.8	14.6	14.5	14.1	13.9
9.7	12.1	14.4	14.2	14.0	13.4
8.7	12.2	14.0	13.6	13.4	13.3
7.7	12.4	12.3	12.3	12.8	12.7
6.7	13.2	10.2	10.3	12.0	12.3
5.7	13.3	11.8	11.2	11.6	11.4
AVG	13.3	13.4	13.2	13.3	13.2

Table A-12 (cont.). Visual Bed Elevations (cm), Run 2

Location (m)	Time (hrs:mins) 02:35	03:00	05:00	06:00	07:00	08:00	10:30	11:30
14.7	14.8	16.2	16.5	16.4	16.4	16.5	16.5	16.2
13.7	14.9	15.9	16.0	15.9	15.9	15.9	16.1	16.1
12.7	14.5	15.2	15.2	15.2	15.1	15.2	15.1	15.2
11.7	14.0	14.2	14.0	13.9	13.9	14.0	13.4	14.0
10.7	13.3	12.8	13.0	13.2	12.8	12.8	12.7	12.6
9.7	12.5	12.2	12.0	11.5	11.6	11.8	12.1	12.2
8.7	12.5	11.6	11.3	11.0	10.9	11.1	11.4	11.6
7.7	12.4	11.3	10.7	10.7	10.7	10.9	11.0	11.3
6.7	12.4	11.2	10.9	10.9	10.9	11.3	10.9	11.3
5.7	11.7	11.3	10.7	10.6	10.4	10.1	10.1	10.2
AVG	13.3	13.2	13.0	12.9	12.9	13.0	12.9	13.1

Table A-13. Wave-Averaged Pressures (kPa), Run 2

Gage #	(cm)	Time (hrs:mins) -0:01	00:00	00:15	00:30	01:00	02:00
		Pore Pressure Gages					
4	4.9	3.82	3.84	3.86	3.86	3.87	3.87
5	7.4	3.45	3.46	3.45	3.47	3.47	3.45
6	9.4	3.16	3.17	3.20	3.24	3.24	3.14
7	3.0	4.10	4.14	4.16	4.17	4.18	4.17
		Total Pressure Gages					
12	7.5	3.47	3.47	3.49	3.49	3.49	3.49
13	9.3	3.20	3.20	3.23	3.24	3.25	3.24
14	4.7	3.92	3.93	3.93	3.93	3.94	3.92
15	3.0	4.18	4.20	4.22	4.21	4.20	4.21

Table A-13 (cont.). Wave-Averaged Pressures (kPa), Run 2

Gage #	(cm)	Time (hrs:mins) 02:35	03:00	04:00	05:00	07:00	08:00	10:30	11:30
		Pore Pressure Gages							
4	4.9	3.87	3.86	3.86	3.86	3.87	3.87	3.87	3.88
5	7.4	3.45	3.44	3.44	3.43	3.43	3.49	3.49	3.51
6	9.4	3.14	3.10	3.17	3.18	3.21	3.22	3.24	3.20
7	3.0	4.17	4.11	4.14	4.14	4.16	4.18	4.23	4.22
		Total Pressure Gages							
12	7.5	3.50	3.46	3.47	3.48	3.50	3.50	3.50	3.50
13	9.3	3.23	3.22	3.19	3.19	3.21	3.20	3.20	3.20
14	4.7	3.93	3.92	3.91	3.92	3.93	3.94	3.94	3.94
15	3.0	4.21	4.21	4.20	4.20	4.21	4.20	4.21	4.21

Table A-14. Dynamic Pressure Amplitudes (0.1 kPa), Run 2

Gage #	Gage (cm)	Time (hrs:mins) 00:00	00:15	00:30	01:00	02:00
		Pore Pressure Gages				
4	4.9	3.1	3.5	3.0	3.3	3.3
5	7.4	3.3	3.6	3.8	3.6	3.9
6	9.4	2.9	3.0	3.1	3.0	2.7
7	3.0	2.3	2.4	2.5	2.3	2.6
		Total Pressure Gages				
12	7.5	4.3	4.8	4.2	4.6	4.1
13	9.3	4.9	5.3	5.2	5.4	5.0
14	4.7	4.0	3.9	3.9	3.7	3.8
15	3.0	4.1	4.2	4.2	4.4	4.1

Table A-14 (cont.). Dynamic Pressure Amplitudes (0.1 kPa), Run 2

Gage #	Gage (cm)	Time (hrs:mins) 02:35	03:00	04:00	05:00	07:00	08:00	10:30	11:30
		Pore Pressure Gages							
4	4.9	4.5	4.6	4.8	4.6	4.6	4.6	4.7	4.7
5	7.4	4.8	5.6	5.0	5.1	4.8	5.0	4.6	4.9
6	9.4	3.6	4.0	3.7	4.2	4.0	4.0	4.0	3.9
7	3.0	2.4	2.7	2.6	2.3	2.4	2.5	2.5	2.2
		Total Pressure Gages							
12	7.5	5.6	5.8	6.0	5.2	6.1	5.5	6.0	5.7
13	9.3	6.9	7.1	7.2	6.4	7.2	7.2	7.5	6.7
14	4.7	5.3	5.4	5.6	5.7	5.4	5.5	5.5	5.3
15	3.0	5.5	5.8	5.6	5.9	6.4	5.8	5.8	5.4

Table A-15. Sediment Bed Concentrations (g/l), Run 2

Elevation (cm)	Time (hrs:mins) 00:00	00:15	00:30	01:00	02:00
12.0	22.4	109.	124.	77.0	132.
10.0	110.	129.	135.	130.	141.
8.0	131.	145.	156.	154.	160.
6.0	160.	145.	159.	170.	164.
4.0	186.	194.	194.	195.	173.
2.0	185.	181.	209.	207.	179.
AVG	132.	151.	163.	156.	158.

Table A-15 (cont.). Sediment Bed Concentrations (g/l), Run 2

Elevation (cm)	Time (hrs:mins) 02:35	03:00	04:00	05:00	07:00	08:00	10:30	11:30
12.0	71.7	64.6	13.5	21.9	15.5	22.8	37.7	19.3
10.0	133.	136.	139.	136.	130.	103.	90.3	103.
8.0	156.	139.	162.	162.	154.	170.	169.	163.
6.0	164.	140.	174.	177.	166.	165.	169.	167.
4.0	163.	192.	196.	198.	194.	183.	180.	164.
2.0	192.	278.	192.	189.	208.	201.	202.	192.
AVG	147.	158.	146.	147.	145.	141	141.	135.

Table A-16. Sediment Concentrations Station A (g/l), Run 2

Elevation (cm)	Time (hrs:mins) 00:00	00:15	00:30	01:00	02:00
26.0	0.00	0.09	0.13	0.17	0.14
20.3	0.00	0.32	0.27	0.31	0.22
17.6	0.00	0.51	0.46	0.63	0.29
15.8	0.05	0.67	0.54	0.47	0.41
14.7	0.05	0.72	-	0.47	0.39

Table A-16 (cont.). Sediment Concentrations Station A (g/l), Run 2

Elevation (cm)	Time (hrs:mins) 02:35	03:00	04:00	05:00	07:00	08:00	10:30	11:30
26.0	0.67	0.61	0.63	0.72	0.70	0.77	0.78	0.79
20.3	0.74	0.62	0.60	0.74	0.70	0.75	0.80	0.80
17.6	0.72	0.61	0.55	0.72	0.67	0.76	0.75	0.82
15.8	0.74	0.62	0.57	0.71	0.68	0.75	0.72	0.79
14.7	-	0.61	0.55	0.69	0.68	0.75	0.76	0.78

Table A-17. Sediment Concentrations Station B (g/l), Run 2

Elevation (cm)	Time (hrs:mins) 00:00	00:15	00:30	01:00	02:00
26.2	0.00	0.03	0.00	0.11	0.10
20.6	0.00	0.10	0.11	0.06	0.16
17.8	0.09	0.32	0.19	0.07	0.12
15.9	0.10	0.46	0.24	0.18	0.16
14.7	0.09	0.47	0.19	0.16	0.20

Table A-17 (cont.). Sediment Concentrations Station B (g/l), Run 2

Elevation (cm)	Time (hrs:mins) 02:35	03:00	04:00	05:00	07:00	08:00	10:30	11:30
26.2	0.16	0.26	0.36	0.48	0.53	0.56	0.62	0.57
20.6	0.23	0.22	0.32	0.44	0.52	0.57	0.64	0.63
17.8	0.31	0.00	0.30	0.44	0.50	0.59	0.60	0.63
15.9	0.74	0.00	0.29	0.47	0.55	0.59	0.66	0.64
14.7	0.14	0.24	0.31	0.49	0.56	0.61	0.71	0.70

Table A-18. Sediment Concentrations Station C (g/l), Run 2

Elevation (cm)	Time (hrs:mins) 00:00	00:15	00:30	01:00	02:00
24.0	0.00	0.03	0.10	0.11	0.12
18.5	0.00	0.04	0.07	0.09	0.12
15.5	0.03	0.16	0.25	0.20	0.18
13.5	0.05	61.43	57.80	25.0	4.80
12.5	0.07	91.03	111.50	88.0	45.26

Table A-18 (cont.). Sediment Concentrations Station C (g/l), Run 2

Elevation (cm)	Time (hrs;mins) 02:35	03:00	04:00	05:00	07:00	08:00	10:30	11:30
24.0	0.09	0.12	0.18	0.27	0.35	0.38	0.43	0.44
18.5	0.10	0.12	0.19	0.29	0.38	0.38	0.43	0.62
15.5	0.20	0.12	0.18	0.28	0.35	0.36	0.38	0.46
13.5	0.44	0.86	0.21	0.31	0.39	0.40	0.43	0.46
12.5	29.44	9.74	0.37	0.34	1.54	1.14	2.63	1.53

Table A-19. Sediment Concentrations Station D (g/l), Run 2

Elevation (cm)	Time (hrs:mins) 00:00	00:15	00:30	01:00	02:00
26.1	0.00	0.00	0.01	0.06	0.06
20.6	0.03	0.02	0.04	0.12	0.12
17.7	0.02	0.03	0.04	0.08	0.10
15.9	0.01	0.05	0.06	0.08	0.09
14.7	0.04	0.06	0.07	0.09	0.12

Table A-19 (cont.). Sediment Concentrations Station D (g/l), Run 2

Elevation (cm)	Time (hrs:mins) 02:35	03:00	04:00	05:00	07:00	08:00	10:30	11:30
26.1	0.12	0.07	0.19	0.23	0.37	0.42	0.39	0.42
20.6	0.22	0.07	0.22	0.21	0.39	0.44	0.46	0.43
17.7	0.06	0.09	0.22	0.28	0.48	0.45	0.48	0.45
15.9	0.08	0.12	0.25	1.07	0.53	0.51	0.52	0.47
14.7	0.11	0.60	1.48	0.81	1.15	1.33	1.14	0.18

Table A-20. Sediment Concentrations Station E (g/l), Run 2

Elevation (cm)	Time (hrs:mins) 00:00	00:15	00:30	01:00	02:00
25.8	-	0.05	0.02	0.04	0.03
20.4	-	0.06	0.03	0.03	0.07
17.6	0.01	0.09	0.04	0.08	0.12
15.7	0.03	74.3	42.8	4.67	1.38
14.7	0.06	89.4	94.5	102.	74.8

Table A-20 (cont.). Sediment Concentrations Station E (g/l), Run 2

Elevation (cm)	Time (hrs:mins) 02:35	03:00	04:00	05:00	07:00	08:00	10:30	11:30
25.8	0.25	0.08	0.35	0.45	0.42	0.38	0.43	0.39
20.4	0.11	0.35	0.66	0.60	0.69	0.75	0.69	0.60
17.6	0.25	36.7	72.3	67.3	62.3	63.4	47.7	36.5
15.7	73.5	87.7	85.3	103.	96.9	91.7	91.4	92.2
14.7	94.1	112.	109.	115.	127.	104.	99.8	108.

APPENDIX C
MODEL SOURCE CODE

```
10  '*****************************************************************
20  '*                      SEDIMENT SUSPENSION MODEL                *
30  '*****************************************************************
40  '
50  '              Definitions - INPUT Data
60  '
70   DEFDBL C
80   DEFINT I,J
90   DIM CPCNT(3),WSO(3),K2(3)
100  INPUT "Input Filename is: 'Filename'<.dat>";FILN$
110  FILNIN$=FILN$+".DAT"
120  OPEN FILNIN$ FOR INPUT AS #1
130  FILN2$=FILN$+".OUT"
140 'INPUT "Output Filename is: <Filename.out>";FILN2$
150  OPEN FILN2$ FOR OUTPUT AS #2
160  INPUT#1, DESCR$
170  INPUT#1, MODE                              'Define: Program Logic
180  READ G,PI,K,RHOSED,RHOFLD,VISC             '        Program Constants
190  DATA 9.81,3.14159,0.4,2700,1000,1e-06
200  INPUT#1, H0,NGRIDS,DTSEC                   '        Discretization
210  INPUT#1, NMNOUT,NMNRUN,NMNTOST             '        Output/Runtime
220  IF(MODE=1)THEN 290
230  INPUT#1, CFLOC,K1,NU,CHNDRD1               '        Settling Velocity
240  INPUT#1, WSO(0),K2(0),BETA,CHNDRD2
250  INPUT#1, NSPECIES
260  FOR J=1 TO NSPECIES
270  INPUT#1, CPCNT(J),WSO(J),K2(J)
280  NEXT J
290  IF(MODE=2) THEN 490
300  INPUT#1,DSK1,DSK2                          '        Diff. Stability
310  INPUT#1, HYDRIVE                           '        Hydrodynamics
320  IF(HYDRIVE<>1) THEN 350
330  INPUT#1,WHEIGHT,WPERIOD,WLENGTH            '        Wave Hydrodynamics
340  INPUT#1,WDIFFK,MFLDMD,TRFLDMD              '        Diffusivity
350  IF(HYDRIVE<>2) THEN 400
360  INPUT#1,VAMP,HAMP                          '        Vel/depth ampls.
370  INPUT#1,PERIOD,TMLAG                       '        Sinusoidal hyd.
380  FREQ=2*PI/PERIOD
390  INPUT#1,MANNGN,CSFLDMD
400  INPUT#1, BEDRIVE                           '        Bed Flux Subr.
410  IF BEDRIVE=0 THEN 490
```

```
420  IF BEDRIVE=1 THEN 430 ELSE 450
430  INPUT#1, TAUDEP,TAUEROS,EROCONST          '          Bed Flux Parameters
440  GOTO 490
450  INPUT#1, TAUDEP,EROCONST                  '          Depth Varying Bed
460  INPUT#1, COBED,DCBDZ                      '              Parameters
470  INPUT#1, TAUA,TAUBETA                     '          Shear Strength Rel.
480  TAUEROS=TAUA*COBED^TAUBETA
490  DIM VEL(99),DVDZ(99),KN(99),KS(99),WVDISP(99)
500  DIM C(99,3),RHO(99),FBED(3)
510  DIM FS(99,3),WS(99,3),DFDDZ(99,3),DFSDZ(99,3)
520  NRUN=NMNRUN*60/DTSEC:NOUT%=NMNOUT*60/DTSEC:NTSTOST%=NMNTOST*60/DTSEC
530  DEF FNSINH(X)=(EXP(X)-EXP(-X))/2
540  DEF FNCOSH(X)=(EXP(X)+EXP(-X))/2
550 '
560 '               Initializations
570 '
580  ON ERROR GOTO 3630
590  SUBRT$="Init"
600  IN=NGRIDS: JN=NSPECIES : IF(JN<>0) THEN 610 ELSE JN=1 : CPCNT(1)=1
610  H=HO:  ITOP=1 : HMAX=H+HAMP : DZ=HMAX/IN
620  RHOCONST=(1-RHOFLD/RHOSED)
630  IF(MODE=1) THEN 640 ELSE WSFLOC=K1*CFLOC^NU : WSMAX=WSO(JN)
640  FOR I=ITOP TO IN
650  INPUT#1,C(I,0)                                    'Input initial concs
660  IF(C(I,0)<.000000000000001#)THEN C(I,0)=.000000000000001#
670  FOR J=1 TO JN
680 'C(I,J)=5/2*(1-COS(PI*I/IN))                       'Posmentier's Data
690 'C(I,J)=C0*CPCNT(J)
700  C(I,J)=C(I,0)*CPCNT(J)
710 'IF(I>IN-3) THEN C(I,J)=C(I-1,J)*3!                'Kirby's Data
720 'C(I,0)=C(I,0)+C(I,J)
730  RHO(I)=RHOFLD+C(I,0)*RHOCONST
740  NEXT J
750  NEXT I
760  T=-NTSTOST% : TIMMIN=T*DTSEC/60 : TIMHR=TIMMIN/60
770  IF(MODE=2) THEN 790 ELSE GOSUB 1780
780  TSAFSGA=0 : TSLFSGL=0
790  GOSUB 2740
800  IF(NTSTOST%>0)THEN CNT%=NOUT%-NTSTOST% ELSE CNT%=0
810  TST%=-NTSTOST%+1
820 '
830 '               MAIN Time Loop
840 '
850  FOR T=TST% TO NRUN
860  CNT% = CNT% + 1
870  TIMMIN=T*DTSEC/60 : TIMHR=TIMMIN/60
880  IF(MODE = 2) THEN GOTO 910
890  GOSUB 1160
900  IF(MODE = 1) THEN GOTO 940
910  GOSUB 1420
920  IF(HYDRIVE>1) THEN GOSUB 1930
930  IF(BEDRIVE>0) THEN GOSUB 2440
```

```
940  FOR I=ITOP TO IN-1
950  C(I,0)=0
960  FOR J=1 TO JN
970  C(I,J)=C(I,J)-DTSEC*(DFSDZ(I,J)+DFDDZ(I,J))
980  IF(C(I,J)<1E-15)THEN C(I,J)=1E-15
990  C(I,0)=C(I,0)+C(I,J)
1000 'PRINT USING " #.##^^^^";C(I,J);DFSDZ(I,J);DFDDZ(I,J)
1010  NEXT J
1020  RHO(I)=RHOFLD+C(I,0)*RHOCONST
1030  NEXT I
1040  C(IN,0)=0
1050  FOR J=1 TO JN
1060  C(IN,J)=C(IN,J)-DTSEC*(FBED(J)/DZ+DFDDZ(IN,J)+DFSDZ(IN,J))
1070 'PRINT USING" #.##^^^^";C(IN,J);DFSDZ(IN,J);DFDDZ(IN,J);FBED(J)
1080  C(IN,0)=C(IN,0)+C(IN,J)
1090  NEXT J
1100  RHO(IN)=RHOFLD+C(IN,0)*RHOCONST
1110  IF (CNT% = NOUT% ) THEN GOSUB 3280
1120  NEXT T
1130  END
1140 '
1150 '               DIFFUSION Flux Subroutine
1160 '
1170  SUBRT$="Diff"
1180  KS(ITOP-1)=0
1190  FOR I=ITOP TO IN-1
1200  RI=0
1205 'IF (HYDRIVE=1) AND (I<IN-1) THEN 1250
1210  DRHODZ=(RHO(I+1)-RHO(I))/DZ
1220  RHOAVG=(RHO(I+1)+RHO(I))/2
1230  IF(ABS(DVDZ(I))<.0001) THEN DVDZ(I)=.0001
1240  RI=G/RHOAVG*DRHODZ/DVDZ(I)^2                    'Local Grad. Rich No.
1250  KS(I)=KN(I)/(1+DSK1*RI)^DSK2                     'Stabilized Diff
1260  NEXT I
1270  FOR J=1 TO JN
1280  FDIM1J=0
1290  KS(ITOP-1)=0!
1300  FOR I=ITOP TO IN-1
1310 'KAVG=.25*KS(I-1)+.5*KS(I)+.25*KS(I+1)
1320  KAVG=KS(I)
1330  FDIJ=-KAVG*(C(I+1,J)-C(I,J))/DZ
1340  DFDDZ(I,J)=(FDIJ-FDIM1J)/DZ
1350  FDIM1J=FDIJ
1360  NEXT I
1370  DFDDZ(IN,J)=-FDIM1J/DZ
1380  NEXT J
1390  RETURN
1400 '
1410 '               SETTLING Flux Subroutine
1420 '
1430  SUBRT$="Set1"
1440  FOR I = ITOP TO IN
```

```
1450  IF (C(I,0) < CHNDRD2) THEN GOTO 1510
1460  WSHND=WSO(0)*(1-K2(0)*C(I,0))^BETA          'Hindered Settling Vel.
1470  FOR J = 1 TO JN
1480  WS(I,J)=WSHND
1490  NEXT J
1500  GOTO 1560
1510  IF(C(I,1)<CHNDRD1) THEN JST=2 ELSE JST=1 AND 1140
1520  IF(C(I,1)<CFLOC)THEN WS(I,1)=WSFLOC ELSE WS(I,1)=K1*C(I,1)^NU
1530 'FOR J=JST TO JN
1540 'WS(I,J)=WSO(J)*(1-K2(J)*C(I,0))^BETA
1550 'NEXT J
1560  FS(I,0)=0
1570  FOR J = 1 TO JN
1580  FS(I,J)=WS(I,J)*C(I,J)
1590  FS(I,0)=FS(I,0)+FS(I,J)
1600  WS(I,0)=FS(I,0)/C(I,0)
1610  NEXT J
1620  NEXT I
1630  FOR J=1 TO JN
1640  FSUPIJ=0
1650  FOR I=ITOP TO IN-1
1660  IF(FS(I+1,0)<FS(I,0)) THEN FS(I,J)=WS(I+1,0)*C(I,J)
1670  DFSDZ(I,J)=(FS(I,J)-FSUPIJ)/DZ
1680  FSUPIJ=FS(I,J)
1690  NEXT I
1700  DFSDZ(IN,J)=-FSUPIJ/DZ
1710  NEXT J
1720  FOR I=1 TO IN
1730  FS(I,0)=0
1740  NEXT I
1750  RETURN
1760 '
1770 '              HYDRODYNAMICS Subroutine
1780 '
1790  SUBRT$="HYDR0"              'Steady-state Hydrodynamics
1800  IF(HYDRIVE=1) THEN 2220
1810  IF(HYDRIVE>1)THEN 1910
1820  FOR I=ITOP TO IN
1830  DVDZ(I)=.1                                  'Stratification Test
1840  Z=I*DZ  : ZM=Z+DZ/2                         'Stratification Test
1850 ''VEL(I)=.2*COS(PI*ZM/H)+.2*(ZM/H)^2         'Postmentier's data
1860 ''DVDZ(I)=.4*Z/(H*H)-.2*PI/H*SIN(PI*Z/H)     'Postmentier's data
1870   KN(I)=(K*Z)*(1-Z/H)*ABS(DVDZ(I))           'Postmentier's data
1880  IF(KN(I)>KMAX) THEN KMAX=KN(I)
1890  NEXT I
1900  GOTO 2470
1910  USTAR=.1*VAMP
1920  KMAX=.1*HMAX*USTAR
1930  SUBRT$="HYDR2"              'Tidal Hyrodynamics Routine
1940  IF(TIMHR<>6.75)THEN 1960                                  'KIRBY DATA
1950  HAMP=2 :VAMP=.8 :FREQ=2*PI/7 : H0=24 :TMLAG=3.5+TMLAG     'KIRBY DATA
1960  WSE=-HAMP*COS((TIMHR-TMLAG)*FREQ)          'TMLAG=0 : Slack Low Tide
```

```
1970  H=H0+WSE
1980  ITOPOLD=ITOP
1990  ITOP=IN-H/DZ+1
2000  IF(ITOP=ITOPOLD) THEN 2060
2010  FOR J=0 TO JN
2020  IF(ITOP<ITOPOLD) THEN C(ITOP,J)=C(ITOPOLD,J)
2030  NEXT J
2040  IF(ITOP<ITOPOLD) THEN TSAFSGA=TSAFSGA+C(ITOPOLD,0)*DZ
2050  IF(ITOP>ITOPOLD) THEN TSLFSGL=TSLFSGL+C(ITOPOLD,0)*DZ
2060  IF(HYDRIVE<>2)THEN 2090
2070  VELAVG=VAMP*SIN((TIMHR-TMLAG)*FREQ)
2080  TAUBED=RHO(IN)*G*MANNGN^2/H^(.33)*VELAVG^2
2090  FOR I=ITOP TO IN-1
2100  Z=(I-ITOP+1)*DZ
2110  ZM=Z+DZ/2
2120 'IF(HYDRIVE<>5)THEN 1475                    'Velocity data from file
2130 ''INPUT#3, VEL(I)                           'Velocity data from file
2140 'IF(HYDRIVE<>4)THEN 1500                    'Special vel. profile data
2150  'Z=h-z  : zm=h-z                           'Postmentier's data
2160 ''KN(I)=DCONST*H/(H-Z)                      'Wolanski's data
2170  KN(I)=(K*Z)*(1-Z/H)*USTAR                  'Diffusivity via Mixing L.
2180  DVDZ(I)=USTAR/(K*H*(1-Z/H))                'Linear Shear Stess Distr.
2190  IF(KN(I)>KMAX) THEN KMAX=KN(I)
2200  NEXT I
2210  GOTO 2410
2220  SUBRT$="HYDR1"                             'Wave Hyd. Routine
2230  WK=2*PI/WLENGTH
2240  WFREQ=2*PI/WPERIOD
2250  WDELTA=(VISC/2/WFREQ)^.5
2260  KH=WK*H
2270  WCONST=WHEIGHT/2*WFREQ/FNSINH(KH)
2280  FOR I=ITOP TO IN-1
2290  Z=H-I*DZ :KZ=WK*Z
2300  VEL(I)=WCONST*FNCOSH(KZ)
2310  DVDZ(I)=WCONST*WK*FNSINH(KZ)
2320 'KN(I)=WDIFFK*WHEIGHT^2*WFREQ*WK*(FNSINH(KZ))^2/(FNSINH(KH)^3) 'Thim
2330 'KN(I)=WDIFFK/2*WHEIGHT^2*WFREQ*(FNSINH(KZ))^2/(FNSINH(KH))^2 'Hwang
2335  WVDISP(I)=WHEIGHT/2*FNSINH(KZ)/FNSINH(KH)
2340  KN(I)=2*WDIFFK*DVDZ(I)*WVDISP(I)           'Ross Spec. Form
2350 'KN(I)=WDIFFK                               'Constant Diff.
2360  IF(KN(I)>KMAX) THEN KMAX=KN(I)
2370  NEXT I
2380  WREYNLS=VEL(IN-1)^2/VISC/WFREQ
2390  WFRIC=2/WREYNLS^.5
2400  TAUBED=RHO(IN)*WFRIC/2*VEL(IN-1)^2
2410  RETURN
2420 '
2430 '              BED FLUX Subroutine
2440 '
2450  SUBRT$="BEDF"
2460  FOR J=1 TO JN
2470  FBED(J)=0
```

```
2480  IF BEDRIVE=0 THEN 2700
2481  IF(C(IN,J)<=TRFLDMD) THEN 2490
2482 'DFLMDDT=MFLDMD*(C(IN,J)/TRFLDMD-1)
2483 'TSLFFML=TSLFFML+DFLMDDT*DTSEC
2490  IF(TAUBED>=TAUDEP)THEN GOTO 2530                    'Deposition Rout.
2500  FBED(J)=WS(IN,J)*C(IN,J)*(1-TAUBED/TAUDEP)
2510  DEPBED=DEPBED+FBED(J)*DTSEC
2515  PRINT FBED(J),DEPBED,"Im in deposition"
2520  GOTO 2700
2530  IF(TAUBED<=TAUEROS) THEN 2640                       'Erosion Routine
2540  M=EROCONST*EXP(-2.33*TAUEROS)
2550 'IF(C(IN,0)>CSFLDMD)THEN 2620
2560  FBED(J)=-M*(TAUBED/TAUEROS-1)
2570  EROBED=EROBED-FBED(J)*DTSEC
2575  IF BEDRIVE=1 THEN 2580 ELSE 2590
2580  TAUEROS=.2+2.5/30*EROBED :GOTO 2700
2590 'ZBEROS=-EROBED/(CBED+COBED)*2
2610 'CBED=COBED+DCBDZ*ZBEROS                             'New Bed Conc.
2620 'TAUEROS=TAUA*CBED^TAUBETA
2630  GOTO 2700
2640  IF(TAUDEP=TAUEROS)THEN 2700                         'Entrnmt. Rout.
2650  FBED(J)=-(TAUBED-TAUDEP)/(TAUEROS-TAUDEP)*DEPBED/DTSEC
2660 'MINTR=EROCONST*EXP(-2.33*TAUDEP)
2670 'FBED(J)=-MINTR*(TAUBED-TAUDEP)/(TAUEROS-TAUDEP)
2680  DEPBED=DEPBED+FBED(J)*DTSEC
2690  IF(DEPBED<.0000001) THEN DEPBED=0
2700  FBED(J)=FBED(J)+DFLMDDT
2701  NEXT J
2710  RETURN
2720 '
2730 '               OUTPUT Subroutine
2740 '
2750  SUBRT$="OUTP"
2760  CLS
2770  PRINT "Program IN PROGRESS - DO NOT TOUCH KEYBOARD"
2780  PRINT#2,DESCR$
2790  PRINT#2, "Time: ";TIME$;" Date: ";DATE$
2800  PRINT#2, "Input Filename was: ";FILN$
2810  PRINT#2, "MODE =";MODE;"(1=Diff, 2=Stlng, 3=Both, 4=3+Eros/Dep)"
2820  IF MODE=2 THEN GOTO 2850
2830  PRINT#2,"The time step for diff. stability is: ";(DZ)^2/(2*KMAX)
2840  IF MODE=1 THEN GOTO 2860
2850  PRINT#2,"The time step for settling stability is: ";DZ/WSMAX
2860  PRINT#2,"The time step used is: ";DTSEC;" (sec)"
2870  PRINT#2,"Discretization Parameters Follow"
2880  PRINT#2,"MEDIAN DEPTH=";H0;" NGRIDS=";IN;" DZ=";DZ;" DTSEC=";DTSEC
2890  PRINT#2,"Settling Velocity Parameters Follow"
2900  PRINT#2," CFLOC      K1        NU       CHNDRD1"
2910  PRINT#2,USING " #.##^^^^";CFLOC;K1;NU;CHNDRD1
2920  PRINT#2," WSO(0)    K2(0)     BETA     CHNDRD2"
2930  PRINT#2,USING " #.##^^^^";WSO(0);K2(0);BETA;CHNDRD2
2940  PRINT#2," J       CPCNT(J)     WSO(J)       K2(J)"
```

```
2950  FOR J=1 TO NSPECIES
2960  PRINT#2, J;
2970  PRINT#2,USING "    #.##^^^^";CPCNT(J);WSO(J);K2(J)
2980  NEXT J
2990  IF MODE=2 THEN GOTO 3280
3000  PRINT#2,"Diffusion Stability Parameters Follow"
3010  PRINT#2,"  Betaconst,SK1    Alpaconst,SK2"
3020  PRINT#2,USING "  ##.##^^^^";DSK1,DSK2
3030  IF(HYDRIVE<>1) THEN GOTO 3110
3040  PRINT#2,"Wave Hydrodynamic Parameters Follow"
3050  PRINT#2,"Wave Height (m), Wave Period (sec), Wavelength (m)"
3060  PRINT#2,USING "  ##.##^^^^";WHEIGHT,WPERIOD,WLENGTH
3070  PRINT#2,"Wave Reynolds#, Friction factor (f), Taubed (N/m^2)"
3080  PRINT#2,USING "  ##.##^^^^";WREYNLS,WFRIC,TAUBED
3090  PRINT#2,"Wave Delta (m), Diffusion Constant"
3100  PRINT#2,USING "  ##.##^^^^";WDELTA,WDIFFK
3102  PRINT#2,"Fluid Mud Horizontal Transport Rate"
3104  PRINT#2,USING "  ##.##^^^^";MFLDMD
3110  IF(HYDRIVE<>2) THEN GOTO 3180
3120  PRINT#2,"Tidal Hydrodynamic Parameters Follow"
3130  PRINT#2,"Tide Period,  Timelag from LWS, Vel Amp, WS Elev Amp"
3140  PRINT#2,USING "  ##.##^^^^";PERIOD,TMLAG,VAMP,HAMP
3150  PRINT#2," MANNGN   CSFLDMD"
3160  PRINT#2,USING "  ##.##^^^^";MANNGN,CSFLDMD
3170  GOTO 3220
3180  FOR I=ITOP TO IN-1 : PRINT#2, USING" .##^^^^";H-I*DZ;:NEXT I
3185  PRINT#2," z(m)"
3190  FOR I=ITOP TO IN-1 : PRINT#2, USING" .##^^^^";VEL(I);:NEXT I
3195  PRINT#2," VEL"
3200  FOR I=ITOP TO IN-1 : PRINT#2, USING" .##^^^^";DVDZ(I);:NEXT I
3205  PRINT#2," DVDZ"
3207  IF(HYDRIVE<>1) THEN 3210
3208  FOR I=ITOP TO IN-1 : PRINT#2, USING" .##^^^^";WVDISP(I);:NEXT I
3209  PRINT#2," wvdisp"
3210  FOR I=ITOP TO IN-1 : PRINT#2, USING" .##^^^^";KN(I);:NEXT I
3215  PRINT#2," Kn"
3220  IF BEDRIVE=0 THEN GOTO 3280
3230  PRINT#2,"Bed Flux Parameters Follow"
3240  PRINT#2,"   TAUDEP     TAUEROS    EROCONST"
3250  PRINT#2,USING "  ##.##^^^^";TAUDEP;TAUEROS;EROCONST
3260  PRINT#2,"   COBED      DCBDZ      TAUA      TAUBETA"
3270  PRINT#2,USING "  ##.##^^^^";COBED;DCBDZ;TAUA;TAUBETA
3290  SUSPMAS = 0
3300  PRINT "Program Progress: Time= ";T*DTSEC/60;" (mins)"
3310  PRINT#2,
3320  PRINT#2, "CONCENTRATIONS (g/l) for time= ";T*DTSEC/60;" (mins)"
3330  IPN=IN
3340  IUN=0
3350  ILN=IUN+1
3360  IF IPN>=10 THEN IUN=IUN+10 ELSE IUN=IUN+IPN
3370  FOR I=ILN TO IUN
3380  IF(I<ITOP)THENPRINT#2,"##.##%";ELSE PRINT#2,USING " ##.##%";C(I,0);
```

```
3390  IF(I>=ITOP) THEN SUSPMAS=SUSPMAS+C(I,0)*DZ
3400  NEXT I
3410  PRINT#2,
3420  IPN=IPN-10
3430  IF IPN>0 THEN GOTO 3350
3440  IF(T=-NTSTOST%)THEN SUSPMAS0=SUSPMAS
3450  PRINT#2, "Total Sediment Now In Suspension: ";SUSPMAS;" (kg/m^2)"
3460  PRINT#2, "Total Sediment Added From Bed Ers: ";EROBED;" (kg/m^2)"
3470  PRINT#2, "Total Sediment Added From Surface: ";TSAFSGA;" (kg/m^2)"
3480  PRINT#2, "Total Sediment Lost From Bed Dep: ";DEPBED;" (kg/m^2)"
3485  PRINT#2, "Total Sediment Lost From Fluid Mud: ";TSLFFML;" (kg/m^2)"
3490  PRINT#2, "Total Sediment Lost From Surface: ";TSLFSGL;" (kg/m^2)"
3500  PRINT#2, "Net Sediment Generated by Model: ";
3510  NSGBM=SUSPMAS-SUSPMAS0-EROBED-TSAFSGA+DEPBED+TSLFSGL+TSLFFML
3520  PRINT#2, USING "##.####  ";NSGBM;:PRINT#2," (kg/m^2)"
3530  IF(BEDRIVE>=1) THEN PRINT#2,"TAUBED=";TAUBED;"(N/m^2), ";
3540  IF(BEDRIVE>=1) THEN PRINT#2," TAUEROS=";TAUEROS;"(N/m^2)"
3550  IF(BEDRIVE>=2) THEN PRINT#2,"Depth of Bed Erosion=";ZBEROS;"(m), ";
3555  BEDC=CBED
3560  IF(BEDRIVE>=2) THEN PRINT#2,"Bed Concentration=";BEDC;"(kg/m^3)"
3570  IF(HYDRIVE>=2) THEN PRINT#2,"Depth=";H;"(m),  Vel=";VELAVG;"(m/s)"
3580  CNT% = 0
3590  IF (MODE<>2) THEN 3620                    'Special time-step increment
3600  IF(TIMMIN=15)THEN NOUT%=T ELSE NOUT%=NOUT%*2 'jump for settl. tests
3610  IF(TIMMIN=0) THEN NOUT%=NMNOUT*60/DTSEC
3620  RETURN
3630 '
3640 '              ERROR TRAP Subroutine
3650 '
3660  PRINT#2, "Error occurred in subroutine: ";SUBRT$
3670  PRINT#2, "Timestep: ";T;" Grid(i): ";I;" J:";J
3680  FOR J=1 TO JN
3690  PRINT#2, "J=";J
3700  PRINT#2, "I  C(I,J)  DFSDZ(I,J)  DFDDZ(I,J)    FBED(J)"
3710  FOR I=ITOP TO IN-1
3720  PRINT#2,USING "###";I;
3730  PRINT#2, USING" #.##^^^^ ";C(I,J);DFSDZ(I,J);DFDDZ(I,J)
3740  NEXT I
3750  PRINT#2,USING "###";IN;
3760  PRINT#2, USING" #.##^^^^ ";C(IN,J);DFSDZ(IN,J);DFDDZ(IN,J),FBED(J)
3770  PRINT#2, "H=";H
3780  PRINT#2, "I    DVDZ(I)    KN(I)    RHO(I)   KS(I)   TAUBED"
3790  FOR I=ITOP TO IN-1
3800  PRINT#2,USING "###";I;
3810  PRINT#2, USING" #.##^^^^ ";DVDZ(I);KN(I);RHO(I);KS(I)
3820  NEXT I
3830  PRINT#2,USING "###";IN;
3840  PRINT#2, USING" #.##^^^^ ";DVDZ(IN);KN(IN);RHO(IN);KS(IN);TAUBED
3850  NEXT J
3860  END
```

REFERENCES

Alishahi, M. R., and Krone, R. B., "Suspension of Cohesive Sediment by Wind-Generated Waves," Technical Report HEL-2-9, Hydraulic Engineering Laboratory, University of California, Berkeley, California, August, 1964.

Been, K. P., "Stress-Strain Behavior of a Cohesive Soil Deposited Underwater," Ph.D. Dissertation, University of Oxford, UK, 1980.

Been, K., and Sills, G. C., "Self-Weight Consolidation of Soft Soils: An Experimental and Theoretical Study," Geotechnique, Vol. 31, No.4, 1981, pp. 519-535.

Bellessort, B., "Movement of Suspended Sediment in Estuaries-Flocculation and Rate of Removal of Muddy Sediment," Tracer Techniques in Sediment Transport, TR145, International Atomic Energy Agency, 1973, pp. 31-40.

Bosworth, R. C. L., "The Kinetics of Collective Sedimentation," Journal of Colloidal Science, Vol. 11, 1956, pp. 496-500.

Burt, T. N., "Field Settling Velocities of Estuary Muds," Estuarine Cohesive Sediment Dynamics, A. J. Mehta, ed., Springer-Verlag, Berlin, 1986.

Cervantes, E. E., "A Laboratory Study of Fine Sediment Resuspension by Waves," M.S. Thesis, University of Florida, Gainesville, 1987.

Chase, R. R. P., "Settling Behavior of Natural Aquatic Particulates," Limnology and Oceanography, Vol. 24, No. 3, 1979, pp. 417-426.

City of Tampa, "Surface Sediment Composition and Distribution in Hillsborough Bay, Florida," Report to the Florida Department of Environmental Regulation, Department of Sanitary Sewers, Tampa, Florida, 1986.

Daily, J. W., and Harleman, D. R. F., Fluid Dynamics, Addison-Wesley, New York, 1966.

Dean, R. G., "Coastal Sediment Processes: Toward Engineering Solutions," Coastal Sediments '87, Specialty Conference on Advances in Understanding of Coastal Sediment Processes, ASCE, Committee on Coastal Engineering, 1987, pp. 1-25.

Dean, R. G., and Dalrymple, R. A., Water Wave Mechanics for Engineers and Scientists, Prentice-Hall, Englewood Cliffs, New Jersey, 1984.

Delft Hydraulics Laboratory, "Momentum and Mass Transfer in Stratified Flows," Report R880, Delft, The Netherlands, December, 1974.

Delft Hydraulics Laboratory, "The Effect of Waves on Kaolinite/Sand Beds," Report M2060, Delft, The Netherlands, August, 1985.

Dixit, J. G., "Resuspension Potential of Deposited Kaolinite Beds," M.S. Thesis, University of Florida, Gainesville, Florida, 1982.

Einstein, H. A., and Chien, N., "Effects of Heavy Sediment Concentration Near the Bed on Velocity and Sediment Distribution," MRD Series No. 8, University of California Institute of Engineering Research and U.S. Army Engineers, Missouri River, Omaha, Nebraska, August, 1955.

Einstein, H. A., and Krone, R. B., "Experiments to Determine Modes of Cohesive Sediment Transport in Salt Water," Journal of Geophysical Research, Vol. 67, No. 4, 1962, pp. 1451-1461.

Engelund, F., and Zhaohui, W., "Instability of Hyperconcentrated Flow," Journal of Hydraulic Engineering, ASCE, Vol. 101, No. 3, 1984, pp. 219-233.

Eskinazi, S., Principles of Fluid Mechanics, Allyn and Bacon, Boston, Massachusetts, 1968.

Faas, R. W., "Rheological Characteristics of Rappahannock Estuary Muds, Southeastern Virginia, U.S.A.," Holocene Marine Sedimentation in the North Sea Basin, I.A.S. Special Publication, Vol. 5, 1981, pp. 505-515.

Faas, R. W., "Viscous Control of Estuarine Resuspension Patterns," Coastal Sediments '87, ASCE Specialty Conference on Advances in Understanding of Coastal Sediment Processes, Nicholas Kraus, ed., 1987.

Fischer, H. B., List, E. J., Koh, R. C. Y., Imberger, J., Brooks, N. H., Mixing in Inland and Coastal Waters, Academic Press, New York, 1979.

Fitch, E. B.,"The Significance of Detention in Sedimentation," Sewage and Industrial Wastes, Vol. 29, No. 10, October 1957, pp. 550-554.

French, R. H., "Interfacial Stability in Channel Flow," Journal of the Hydraulics Division, ASCE, Vol. 105, No. HY8, 1979, pp. 955-979.

French, R. H., and McCutcheon, S. C., "Vertical Momentum Transfer in Continuously Stratified Channel Flow," Water Resources Center, Desert Research Institute, Las Vegas, Nevada, 1983.

French, R. H., Open Channel Hydraulics, McGraw-Hill, New York, NY, 1985.

Guy, H. P., "Pipette Method," Sedimentation Engineering, Manuals and Reports on Engineering Practice No. 54, V. A. Vanoni, ed., ASCE, New York, New York, 1975, pp. 416-418.

Hayter, E. J., "Prediction of Cohesive Sediment Movement in Estuarial Waters," Ph.D. Dissertation, University of Florida, Gainesville, Florida, December 1983.

Hayter, E. J. and Mehta, A. J., "Modeling of Estuarial Fine Sediment Transport for Tracking Pollutant Movement," UFL/COEL-82/009, Coastal and Oceanographic Engineering Department, University of Florida, Gainesville, Florida, December 1982.

Heltzel, S. B., and Teeter, A. M., "Settling of Cohesive Sediments," Coastal Sediments '87, ASCE Specialty Conference on Advances in Understanding of Coastal Sediment Processes, Nicholas Kraus, ed., 1987, pp. 63-70.

Holzman, B., "The Influence of Stability on Evaporation," Boundary Layer Problems in the Atmosphere and Ocean, W. G. Valentine ed., Vol. XLIV, Article 1, 1943 pp. 13-18.

Hunt, J. R., "Prediction of Oceanic Particle Size Distribution from Coagulation and Sedimentation Mechanisms," Advances in Chemistry Series No. 189 -- Particles in Water, M.C. Kavanaugh and J. O. Leckie eds., Amer. Chem. Soc., Washington, DC, 1980, pp. 243-257.

Hunt, S. D., "A Comparative Review of Laboratory Data on Erosion of Cohesive Sediment Beds," Report No. UFL/COEL - 81/17, Coastal and Oceanographic Engineering Department, University of Florida, Gainesville, Florida, 1981.

Hwang, P. A., and Wang, H., "Wave Kinematics and Sediment Suspension at Wave Breaking Point," Technical Report No. 13, Department of Civil Engineering, University of Delaware, Newark, Delaware, 1982.

Imai, G., "Settling Behavior of Clay Suspensions," Soils and Foundations, Vol. 20, No. 1, 1980, pp. 7-20.

Imai, G., "Experimental Studies on Sedimentation Mechanism and Sediment Formation of Clay Minerals," Soils and Foundation, Vol. 21, No. 1, 1981, pp. 7-20.

Inglis, C. C., and Allen, F. H., "The Regimen of the Thames Estuary as Affected by Currents, Salinites, and River Flow," Institute of Civil Engineering, Vol. 7, 1957, pp. 827-868.

Inter-Agency River Basin Committee, "Methods of Analyzing Sediment Samples; Report No. 4, Measurement and Analysis of Sediment Loads in Streams," Hydraulics Laboratory, University of Iowa, Iowa City, Iowa, 1941.

Inter-Agency River Basin Committee, "A Study of New Methods for Size Analysis of Suspended Sediment Samples; Report No. 7, Measurement and Analysis of Sediment Loads in Streams," Hydraulics Laboratory, University of Iowa, Iowa City, Iowa, 1943.

Kamphuis, J. W., "Friction Factor under Oscillatory Waves," Journal of the Waterways, Harbors and Coastal Engineering Division, ASCE, Vol. 101, No. WW2, May, 1975, pp. 135-144.

Kandiah, A., "Fundamental Aspects of Surface Erosion of Cohesive Soils," Ph.D. Dissertation, University of California, Davis, California, 1974.

Kassab, V., Technical BASIC, Prentice-Hall, Englewood Cliffs, New Jersey, 1984.

Kato, H., and Phillips, O. M., "On the Penetration of a Turbulent Layer Into a Stratified Fluid," Journal of Fluid Mechanics, Vol. 37, 1969, pp. 643-655.

Kendrick, M. P., and Derbyshire, B. V., "Monitoring of Near-bed Turbid Layers," Report SR 44, Hydraulics Research, Wallingford, United Kingdom, 1985.

Kennedy, J. F., and Locher, F. A., "Sediment Suspension by Waves," Waves on Beaches and Resulting Sediment Transport, R. E. Meyer ed., Academic Press, Inc., New York, 1972, pp. 249-296.

Kent, R. E., and Pritchard, D. W., "A Test of Mixing Length Theories in a Coastal Plain Estuary," Journal of Marine Research, Vol. 1, 1957, pp. 456-466.

Kirby, R., "Suspended Fine Cohesive Sediment in the Severn Estuary and Inner Bristol Channel, U.K.," Report ETSU-STP-4042, Department of Atomic Energy, Harwell, United Kingdom, 1986.

Kirby, R., and Parker, W. R.,"The Physical Characteristics and Environmental Significance of Fine Sediment Suspensions in Estuaries," Estuaries, Geophysics and the Environment, National Research Council, NAS, USA, Studies in Geophysics, 1977, pp. 110-120.

Krone, R. B., "Flume Studies of the Transport of Sediment in Estuarial Shoaling Process," Final Report, Hydraulic Engineering Laboratory and Sanitary Engineering Research Laboratory, University of California, Berkeley, California, 1962.

Krone, R. B., "A Study of Rheologic Properties of Estuarial Sediments," Technical Bulletin No. 7, Committee on Tidal Hydraulics, U.S. Army Engineers, Waterways Experiment Station, Vicksburg, Mississippi, September, 1963.

Krone, R. B., ed., Sedimentation Control to Reduce Maintenance Dredging of Navigational Facilities in Estuaries, Marine Board, Commission on Engineering and Technical Systems, National Research Council, National Academy Press, Washington, DC, 1987.

Lamb, H., Hydrodynamics, Dover Publications, New York, NY, 1945.

Lavelle, J. W., and Thacker, W. C., "Effects of Hindered Settling on Sediment Concentration Profiles," Journal of Hydraulic Research, Vol. 16, No. 4, 1978, pp. 347-355.

Lott, J. W., "Laboratory Study on the Behavior of Turbidity Current in a Closed-end Channal," M.S. Thesis, University of Florida, Gainesville, Florida, 1987.

Maa, P.-Y., "Erosion of Soft Muds by Waves," Ph.D. Dissertation, University of Florida, Gainesville, Florida, 1986.

Maa, P.-Y., and Mehta, A. J., "Considerations on Bed Response in Wave Resuspensions of Muds," Coastal And Oceanographic Engineering Department, University of Florida, Gainesville, Florida, 1985.

Maa, P.-Y., and Mehta, A. J., "Mud Erosion by Waves: A Laboratory Study," Continental Shelf Research, Vol. 7, Nos. 11/12, 1987, pp. 1269-1284.

Malvern, L. E., Introduction to the Mechanics of a Continuous Medium, Prentice-Hall, Englewood Cliffs, New Jersey, 1969.

McCutcheon, S. C.,"Vertical Mixing in Models of Stratified Flow," Proc. Conference on Frontiers in Hydraulic Engineering, ASCE, 1983, pp. 15-20.

McDowell, D.M., and O'Connor, B.A., Hydraulic Behavior of Estuaries, John Wiley and Sons, New York, 1977.

Mclaughlin, R. J., Jr., "On The Mechanics of Sedimentation in Artificial Basins," Ph.D. Thesis, California Institute of Technology, Pasadena, 1958.

McLaughlin, R. J., Jr., "The Settling Properties of Suspensions," Journal of the Hydraulics Division, ASCE, Vol. 85, No. HY12, 1961, pp. 9-41.

McNown, J. S., and Lin, P. N., "Sediment Concentration and Fall Velocity," Proc. the 2nd Midwestern Conference on Fluid Mechanics, Ohio State University, Columbus, Ohio, 1952, pp. 401-411.

Mehta, A. J., "Depositional Behavior of Cohesive Sediments," Ph.D. Dissertation, University of Florida, Gainesville, Florida, 1973.

Mehta, A. J., "Characterization of Cohesive Sediment Properties and Transport Processes in Estuaries," Estuarine Cohesive Sediment Dynamics, A. J. Mehta, ed., Springer-Verlag, Berlin, 1986.

Mehta, A. J., Lott, J. W., "Sorting of Fine Sediment During Deposition," Coastal Sediments '87, ASCE Specialty Conference on Advances in Understanding of Coastal Sediment Processes, Nicholas Kraus, ed., 1987, pp. 348-362.

Mehta, A. J., and Maa, P. -Y., "Waves Over Mud: Modeling Erosion," The Third International Symposium on River Sedimentation, Jackson, Mississippi, April, 1986.

Mehta, A. J., Parchure, T. M., Dixit, J. G., and Ariathurai, R., "Resuspension Potential of Deposited Cohesive Sediment Beds," Estuarine Comparisons, V. S. Kennedy, ed., Academic Press, New York, 1982, pp. 591-609.

Mehta, A. J., Ariathurai, R., Maa, P. and Hayter, E. J.,"Fine Sedimentation in Small Harbors," UFL/COEL - TR/051, Coastal and Oceanographic Engineering Department, University of Florida, Gainesville, 1984.

Munk, W. H., and Anderson, E. R., "Notes on the Theory of the Thermocline," Journal of Marine Research, Vol. 1, 1948, pp. 276-295.

Narimousa, S., and Fernando, H. J. S., "On The Sheared Density Interface of an Entraining Stratified Fluid," Journal of Fluid Mechanics, Vol. 171, 1987, pp. 1-22.

Neilson, P., "Sime Basic Concepts of Wave Sediment Transport," Paper No. 20, Institute of Hydrodynamics and Hydraulic Engineering, Technical University of Denmark, Lyngby, Denmark, 1979.

Nelson, J. E., "Vertical Turbulent Mixing in Stratified Flow-A Comparision of Previous Experiments," Report No. WHM-3, Hydraulic Engineering Laboratory, University of California, Berkeley, California, 1972.

Nichols, M. M., "Fluid Mud Accumulation Process in an Estuary," Geo-Marine Letters, Vol. 4, 1985, pp. 171-176.

O'Brien, M. P., "Review of the Theory of Turbulent Flow and its Relation to Sediment Transportation," Transactions, American Geophysical Union, Washington, DC, April, 1933, pp. 487-491.

O'Melia, C. R., Physicochemical Processes for Water Quality Control, W. J. Weber, ed., Wiley-Interscience, New York, 1972, pp. 61-109.

Odd, N. V. M., and Rodger, J. G., "Vertical Mixing in Stratified Tidal Flows," Journal of the Hydraulics Division, ASCE, Vol. 104, No. HY3, 1978, pp. 337-351.

Odd, N. V. M., and Rodger, J. G., "An Analysis of the Behavior of Fluid Mud in Estuaries," Report SR84, Hydraulics Research, Wallingford, United Kingdom, 1986.

Oduyemi, K. O. K., "Turbulent Transport of Sediments in Estuaries," Ph.D. Dissertation, Department of Civil Engineering, University of Birmingham, Birmingham, Alabama, 1986.

Owen, M. W., "A Detailed Study of the Settling Velocities of an Estuary Mud," Report No. INT 78, Hydraulics Research Station, Wallingford, United Kingdom, 1970.

Owen, M. V., "The Effect of Turbulence on Settling Velocities of Silt Flocs," Proc. XIVth Congress, International Association for Hydraulic Research, XIVth Congress, Paris, France, 1971, pp. 27-32.

Owen, M. V., "Determination of the Settling Velocities of Cohesive Muds," Report No. INT 161, Hydraulics Research Station, Wallingford, United Kingdom, 1976.

Parchure, T. M., "Erosional Behavior of Deposited Cohesive Sediments," Ph.D. Dissertation, University of Florida, Gainesville, Florida, 1984.

Parchure, T. M., and Mehta, A. J., "Erosive Shear Strength of Soft Muddy Deposits," Second Indian Conference in Ocean Engineering, Poona, India, December, 1983, pp. 871-884.

Parchure, T. M., and Mehta, A. J., "Erosion of Soft Cohesive Sediment Deposits," Journal of Hydraulic Engineering, ASCE, Vol. 3, No. 10, 1985, pp. 1308-1326.

Parker, W. R., "On the Observation of Cohesive Sediment Behavior for Engineering Purposes," Estuarine Cohesive Sediment Dynamics, A. J. Mehta ed., Springer-Verlag, Berlin, 1986.

Parker, W. R., "Observations on Fine Sediment Transport Phenomena in Turbid Coastal Environments," Continental Shelf Research, Vol. 7, Nos 11/12, 1987, pp. 1285-1293.

Parker, W. R., and Kirby, R., "Fine Sediment Studies Relevant to Dredging Practice and Control," Proc. Second International Symposium on Dredging Technology, BHRA, Papper B2, Texas A & M University, College Station, 1977.

Parker, W. R., and Kirby, R., "Observation of Fine Sediment Behavior," First International Conference on Coastal Sediments, EBSA, Churchill College, Cambridge, UK, 1979.

Partheniades, E., "Erosion and Deposition of Cohesive Materials," River Mechanics, Vol. 2, H. W. Shen ed., Fort Collins, Colorado, 1971.

Partheniades, E., "A Summary of the Present Knowledge of the Behavior of Fine Sediments in Estuaries," Technical Report No. 8, M.I.T., Hydrodynamic Lab, June 1984.

Perloff, W. H., and Baron, W., Soil Mechanics Principles and Applications, John Wiley and Sons, New York, 1976.

Phan-Thien, N., "A Similarity Solution for Rayleigh Flow of a Bingham Fluid," Journal of Fluid Mechanics, Vol. 50, 1983, pp 229-230.

Phillips, O. M., "Entrainment", Modeling and Prediction of the Upper Layers of the Ocean, E. G. Kraus, ed., Pergamon Press, New York, 1977, pp. 92-101.

Posmentier, E., "The Generation of Salinity Finestructure by Vertical Diffusion," Journal of Physical Oceanography, Vol. 7, 1977, pp. 298-300.

Price, J. F., "On the Scaling of Stress-Driven Entrainment Experiments," Journal of Fluid Mechanics, Vol. 90, 1979.

Price, J. F., Mooers, C. N. K., and van Leer, J. C.,"Observation and Simulation of Storm-induced Mixed Layer Deepening," Journal of Physical Oceanography, Vol. 8, 1978, pg. 582-599.

Raudkivi, A. J., Loose Boundary Hydraulics, Pergamon Press, Oxford, 1967.

Richardson, J. F., and Zaki, W. N., "The Sedimentation of a Suspension of Uniform Spheres under Conditions of Viscous Flow," Chemical Engineering Science, Vol. 3, 1954, pp. 65-72.

Roache, P. J., Computational Fluid Dynamics, Hermosa Publishers, Albuquerque, New Mexico, 1972.

Ross, M. A., Lin, C.-P., and Mehta, A. J., "On the Definition of Mud," Proc. 1987 Conference of Hydraulic Engineering, ASCE, Robert M. Ragan, ed., Williamsburg, Va., 1987, pp. 231-236.

Rossby, C. G., and Montgomery, R. B., "The Layer of Friction Influence in Wind and Ocean Currents," Physical Oceanography and Meteorology, Vol. 3, No. 3, 1935.

Rouse, H., "Modern Conceptions of the Mechanics of Fluid Turbulence," Transactions, ASCE, Vol. 102, Paper No. 1965, 1937, pp. 463-543.

Rouse, H., Fluid Mechanics for Hydraulic Engineers, Dover Publications, New York, 1938.

Schiffman, R. L., Pane V., and Sunara, V., "Sedimentation and Consolidation," Engineering Foundation Conference, Flocculation,

Sedimentation, and Consolidation, Brij M. Moudgil and P. Somasundaran, eds., AICE, New York, NY, 1986.

Schlichting, H., Boundary Layer Theory, Pergamon Press, Oxford, UK, 1979.

Seed, B. H., "Evaluation of Soil Liquifaction Effects on Level Ground During Earthquakes," Liquifaction Problems in Geotechnical Engineering, ASCE National Convention, Philadelphia, 1976, pp. 1-104.

Sheng, Y. P., "Mathematical Modeling of Three-Dimensional Coastal Currents and Sediment Dispersion: Model Development and Application," CERC Technical Report, Vol. 83, No. 2, U.S. Army Engineers, Waterways Experiment Station, Vicksburg, Mississippi, 1983.

Sherman, F. S., Imberger, J., and Corcos, G. M., "Turbulence and Mixing in Stably Stratified Waters," Ann. Rev. Fluid Mechanics, 1978, Vol. 10, pp. 267-288.

Sills, G. C. and Elder, D.McG., "The Transition from Suspension To Settling Bed," Estuarine Cohesive Sediment Dynamics, A. J. Mehta ed., Springer-Verlag, Berlin, 1986, pp. 192-205.

Sowers, G. F., Introductory Soil Mechanics and Foundations: Geotechnical Engineering, Macmillan Publishing, New York, 1976.

Stokes, G. G., "On the Effect of the Internal Friction of Fluids on the Motion of Pendulums," Math. and Phys. Papers, Vol. III, No. 1, Cambridge, UK, 1901.

Sumer, S. M., "Transverse Dispersion in Partially Stratified Tidal Flow," Report No. WHM-20, Hydraulic Engineering Laboratory, University of California, Berkeley, May, 1976.

Teeter, A. M., "The Atchafalaya River Delta; Report 2, Volume 2; Settling Characteristics of Bay Sediments," HL-82-15, United States Army Engineers, Waterways Experiment Station, Vicksburg, Mississippi, 1986a.

Teeter, A. M., "Vertical Transport in Fine-Grained Suspension and Newly-Deposited Sediment," Estuarine Cohesive Sediment Dynamics, A. J. Mehta, ed., Springer-Verlag, Berlin, 1986b.

Terzaghi, K., "Die Berchnung der Durchlassigkeitsziffer des Tones aus dem Verlauf der Hydrodynamischen Spannungserscheinungen," Akademie der Wissenchaften in Wien, Sitzungsberichte, Mathematischnaturwissenschaftliche Klasse, Part IIa, Vol. 132, No. 3/4, 1923, pp. 125-138.

Thimakorn, P., "Resuspension of Clays Under Waves," in Seabed Mechanics, B. Denness, ed., Graham & Trotman Ltd., London, 1984, pp. 191-196.

Thompson, R.O.R.Y., "A Re-examination of Entrainment Process in Some Laboratory Flows," Dyn. Atmosphere and Oceans, Vol. 4, No. 45, 1979.

Thorn, M. F. C., "Physical Processes of Siltation in Tidal Channels," Proc. Hydraulic Modelling Applied to Maritime Engineering Problems, ICE, London, 1981, pp. 47-55.

Turcotte, B. R., Liu, P.L.-F., and Kulhawy, F.H., "Laboratory Evaluation of Wave Tank Parameters for Wave-Sediment Interaction," Joseph H. DeFrees Hydraulics Laboratory Report 84-1 and Geotechnical Engineering Report 84-6, School of Civil and Environmental Engineering, Cornell University, Ithaca, New York, August, 1984.

Turner, J. S., Buoyancy Effects in Fluids, Cambridge University Press, Cambridge, Massachusetts, 1973.

van Olphen, H., An Introduction to Clay Colloid Chemistry, Interscience Publishers, New York, 1963.

Vanoni, V. A., "Sedimentation Engineering," Report of Engineering Practice No. 54, American Society of Civil Engineers, New York, 1975.

Wells, J. T., "Dynamics of Coastal Fluid Muds in Low-, Moderate-, and High Tide-Range Environments," Canadian Journal of Fisheries and Aquatic Sciences, Vol. 40 (Suppl. 1), 1983, pp. 130-142.

Wells, J. T., Coleman, J. M., and Wiseman, W. J., "Suspension and Transportation of Fluid Mud by Solitary-Like Waves," Proc. 16th Coastal Engineering Conference, Vol. 2, Hamburg, Federal Republic of Germany, 1978, pp. 1932-1952.

Wells, J. T., and Kemp, G. P., "Interaction of Surface Waves and Cohesive Sediments: Field Observations and Geologic Significance," Estuarine Cohesive Sediment Dynamics, A. J. Mehta, ed., Springer-Verlag, Berlin, 1986.

Whitehouse, U. G., Jeffrey, L. M., and Debrecht, J. D., "Differential Settling Tendencies of Clay Minerals in Saline Waters," Clays and Clay Minerals, Seventh National Conference, 1960, pp. 1-79.

Yeh, H.-Y., "Resuspension Properties of Flow Deposited Cohesive Sediment Beds," M.S. Thesis, University of Florida, Gainesville, Florida, 1979.

Yih, C.-S., "Stability of and Waves in Stratified Flows," 8th Symposium of Naval Hydrodynamics, Pasadena, California, 1970.

Yih, C.-S., "Instability of Surface and Internal Waves," Advances in Applied Mechanics, No. 16, 1976, pp. 369-419.

Yih, C.-S., Stratified Flows, Academic Press, New York, 1980.

Yong, R. N., and Elmonayeri, D. S., "Convection-Diffusion Analysis of Sedimentation in Initially Dilute Solids Suspensions," Sedimentation Consolidation Models, Predictions and Validation, R. N. Yong and F. C. Townsend eds., ASCE, New York, NY, 1984, pp. 260-274.

Zeman, O., and Lumley, J. L., "Buoyancy Effects in Entraining Turbulent Boundary Layers: a Second-order Closure Study," Proc. Turbulent Shear Flow Symp., Penn. State University, Pennsylvania, April, 1977, pp. 6.21-6.28.

BIOGRAPHICAL SKETCH

The author was born May 1959, in Nashville, Tennessee, but grew up in Florida. Having been reared by professor-parents he developed a unique and unusual set of academic ideals, to which he rebelled intermittently and, in the tradition of Huckleberry Finn, opted for a boat and fishing pole (sans books). In 1974, the author met wife to be Susan, a beautiful, strong-minded woman of Italian descent, who quickly communicated to him the virtues of success. After graduating from high school in 1977, he began his higher education at the University of South Florida, Tampa, Florida, and, in 1979, was accepted to an accelerated five year bachelor's/master's program in the College of Engineering. Following a courtship of six years, the author married his childhood sweetheart. In 1982, the author formally received his baccalaureate and master's degrees in civil engineering (water resources) and became gainfully employed for two years in consulting/research activities. The decision was made in 1984 to return to school for the doctorate in civil engineering. Three and one-half years later, it is with a slight hint of melancholy but an overall sense of satisfaction that the author now concludes his tenure as a graduate student. He hopes that he will make his teachers proud.

I certify that I have read this study and that in my opinion it conforms to acceptable standards of scholarly presentation and is fully adequate, in scope and quality, as a dissertation for the degree of Doctor of Philosophy.

Ashish Mehta, Chair
Professor of Civil Engineering

I certify that I have read this study and that in my opinion it conforms to acceptable standards of scholarly presentation and is fully adequate, in scope and quality, as a dissertation for the degree of Doctor of Philosophy.

Robert Dean, Cochair
Graduate Research Professor of
Coastal and Oceanographic
Engineering

I certify that I have read this study and that in my opinion it conforms to acceptable standards of scholarly presentation and is fully adequate, in scope and quality, as a dissertation for the degree of Doctor of Philosophy.

David Bloomquist
Assistant Engineer of Civil
Engineering

I certify that I have read this study and that in my opinion it conforms to acceptable standards of scholarly presentation and is fully adequate, in scope and quality, as a dissertation for the degree of Doctor of Philosophy.

Wayne Huber
Professor of Environmental
Engineering Sciences

I certify that I have read this study and that in my opinion it conforms to acceptable standards of scholarly presentation and is fully adequate, in scope and quality, as a dissertation for the degree of Doctor of Philosophy.

James Kirby
Associate Professor of Coastal
and Oceanographic Engineering

I certify that I have read this study and that in my opinion it conforms to acceptable standards of scholarly presentation and is fully adequate, in scope and quality, as a dissertation for the degree of Doctor of Philosophy.

Dan Spangler

Dan Spangler
Professor of Geology

This dissertation was submitted to the Graduate Faculty of the College of Engineering and to the Graduate School and was accepted as partial fulfillment of the requirements for the degree of Doctor of Philosophy.

August 1988

Herbert A. Bowers

Dean, College of Engineering

Dean, Graduate School

UNIVERSITY OF FLORIDA
3 1262 08556 8045